AN ABSTRACT OF THE THESIS OF

Annabel B. Shephard for the degree of Master of Science in Civil Engineering and Wood Science presented on August 24, 2020.

Title: The Fundamental Behavior of Timber-Concrete Composite Floors in Fire

Abstract approved: _____
Erica C. Fischer Arijit Sinha

Timber-concrete composite (TCC) floors have improved strength and stiffness when compared to timber-only floors, allowing for longer spans in buildings and improved life safety. However, North America does not have codes and standards that recognize TCC floors, particularly the improved life safety performance of these floors in fire. Therefore, alternate means and methods, structural fire engineering, or extensive structural testing is required for structural engineers to design the fire protection for TCC floors. This becomes a large burden on the building owner, as these calculation and testing methods are costly and add time to the project. The objective of this research is to fundamentally understand the behavior of TCC floors during a fire and benchmark existing analytical models for predicting the flexural capacity and deflection of TCC floors in fire against the experimentally collected data. This thesis presents an experimental investigation consisting of two experimental studies conducted to examine (1) properties of shear connectors used in TCC floors through ambient temperature direct shear tests and (2) the behavior of TCC floors through large-scale fire tests performed at the National Research Council (NRC) in Canada. An analytical investigation is performed consisting of benchmarking and improving existing analytical models for the prediction of flexural capacity and deflection of TCC floors during a standard fire. These models are benchmarked against experimental data from the experimental investigation and from previously published large-scale fire tests of TCC floors.

The results indicate that TCC floors have improved fire performance when compared to mass timber floors. The calculated experimental char rates are comparable to prescribed char rates for timber-only, indicating existing char rates can be used for TCC floors. The presence of shear connectors and a concrete topping was found to have a negligible impact on the char rate of timber. Existing analytical models can reasonably predict the temperature-dependent flexural capacity and deflection of TCC floors in fires. This research quantifies the force-slip behavior of the shear connectors used as well as calculating the slip modulus of TCC floor shear connectors using the simplified design method (CEN 2004a). The use of both shear connector slip moduli demonstrated comparable results when calculating deflection

using existing analytical models. The work presented in this thesis is intended to aid practicing engineers in the design of TCC floors for fire.

The Fundamental Behavior of Timber-Concrete Composite Floors in Fire

by

Annabel B. Shephard

A THESIS

Submitted to

Oregon State University

In partial fulfillment of
the requirements for the
degree of

Master of Science

Presented August 24, 2020
Commencement June 2021

Master of Science thesis of Annabel B. Shephard presented on August 24, 2020.

APPROVED:

_____

Co-Major Professor, representing Civil Engineering

_____

Co-Major Professor, representing Wood Science

_____

Head of the School of Civil and Construction Engineering

_____

Head of the Department of Wood Science and Engineering

_____

Dean of the Graduate School

I understand that my thesis will become part of the permanent collection of Oregon State University libraries. My signature below authorizes release of my thesis to any reader upon request.

_____

Annabel B. Shephard, Author

ACKNOWLEDGEMENTS

To begin, I want to thank my advisor Dr. Erica C. Fischer. You encouraged me to attend graduate school when I had not considered continuing my education. I have immense gratitude for your setting me on this path and all the doors you opened for me along the way.

I would like to thank my co-major advisor, Dr. Arijit Sinha, and committee member, Dr. Andre R. Barbosa, for providing their insight, expertise, and asking all the hard questions throughout the development and execution of the experimental and analytical investigations herein. To my committee members, Dr. Mariapaola Riggio and Dr. John Sessions, thank you for your contributions and support throughout this process.

I owe a very special thanks to Milo Clausen for his help in preparing and performing the direct shear testing, including his direction, oversight, and wisdom.

Thank you to my peers for your willingness to lend a hand throughout this project. In particular, thank you to Ian, Hunter, Cody Beairsto, Brad, Kolton, Cody Knight, Shrenik, and Byrne for getting messy during the concrete pour, and to Walker for staying late in the lab to help me calibrate sensors. To Julie, Stefanie, and Tiana, thank you for eagerness to aid in the revision process, and being a reliable, supportive community.

To my father, Scott, who instilled in my brother and I the importance of working hard and spending our days doing what brings us joy, and to my mother, Martha, who demonstrated patience, poise, and fierce determination to do things her own way - thank you for your unwavering support and love all these years.

Finally, to my partner Zachariah. Every moment I spent in doubt, you met with clarity. Thank you for your sturdiness and care.

This work is in collaboration with many industry partners actively working on mass timber buildings. I would like to thank Holmes Structures, Skidmore Owings & Merrill, Katerra, Arup, Forest Products Laboratory, and WoodWorks for their participation in technical advisory committees. The research presented in this paper was funded by the TallWood Design Institute through the US Department of Agriculture, award number 58-0204-6-002.

CONTRIBUTION OF AUTHORS

Dr. Erica C. Fischer, Dr. Andre R. Barbosa, and Dr. Arijit Sinha co-authored Chapter 2 and assisted in the development and execution of the experimental and analytical investigations described within the chapter. Dr. Erica C. Fischer, Dr. Andre R. Barbosa, and Dr. Arijit Sinha assisted in the development and execution of the analytical investigations described within Chapter 3.

TABLE OF CONTENTS

TABLE OF CONTENTS (Continued)

TABLE OF CONTENTS (Continued)

LIST OF FIGURES

LIST OF FIGURES (Continued)

LIST OF FIGURES (Continued)

LIST OF TABLES

LIST OF APPENDICES

For Bella Gazzola.

“Be present in this moment. And the next. And so on.”

CHAPTER 1: INTRODUCTION

Timber construction and fire perception

Timber construction has experienced a resurgence in recent years (Buchanan et al. 2014). Traditionally used for residential homes, the advent of mass timber products, characterized by timber member sizes greater than 150 mm x 150 mm (6 in x 6 in), has made construction above 6 stories (high-rise buildings) feasible (Buchanan et al. 2014; Gerard et al. 2013; White 2008). Examples of mass timber products include cross-laminated timber (CLT), nail-laminated timber (NLT), laminated veneer lumber (LVL), screw-laminated timber (SLT), dowel-laminated timber (DLT), and mass plywood panels (MPP). CLT is comprised of dimensional lumber in layers of alternating direction joined with adhesive. NLT is constructed from dimensional lumber stacked on edge joined with nails. LVL is formed from thin slices of wood veneers bonded through heat and pressure. SLT is constructed from dimensional lumber stacked on edge joined with screws. DLT is constructed from dimensional lumber stacked on edge joined with dowels. MPP is manufactured using structural composite lumber.

The growing popularity of mass timber products for use in North American high-rise buildings (Gerard et al. 2013; Dias et al. 2016; Emberley et al. 2017; Pei et al. 2014) is due in part to the suitability of timber for prefabrication and precision production, subsequently improving construction efficiency and shortening construction times. In addition, mass timber has a lower density than other traditional building construction materials (e.g. steel, concrete) leading to lighter foundations and potentially reduced seismic demands in high-rise mass timber buildings. Lastly, mass timber has gained additional attention as sustainable infrastructure becomes more popular (Buchanan et al. 2017; Gerard et al. 2013) because mass timber is a low-carbon, renewable product that has potential to reduce the embodied carbon of a structure (Gerard et al. 2013; Sathre and O'Connor 2010).

However, despite the known benefits, one of the perceived barriers of utilizing mass timber in high-rise buildings is the behavior of mass timber during a fire. Timber is a combustible material, but the fire performance of timber varies by construction type. Timber construction is commonly classified as either light frame or heavy timber construction. Timber chars when exposed to fire temperatures exceeding 300°C. Formation of a char layer, which has no strength or stiffness, delays the onset of combustion subsequently decreasing the char rate of the unexposed timber (Wood Handbook 2010). For timber members with larger cross-sections (heavy timber, mass timber products) there is a longer fire

exposure time, compared to timber members with smaller cross-sections (light frame, dimensional lumber), before all mechanical resistance is lost.

Timber-concrete composite floors

The steel shortage following World War I and II created a need for an alternative to concrete reinforced with steel (Yeoh et al. 2011b). As a result, TCC floors were developed and during the 1930s and 1940s several patents were filed for shear connections to join timber beams to concrete toppings (Schaub 1931; Yeah et al. 2011b). During this period, TCC structures, particularly TCC bridges, had become common in the United States (US) (Richart and Williams 1943). The global use of TCC structures increased first with bridges in Australia and New Zealand (Rodrigues et al. 2013) and later in Europe (Rodrigues et al. 2013; Yeoh et al. 2011b). An additional application of TCC structures in Europe was the refurbishment of timber-only floors with a concrete topping to meet sound insulation and fire resistance requirements (Yeoh et al. 2011b). This practice continues today for both refurbishment of existing timber-only floors and the construction of new TCC floors.

To meet the International Building Code (IBC) (2018) performance requirements for acoustics and vibration, engineers often add a concrete topping to mass timber floors (Boccadoro and Frangi 2013; Ceccotti et al. 2006; Deam et al. 2007; Dias et al. 2016; Gelfi et al. 2002). Steel mesh is used in the concrete topping for reinforcement (Ceccotti et al. 2006; Deam et al. 2007). The thickness of these concrete toppings is typically 57 mm to 102 mm (2.25 inches to 4 inches). The mass timber floor and concrete topping can be made composite with a shear connection, increasing the strength and stiffness of the floor (Higgins et al. 2017). Compared to timber- or concrete-only floors, timber-concrete composite (TCC) floors have been shown to have superior performance in gravity, seismic, and fire loading (Barbosa et al. 2018; Boccadoro and Frangi 2013; Deam et al. 2007; Dias et al. 2016; Lukaszewska et al. 2008; Yeoh et al. 2011a). Despite these benefits, there are no design methodologies for TCC floors in any current North American codes and standards (AWC 2018) nor does the prescriptive approach for fire resistant design (ICC 2018) consider the superior fire resistance of TCC floors compared to timber-only floors.

Previous research on TCC floors has focused on the performance of shear connectors in direct shear (Branco et al. 2015; Deam et al. 2007; Gelfi et al. 2002; Mai et al. 2018; Miotto and Dias 2011), out-of-plane loading (Barbosa et al. 2018; Higgins et al. 2017), and the behavior of glulam-concrete composite floors. There has been some experimental investigation into the performance of TCC floors and other structural components during a fire, including investigation of char rates (Emberley et al. 2017;

Fragiacomo et al., 2012; Frangi et al. 2008; Klippel et al. 2014; Lineham et al. 2016; Wiesner et al. 2017), and the behavior of TCC floors in fire (Dagenais et al. 2016; Frangi et al. 2010; O'Neill et al. 2011). Recently, a TCC floor design guide was published (Cuerrier-Auclair 2020), and the work in this thesis supports the design methodologies of this guide and the application to US building design.

State-of-the-practice for fire protection design of TCC floors

Buildings are characterized by construction type in the prescriptive approach for fire resistant design (ICC 2018). The perception of timber products as an increased fire hazard is reflected in the prescriptive fire protection design approach, where maximum allowable height and fire resistance requirements are designated based on the fire resistance of the structural material. The current IBC (2018) contains five construction types, Type I, II, III, IV, and V, four of which have sub-types, A and B. Noncombustible construction materials are designated as Type I and II, with maximum allowable heights of "unlimited" and 26 m (85 ft), respectively. Light-frame timber construction is designated as Type III and V, with maximum allowable heights of 26 m and 21 m (85 ft and 70 ft), respectively. Heavy timber construction is designated as Type IV, with a maximum allowable height of 26 m (85 ft). For high-rise mass timber structures to bypass code limitations an alternative engineering approach is required (IBC 2018) that demonstrates that the design meets the intent of the code.

In response to the adoption of mass timber products for high-rise building construction the governing body for the IBC, the International Code Council (ICC), commissioned the ICC Tall Wood Building (TWB) Ad Hoc Committee with the intention of investigating the possibility and development of code changes pertaining to tall wood buildings (Breneman et al. 2019). The results of this committee were the forthcoming adoption of three new construction types for heavy timber into IBC 2021: Type IV-A, IV-B, and IV-C (with Type IV transformed into IV-HT). The maximum allowable heights for heavy timber classifications increased to 82 m (270 ft; Type IV-A) and 55 m (180 ft; Type IV-B).

The IBC prescriptive approach prescribes performance requirements as the period of time (hr) a structural member withstands the ASTM E119 standard fire curve before critical behavior is observed. This period of time is referred to as a fire-resistance rating (FRR) and minimum values are based on individual fire testing of a structural member. Critical behavior varies by structural member type (IBC 2018; ASTM 2018). Required FRR for floor elements by construction type range from 2 hr (Type I-A and I-B), 1hr (Type II-B, III-B, and V-B), to 0 hr (Type II-B, III-B, and V-B). For Type IV, no FRR is required, rather minimum dimensions of the timber members are prescribed with the intention the members have inherent fire resistance. The required FRR for all new construction types, Type IV-A, -B,

and -C, is 2 hr. The changes in the IBC from 2018 to 2021 is a reflection of the recent research developments and is progress for high-rise mass timber construction, but prescriptive approach has yet to account for the improved fire resistance of TCC floors over timber-only floors.

Prescriptive fire protection design assumes the effects of real building fires are sufficiently represented by the ASTM E119 standard fire curve and that the results from fire testing of isolated structural components (ASTM 2018) can be scaled to the full building behavior. The method only allows for the singular objective of identifying critical behavior and neglects to incorporate other design goals such as conservation, business continuity, or sustainability (Hopkin et al. 2014). For floors, one of the critical failure criteria is flame-through which is an integrity failure mode, rather than a structural failure mode. The structural floor assembly (structure and fire protection) must sustain load without developing temperatures on the unexposed surface that would ignite cotton waste (ASTM 2018). This criteria is not related to the structural performance of the floor, but meets the fire integrity provisions to prevent fire spread throughout a building. The presence of a concrete topping on a timber floor can prevent or significantly delay flame-through or integrity failure modes, which would result in a greater fire resistance than a floor without a concrete topping. To take advantage of this behavior, building owners are burdened with funding experimental testing on TCC floors in fire to demonstrate code equivalence and bypass and reassess current code restrictions.

Other fire protective design approaches include engineering analysis, alternative protection methods, and performance-based design (ICC 2018, ASCE 2016). First, engineering analysis is an alternative to the prescriptive approach. Engineering analysis determines the FRR of building elements, components, or assemblies per testing procedures defined by ASTM E119 or the *UL Standard for Fire Tests of Building Construction and Materials* (ASTM 2018; UL 2011). Engineering analysis requires experimental testing data and benchmarked analytical models that can be used by practicing engineers to calculate the behavior of said structural components. This thesis focuses on engineering analysis as an alternative for the prescriptive approach. Second, the alternative protection method is an alternative to the prescriptive approach. The IBC (2018) Section 104.11 allows for an alternative material, design, or method of construction to be used when approved by a building official to not be less than the equivalent of that prescribed in the IBC (2018). The alternative protection method is an expensive alternative, requiring experimental testing to demonstrate equivalence to that prescribed by the code. Finally, in the US, the ASCE *Minimum Design Loads for Buildings and Other Structures* (ASCE 2016) Appendix E has introduced a performance-based approach as an alternative to the prescriptive approach. Performance-based design accounts for the effects of real building fires and considers the response of the structure using the concepts of structural mechanics. This method allows for the design of structural members for

performance objectives beyond the critical failure criteria defined in the prescribed method. Appendix E provides an introduction into performance-based design including general requirements, performance objectives, and analysis of fire effects (ASCE 2016). Appendix E can be used to bypass the restrictions set by the prescriptive method. However, this method can be time-consuming, expensive, and add additional risk to the project as the performance-based design approach often requires additional experimental testing or finite element analysis.

Motivation and research need

This thesis focuses on fundamentally understanding the behavior of TCC floors during a fire scenario and developing and benchmarking methods for predicting this behavior to aid in the design of TCC floors. Both experimental and analytical investigations were performed on TCC floors designed using typical US construction and design practices. The experimental and analytical work performed as a part of this research project were aimed at understanding the fundamental behavior of TCC floors in fire and investigating design parameters to be used in TCC floor design. Small-scale direct shear tests were performed to quantify the force-slip behavior of the shear connectors used in TCC floors for use in analytical and numerical models. Large-scale TCC floors were tested under gravity and thermal loads to characterize the fire behavior of CLT- and NLT-concrete composite floors. Inter-panel connections were included within the floor constructions to determine whether they triggered integrity failures in the floor. Temperature data collected was used to determine that char rates prescribed for solid timber were applicable to TCC floors. The quantitative and qualitative data collected during the experiments were used to benchmark an existing calculation method for the flexural capacity and deflections of TCC floors in fire, and both methods were modified to account for the tensile capacity of truss plate-type shear connectors. For further investigation, the existing calculation method was benchmarked against the data collected during Dagenais et al. (2016) full-scale fire tests. The simplified calculation method to calculate the slip modulus of dowel-type shear connectors (CEN 2004a) is used in the existing calculation method for deflection and the results are compared to the experimental deflection data of TCC floors with dowel-type shear connectors.

Research goals and objectives

The primary goal of this research was to investigate and quantify behavior of CLT- and NLT-concrete composite floors. The qualitative and quantitative results of the tests are used to enhance existing design models that will allow practicing engineers to design TCC floors for fire scenarios, while ensuring life

safety performance. The author intends for these models to aid practicing engineers in employing structural fire engineering on mass timber buildings.

The research objectives of this project were:

1. To experimentally quantify the force-slip behavior of shear connectors used in TCC floors with direct shear tests,
2. To evaluate the structural resistance and fire integrity of TCC floors when exposed to a standard fire (ASTM 2018) and subjected to gravity loads,
3. To compare experimentally measured char rates to those prescribed in international codes (AWC 2018; CEN 2004b; CSA Group 2016),
4. To benchmark and improve upon analytical models for calculating the flexural load-carrying capacity of TCC floors at ambient temperature and throughout a standard fire,
5. To benchmark and improve upon analytical models for determining the deflection of TCC floors throughout a standard fire (ASTM 2018).

To complete these research objectives, the research project was divided into the following tasks:

- **TASK I – Experimental investigation of shear connections:** Testing of CLT- and NLT-concrete composite specimens to measure the force-slip behavior of shear connectors commonly used in TCC floors. The tests were performed at ambient temperature. The specimens were loaded monotonically and uniaxially by an actuator. Loading protocol followed ISO 6891 (1983) and was modified to be controlled through displacement of the crosshead at a constant rate. Slip moduli and shear connector ultimate capacities were calculated using the data from the experiments, which are essential parameters for the design of TCC floors.
- **TASK II – Experimental investigation of large-scale TCC floors:** Testing of two large-scale TCC floors (side-by-side) in a gas-fired floor furnace to evaluate the structural and fire resistance behavior of the TCC floors. The floors used the same shear connector layout, depth of timber, and thickness of concrete as was tested in the direct shear tests (**Task I**). Floors were exposed to the ASTM E119 standard fire (ASTM 2018) and loaded with a distributed service live load using hydraulic rams and a load distribution system. Vertical deflections of the two floors were permitted to be independent. Temperatures and vertical displacements were measured throughout the test.
- **TASK III – Benchmarking of existing char rates for solid timber for TCCs:** Existing char rates for solid timber were evaluated for their application to TCC floors using the temperature data from the experimental fire tests (**Task II**). Temperature data from the fire tests was used to calculate the

experimental char rate for CLT- and NLT-concrete composite floors. The char rates prescribed in both NDS, Eurocode 5, and the Canadian Standard CSA 086-14 (AWC 2018; CEN 2004b; CSA Group 2016) for timber-only are comparable to the experimental char rates observed for the TCC floors.

- **TASK IV – Benchmarking and modification of an existing analytical model for predicting flexural capacity of TCC floors during a fire:** Two existing analytical models for calculating the flexural capacity of TCC floors in fire (Frangi and Fontana 2003; CEN 2004b; Cuerrier-Auclair 2020) were benchmarked using the quantitative and qualitative data from the experimental fire tests (**Task II**). Results from the two analytical models were compared and found to be similar for dowel-type fasteners and agree well with the experimental observations; however, both models required modifications to be applied to TCC floors with truss plate-type shear connectors. Modifications were made to account for the full elastic section modulus of the subcomponents in the neutral axis calculations and to account for the additional tensile reinforcement provided by the truss plate-type shear connectors. The modified model was determined to reasonably predict the flexural capacity of the TCC floors in fire.
- **TASK V – Benchmarking and modification of an existing analytical model for predicting deflection of TCC floors during a fire:** An existing analytical model for calculating the deflection of TCC floors in fire (CEN 2004a; CEN 2004b) was benchmarked using the data from the experimental fire tests (**Task II**). The model was determined to reasonably predict throughout a standard fire the deflection of the TCC floors from **Task II** and the CLT- and SLT-concrete composite floors from Dagenais et al. (2016) using char rates calculated from experimental data and experimentally measured slip moduli. In addition, deflections of CLT-concrete composite floors using dowel-type fasteners were predicted using prescriptive char rates (CEN 2004a) and simplified calculation method to calculate the slip modulus (CEN 2004a).

Thesis outline

This thesis is in manuscript format and comprised of four chapters. Chapter 2, the first manuscript, discusses two different experimental investigations designed to quantify the behavior of shear connectors used to develop composite action between timber and concrete and evaluate the structural resistance and fire integrity of TCC floors when exposed to a standard fire (ASTM 2018). First, direct shear tests were performed to quantify the force-slip behavior of the shear connectors used in TCC floors. Second, large-scale fire tests were performed to measure and demonstrate the fire resistance of TCC floors when exposed to fire. The chapter compares experimentally measured char rates for TCC floors with code-prescribed char rates for solid timber. The chapter presents analytical models for predicting the

flexural capacity of TCC floors and modifies the methods to represent the behavior of TCC floors, benchmarked against the experimental data collected during the fire tests. Chapter 3, the second manuscript, discusses an analytical model for calculating the deflection of TCC floors throughout a standard fire and benchmarks the calculated deflection against the deflection data from experimental fire tests. This model demonstrated good agreement with the experimental tests for dowel-type and truss plate-type shear connectors in NLT-, CLT-, and SLT-concrete composite floors using experimentally calculated char rates and experimentally measured slip moduli. Furthermore, the model demonstrated good agreement with the experimental tests when using prescribed char rates and a simplified model for calculating dowel-type shear connectors slip modulus. Chapter 4 summarizes the research presented in this thesis and provides recommendations for future work.

FUNDAMENTAL BEHAVIOR OF TIMBER-CONCRETE COMPOSITE FLOORS IN FIRE

Annabel B. Shephard

Dr. Erica C. Fischer

Dr. Andre R. Barbosa

Dr. Arijit Sinha

Journal of Structural Engineering

1801 Alexander Bell Drive

Reston, VA 20191-4400

Submitted for review and possible publication

CHAPTER 2: EXPERIMENTAL TESTING AND FLEXURAL CAPACITY ANALYTICAL MODELING OF TIMBER-CONCRETE COMPOSITE FLOORS IN FIRE

Introduction and motivation

Mass timber and building codes

North America is rapidly adopting mass timber products in tall building construction (Gerard et al. 2013; Dias et al. 2016; Emberley et al. 2017; Pei et al. 2014). The popularity of mass timber products is in part due to the potential for prefabrication, precision production, shorter construction time, lighter foundations, and reduced seismic demands.

Acoustical and vibration demands in mass timber buildings are often met by adding a concrete topping to the mass timber deck (Boccadoro and Frangi 2013; Ceccotti et al. 2006; Deam et al. 2007; Dias et al. 2016; Gelfi et al. 2002). Engineers have made these reinforced concrete topping slabs composite with the timber deck to increase strength and stiffness (Higgins et al. 2017) of the floors through the use of shear connectors. Timber-concrete composite (TCC) floors also have improved behavior under gravity, seismic, and fire loading as compared with timber-only floors (Barbosa et al. 2018; Boccadoro and Frangi 2013; Deam et al. 2007; Dias et al. 2016; Lukaszewska et al. 2008; Yeoh et al. 2011a). However, current North American codes and standards do not provide design methodologies for TCC floors (AWC 2018). In addition, the improved fire resistance of TCC floors over timber-only floors is not considered in the prescriptive approach for fire resistant design in the International Building Code (IBC) (ICC 2018). Rather, the only design guidance North American engineers have for TCC floors both at ambient temperature and during a fire is the newly published *Design Guide for Timber-Concrete Composite Floors in Canada* (Cuerrier-Auclair 2020). The calculated methods presented in this chapter will closely align with this design guide.

The IBC prescriptive approach for fire resistant design (ICC 2018) is based on characterizing buildings according to construction type. Prescriptive fire-resistance ratings are developed by testing individual structural members to achieve a fire-resistance rating (FRR) with the units of time (hours). This time corresponds to the amount of time a member withstood exposure to the standard fire (ASTM E119) within a gas-fire furnace before reaching critical behavior prescribed by ASTM E119 (ASTM 2018). The critical behavior changes from member to member. For floors, the acceptance criterion consists of sustaining the applied load during the classification period without flame-through and limiting the transmission of heat through the specimen. These criteria are not related to the structural performance of

the floor but meet the fire integrity provisions to prevent fire spread throughout a building. The presence of a concrete topping on a timber floor (such is the case for TCC floors) can prevent or significantly delay flame-through or integrity failure modes, which would result in a greater fire resistance than a floor without a concrete topping.

The behavior of cross-laminated timber (CLT), commonly used in TCC floors, in fire is highly dependent upon the performance of the adhesive (Barber and Gerard 2015; Frangi et al. 2009; Li et al. 2016). Poor performing adhesives can cause the timber to fall off, or delaminate, exposing uncharred timber. Exposure of uncharred timber can cause re-ignition of a fire during the decay phase. This behavior can prevent the fire from ever decaying (or burning out) and can lead to an increased char rate. ANSI/APA PRG 320 *Standard for Performance-Rated Cross Laminated Timber* was developed to standardize the manufacturing of CLT, including adhesives. In the most recent version (ANSI 2018), fire and moisture testing of the adhesives are required to prevent delamination, thereby preventing re-ignition of the fire. When considering the fire behavior of nail-laminated timber (NLT), another common mass timber product for TCC floors, delamination is not a concern as NLT is not constructed with adhesive or horizontal panels of timber.

Previous research on TCC floors in fire

TCC shear connectors have been widely tested under direct shear (Branco et al. 2015; Deam et al. 2007; Gelfi et al. 2002; Mai et al. 2018; Miotto and Dias 2011) and out-of-plane loading (Barbosa et al. 2018; Higgins et al. 2017). However, there is limited experimental data on the fire performance of TCC floors. Previous researchers have investigated the fire performance of TCC structural components by studying char rates (Emberley et al. 2017; Fragiacomo et al., 2012; Frangi et al. 2008; Klippel et al. 2014; Lineham et al. 2016; Wiesner et al. 2017), and the fundamental behavior of TCC floors (Dagenais et al. 2016; Frangi et al. 2010; O'Neill et al. 2011). Recently, Hozjan et al. (2019) conducted a comprehensive literature review of TCC structures in fire.

O'Neill et al. (2011) performed full-scale fire tests on two TCC floors with dimensions 4 m x 3 m (13 ft x 9.8 ft) and loaded with a live load of 2.5 kPa (52 psf). Floors were double laminated veneer lumber (LVL) beams with a concrete topping with different shear connectors for each test: (1) partially threaded timber screws and (2) truss plates. Both floors failed in flexure due to the reduction of timber through charring. Floors demonstrated a higher level of fire resistance compared to timber-only counterparts (37 minutes under fire exposure before failure compared to 75 minutes) (O'Neill et al. 2011).

These tests provided valuable data on the fire performance of LVL-concrete composite floors but did not address other timber material options for TCC floors.

Frangi et al. (2010) investigated the performance of one type of shear connector for glulam beam-concrete floors. The research focused on self-drilling screw connectors that use a collar to limit the embedment depth of the screw in the timber and a head to engage the concrete. Researchers developed a design model to calculate the stresses of the subcomponents for TCC floors with screw connectors exposed to fire. This design model was based on the reduced cross-section method (RCSM) (CEN 2004b) and the "γ-method," a simplified calculation method for calculating the stiffness of and the stress distribution through timber elements joined with mechanical fasteners (CEN 2004a). Frangi et al. (2010) performed a full-scale fire test of a TCC floor comprised of four 180 mm x 240 mm (7.1 inches x 9.5 inches) glulam beams supporting an 80 mm (3.1 inches) concrete slab. The developed model was used to predict the experimental behavior of the floor throughout the test. The concrete and timber were composite through the use of self-drilling screws arranged at 45°. The failure of the floor was controlled by the loss of strength and stiffness of the shear connector (Frangi et al. 2010). This test highlighted that the structural behavior of TCC floors is primarily governed by the behavior of the shear connectors and the importance of understanding how this behavior may change with temperature. The design model developed by Frangi et al. (2010) also demonstrated the ability to use structural mechanics to design and predict the fire behavior of TCC floors.

Dagenais et al. (2016) performed full-scale fire tests on three different TCC floors: CLT-, screw-laminated timber (SLT), and LVL-concrete composite floors loaded with a live load of 2.4 kPa (50 psf). The shear connectors varied on each of the floors. Self-tapping screws arranged at 45° were used to join the concrete and CLT compositely, conventional steel truss plates were used with the SLT, and lag screws placed at 90° were used with the LVL. All three of the assemblies maintained load-carrying capacity when exposed to the standard CAN/ULC-S101 fire curve for three hours (Dagenais et al. 2016; ULC 2014). This fire curve is similar to that of ASTM E119 (ASTM 2018). The results from these tests indicate that the shear connectors had a negligible impact on the char rates measured throughout the tests. While the LVL-concrete composite floor included an inter-panel joint, the CLT- and SLT-concrete composite floors did not. These joints are often the location of integrity failures in floor fire tests (Osborne et al. 2012), though the LVL-concrete composite floor did not experience an integrity failure due to the inter-panel joints (Dagenais et al. 2016).

Chapter objectives

The objectives of this chapter are to quantify the behavior of shear connectors used to develop composite action between timber and concrete and to evaluate the structural resistance and fire integrity of TCC floors when exposed to a standard fire (ASTM 2018). This chapter accomplishes these objectives through experimental testing and the evaluation of TCC floors through analytical modeling. The author conducted ambient direct shear tests on TCC specimens to quantify the force-slip behavior of the shear connectors. The author then performed large-scale structural fire tests on two TCC floors in a gas-fire furnace to measure and demonstrate the integrity and fire resistance of TCC floors when exposed to fire. The qualitative and quantitative results of these experimental programs were used to enhance an existing design method, the elasto-plastic model (Frangi and Fontana 2003). This model was benchmarked against the experimental tests, compared to a second analytical model (Cuerrier-Auclair 2020), and demonstrated that practicing engineers can design TCC floors for fire scenarios while ensuring life safety performance.

In this chapter, the author will first present the materials and methods for both the direct shear tests and the large-scale fire tests. This section includes material grades and properties, instrumentation, and loading protocols. The author will then present and discuss the results from both the direct shear tests and the large-scale fire tests. These results will be qualitative (observations) and quantitative (calculated slip moduli, calculated char rates). Lastly, the author will use the results from both the direct shear tests and the large-scale fire tests to enhance an existing design model (Frangi and Fontana 2003) and benchmark the model against the experimental tests performed in this experimental program and a second experimental program (Dagenais et al. 2016). The results of the existing design model (Frangi and Fontana 2003) is compared to the results of a second analytical model (Cuerrier-Auclair 2020).

Materials and methods

Direct shear tests

Slip moduli and ultimate shear capacities of shear connectors can be calculated using experimentally measured force-slip behavior of shear connectors. Six CLT-concrete composite specimens with fully-threaded timber screws and six nail-laminated timber (NLT) concrete composite specimens with truss plate shear connectors were tested at Oregon State University.

CLT-concrete composite specimens

The CLT-concrete composite specimen consisted of ANSI/APA PRG 320 (ANSI 2017) compliant 5-ply, 175 mm (6.88 inches) thick, grade V2 CLT manufactured by Structurlam with a 57.2

mm (2.25 inches) normal-weight concrete topping. The concrete design compressive strength was 34.5 MPa (5 ksi) at 28 days. The concrete design included a water reducer admixture. The concrete cylinder compression tests were performed per ASTM C39 (ASTM 2012), and the results are provided in Table 2.1. Tensile reinforcement in the concrete was W152 x 152 (W6 x 6) gauge 9/9.

The CLT-concrete composite specimens were 305 mm (12 inches) wide and 610 mm (24 inches) in length. Fully-threaded ASSY VG CYL timber screws 9.53 mm (0.375 inches) in diameter and 200 mm (7.875 inches) in length were used as shear connectors between the timber and concrete to develop the composite action. The fully-threaded screws were oriented in the same direction at 45° and embedded in the CLT for a depth of 150 mm (5.9 inches) (Figure 2.1c). The remainder of the fully-threaded screw was embedded in the concrete topping. Fully-threaded screws were spaced at 305 mm (12 inches) along the length of the specimen resulting in two fully-threaded screws, with 152 mm (6 inches) of edge distance in each direction.

NLT-concrete composite specimens

The NLT-concrete composite specimens consisted of 38 mm x 140 mm (1.5 inches x 5.5 inches) solid sawn Ponderosa Pine, 0.40 specific gravity, Grade No. 2 with a 76.2 mm (3 inches) normal-weight concrete topping. The nails joining the timber laminations were smooth shank 76.2 mm (3 inches) in length and 3.05 mm (0.120 inches) in diameter. Per the NLT Design Guide (2017), the lamination nailing pattern was two rows of nails spaced 127 mm (5 inches) staggered (Figure 2.2). The concrete was of the same mix and utilized the same tensile reinforcement as the CLT-concrete composite specimen shown in Table 2.1 and discussed in the previous section.

Table 2.1. Concrete cylinder compression testing results for direct shear tests

Age	Cylinders tested	Avg. Compressive Strength	Max. Compressive Strength	Min. Compressive Strength	COV
days	**#**	**Mpa (ksi)**	**Mpa (ksi)**	**Mpa (ksi)**	**%**
7	3	27.4 (3.97)	28.1 (4.07)	26.7 (3.88)	2.53
28[1]	3	41.1 (5.96)	41.4 (6.00)	40.9 (5.93)	0.89
57 Day of test, NLT-concrete	3	39.6 (5.74)	40.9 (5.93)	38.8 (5.63)	2.82
61 Day of test, CLT-concrete	3	38.5 (5.59)	40.1 (5.81)	37.5 (5.45)	3.50

[1]Average compressive strength and COV calculated using two data points. The third data point was removed because COV was outside the allowable range (ASTM 2012).

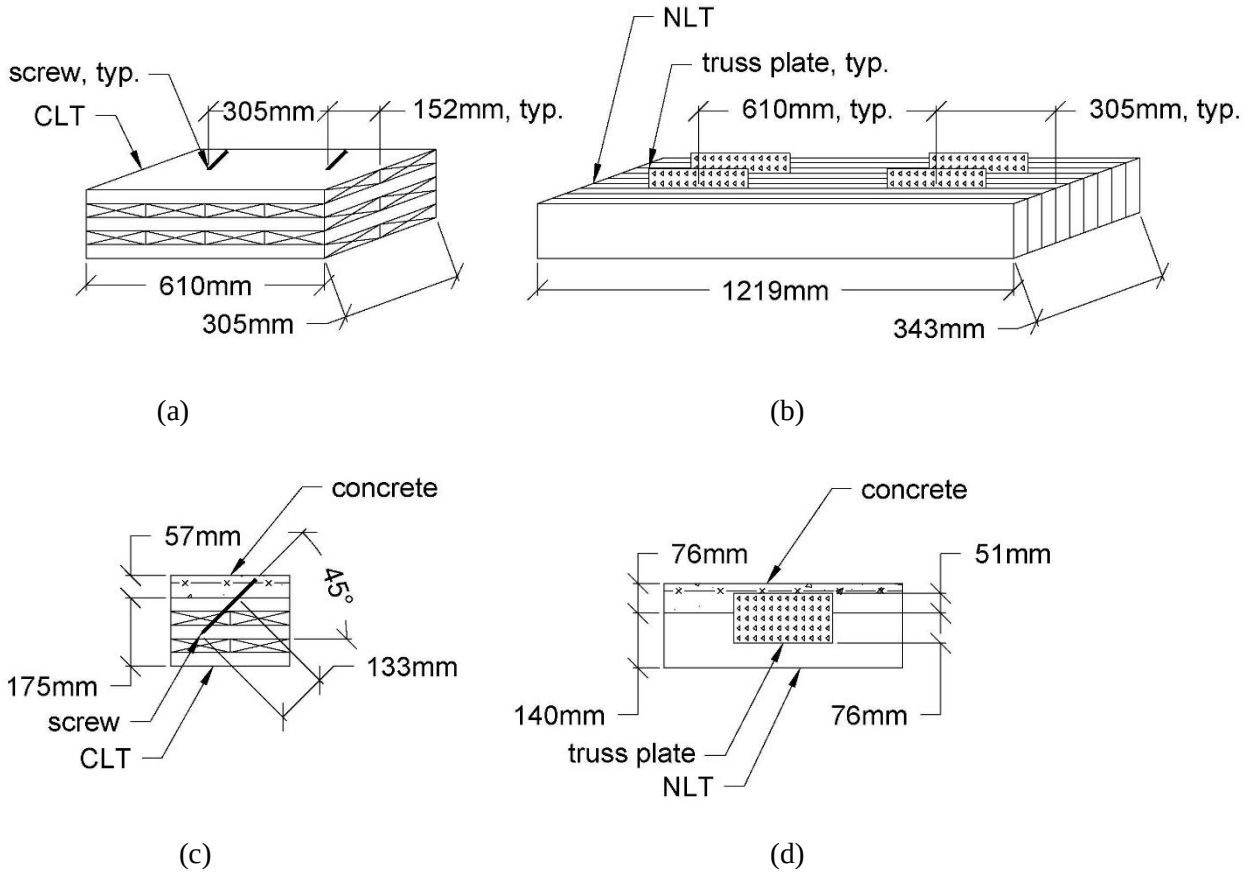

Fig. 2.1. Cross-section through direct shear tests showing connector geometry for the (a, c) CLT- and (b, d) NLT-concrete composite specimens

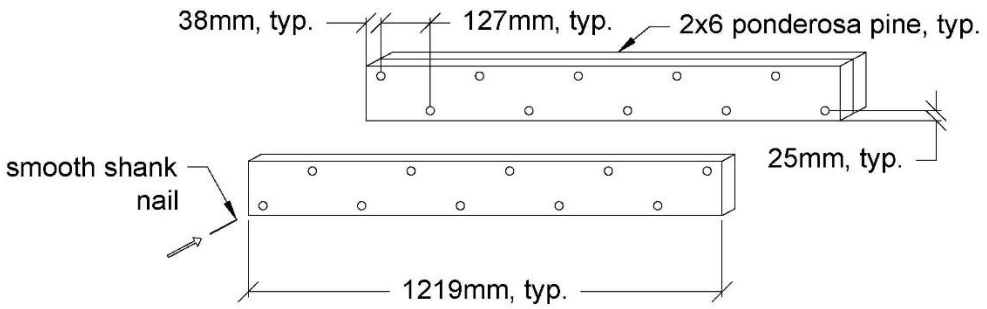

Fig. 2.2. Nail pattern used for the construction of the NLT-concrete composite specimen

The NLT-concrete composite specimens were 343 mm (13.5 inches) wide and 1219 mm (48 inches) in length. MiTek MT20 truss plates were used as shear connectors between the timber and concrete to develop composite action. The truss plates were embedded in the NLT by a hydraulic press every third lamination, per manufacturer's standard (ICC-ES 2016). Shown in Figure 2.1d, 76.2 mm of the truss plate depth was embedded in the NLT, while the remainder was embedded in the concrete

topping. Truss plates were spaced at 610 mm (24 inches) along the length of the specimen with 305 mm (12 inches) of edge distance. A total of four truss plates were utilized for each specimen.

Loading protocol

Each specimen was tested individually and loaded monotonically and uniaxially by a 179 kN (40 kips) actuator with a 44.5 mm (1.75 inches) extension. The loading protocol, shown in Figure 2.3, followed ISO 6891 (1983) and was modified to be controlled through the displacement of the crosshead at a rate of 0.5 mm/min (0.02 inches/min). The loading protocol is shown in Figure 2.3. The load was applied until 0.4 of the estimated maximum force (F_{est}). For Test 1, F_{est} was estimated from previous experimental tests (Branco et al. 2015; Mai et al. 2018). For Tests 2-6, the F_{est} was the maximum experimentally measured force from Test 1. At $0.4F_{est}$, the applied force was maintained for 30 seconds. The specimen was then unloaded at the same rate to $0.1F_{est}$, the load was held for 30 seconds, and then the specimen was loaded until failure or until the load had decreased to $0.5F_{est}$ in the post-peak behavior. A steel bulkhead was welded to the strong floor to prevent movement of the timber in the direction of the applied load, as shown in Figures 2.4a and 2.5a. The concrete was not restrained during the tests.

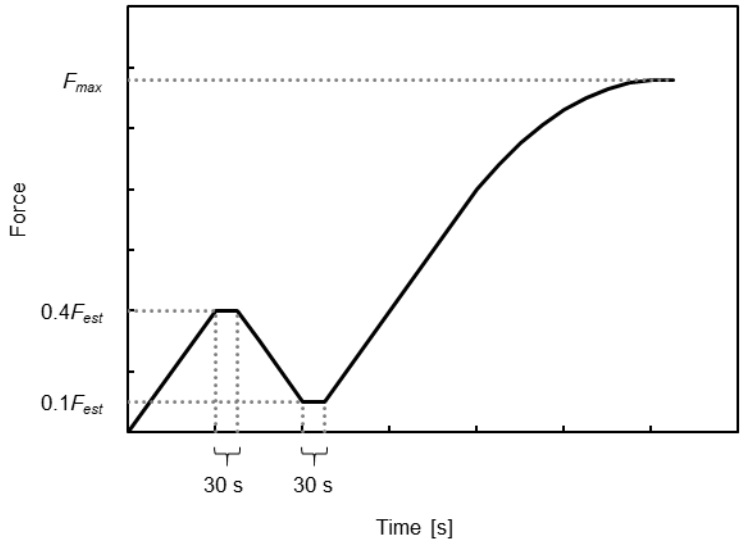

Fig. 2.3. Loading protocol per ISO 6891 (1983) modified to allow for displacement control

Instrumentation

Displacements and applied load were measured throughout the direct shear tests. The displacements were measured using linear variable differential transformers (LVDTs) to measure the horizontal movement of the timber with respect to the concrete, rotation of the specimen in-plane, and

uplift of the specimen. Two LVDTs were utilized to measure each of these displacements and provide redundancy in the measurements, for a total of six LVDTs on each specimen. The applied load was measured using a 222 kN (50 kips) load cell. The location of the LVDTs and load cell are shown in Figures 2.4 and 2.5.

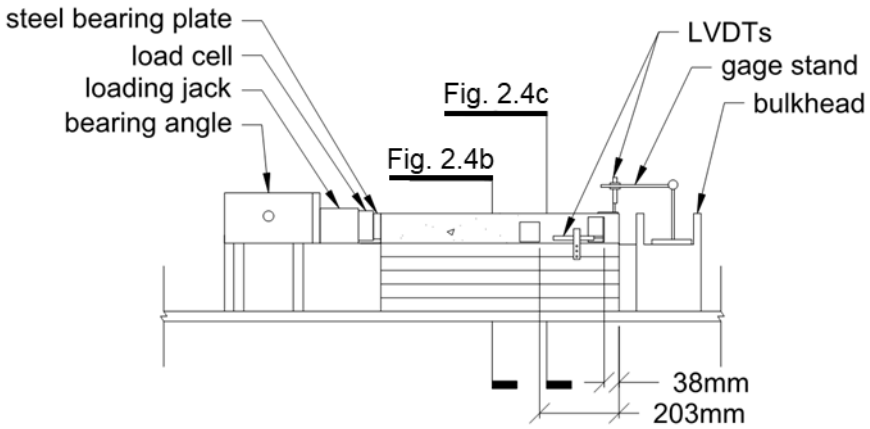

(a)

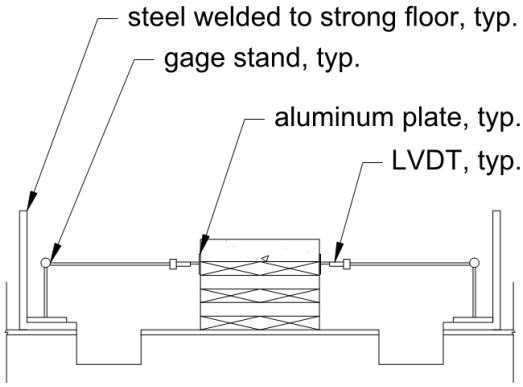

(b)

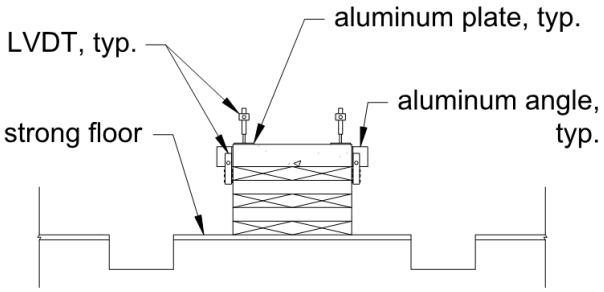

(c)

Fig. 2.4. Test set-up for the CLT-concrete composite specimen (a) elevation view of test set-up, (b) section showing the location of LVDTs measuring the in-plane rotation of the specimen, and (c) section showing the location of LVDTs measuring uplift and horizontal movement of the timber relative to the concrete

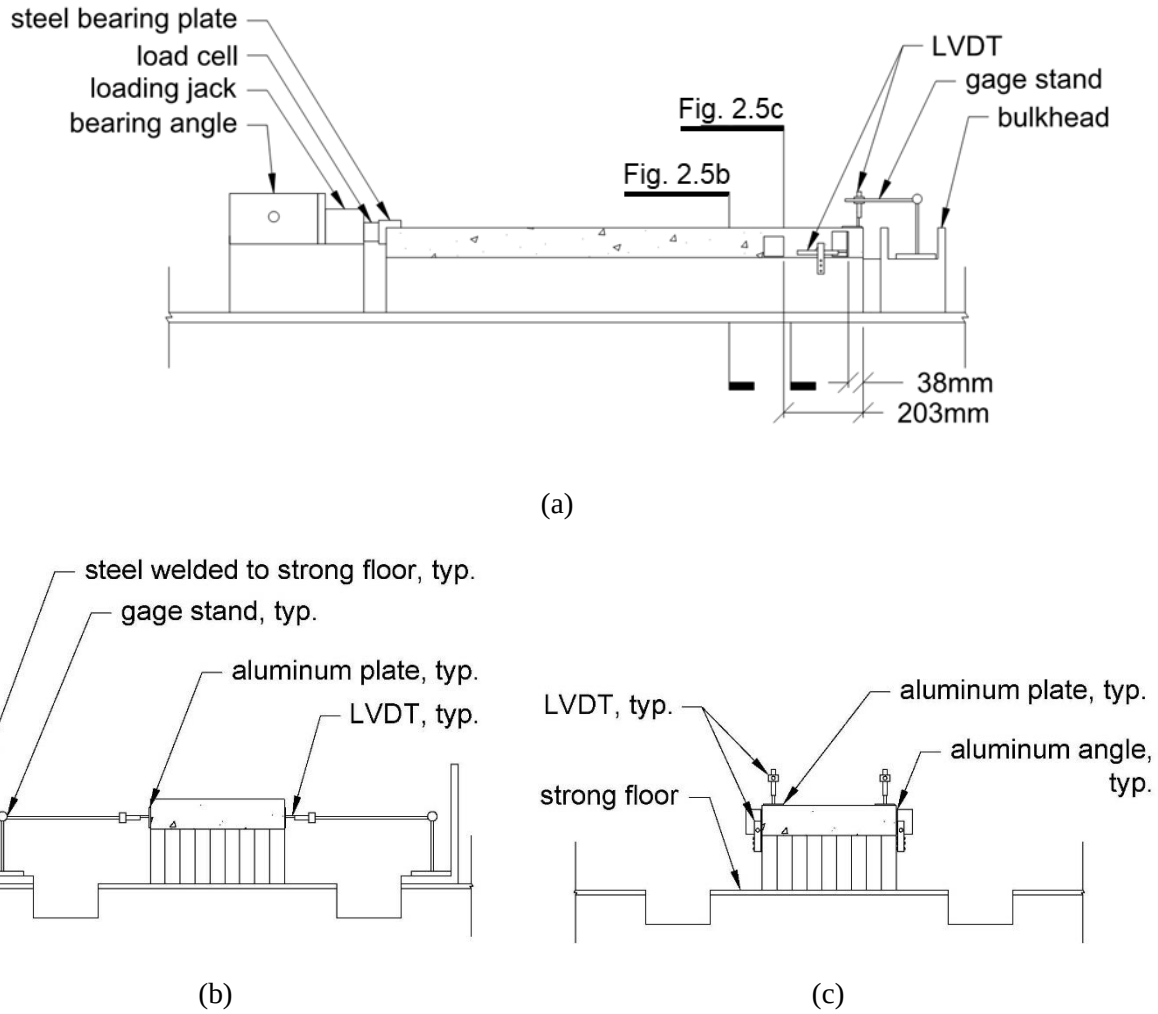

Fig. 2.5. Test set-up for the NLT-concrete composite specimen (a) elevation view of test set-up, (b) section showing the location of LVDTs measuring the in-plane rotation of the specimen, and (c) section showing the location of LVDTs measuring uplift and horizontal movement of the timber relative to the concrete

Large-scale fire tests

Fire tests were performed on one CLT- and one NLT-concrete composite floor in the gas-fired floor furnace at the National Research Council (NRC) of Canada in Ottawa, Ontario. The objective of these tests was to evaluate the structural and fire resistance behavior of the TCC floors. The floors used the same shear connector layout, depth of timber, and thickness of concrete as was tested in the direct shear tests.

CLT-concrete composite floor

The CLT-concrete composite floor used the same dimensional configuration as the direct shear tests previously described. The CLT was manufactured by Smartlam and met the specification of the 2017 ANSI/APA PRG 320 (ANSI 2017). The properties of the different CLT panels used for the experimental tests are compared in Table 2.2. The concrete design compressive strength was 34.5 MPa (5 ksi) at 28 days. The concrete design included a water reducer admixture. The concrete cylinder compression tests were performed per ASTM C39 (ASTM 2012), and the results are provided in Table 2.3. The tensile reinforcement in the concrete was W152 x 152 (W6 x 6) gauge 9/9.

Table 2.2. Design values for CLT utilized in the direct shear tests and the large-scale fire tests

	Direct shear tests (Structurlam[1])	**Large-scale fire tests (Smartlam[2])**
Grade	V2M1.1	SL-V4
Specific gravity	0.42 (SPF)[3]	0.36 (SPF-S)
Bending strength	875 psi	775 psi
Tensile strength	450 psi	350 psi
Elastic modulus	$1.4 \cdot 10^6$ psi	$1.1 \cdot 10^6$ psi

[1]All values from Structurlam's *CrossLam CLT Technical Design Guide* (Structurlam 2020) unless otherwise noted
[2]Values from Smartlam's *Cross-Laminated Timber 2020 Specification Guide* (Smartlam 2020)
[3]Value from ANSI/AWC *National Design Specification for Wood Construction* (AWC 2018)

The floor was 1200 mm (48 inches) wide and 4800 mm (189 inches) in length. The same fully-threaded timber screws were used as shear connectors with the same spacing and embedment into the CLT and the concrete as described for the direct shear tests. The fully-threaded screws were oriented in the strong position, facing toward the nearest support, with 152 mm (6 inches) of edge distance in the transverse direction and 76 mm (3 inches) of edge distance in the longitudinal direction of the floor. The screw pattern is similar to ambient tested specimens by Higgins et al. (2017) adjusted for furnace dimensions (Figure 2.6).

A spline connection was placed at the center of the floor, as shown in Figure 2.6. The spline was 152 mm (6 inches) in width and connected two 610 mm (24 inches) wide CLT floors to form the single 1219 mm (48 inches) wide floor. The spline consisted of two 152 mm (6 inches) long SDWS timber screws spaced at 76.2 mm (3 inches) in the transverse direction joining a 152 mm (6 inches) wide and 28.6 mm (1.13 inches) thick plywood board embedded into the first lamination of the CLT floor. The

SDWS timber screws were spaced longitudinally 102 mm (4 inches) on center. The exposed shear connectors and the surface of the spline can be seen in Figure 2.6 and Figure 2.8b.

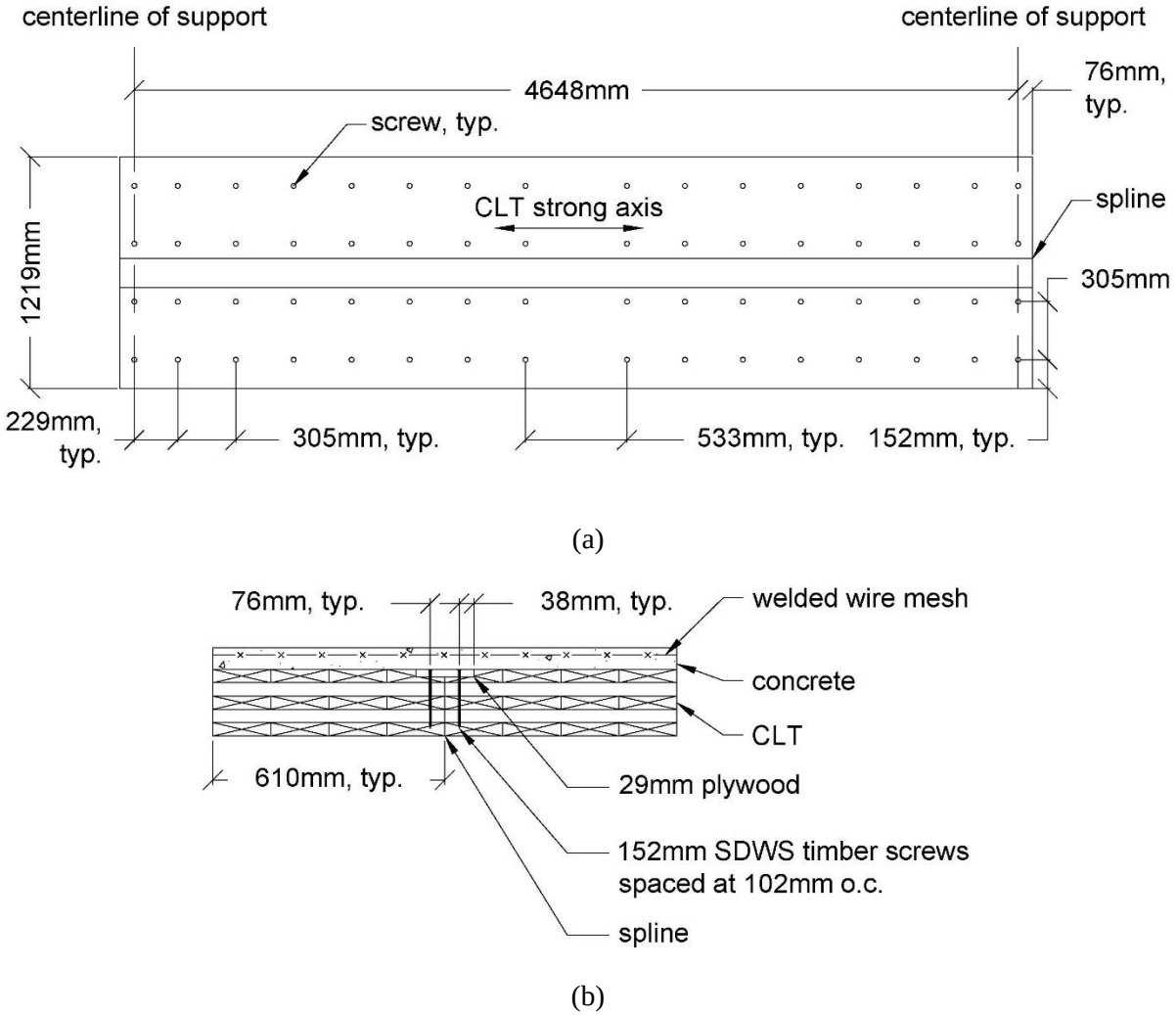

Fig. 2.6. CLT-concrete composite floor layout (a) plan view showing shear connector layout and (b) section through the spline joint detail

NLT-concrete composite floor

The NLT-concrete composite floor used the same dimensional configuration as the direct shear test. The NLT was constructed from 38 mm x 140 mm (1.5 inches x 5.5 inches) solid sawn Grade No. 2 spruce-pine-fir (SPF), which has a similar specific gravity as Ponderosa Pine (0.42). The lamination nailing was the same design as the direct shear test (NLT Design Guide 2017). The concrete was of the same mix and utilized the same tensile reinforcement as the large-scale fire test CLT-concrete composite floor.

The floor was 1257 mm (49.5 inches) wide and 4801 mm (189 inches) in length. The same MiTek MT20 truss plates were used as shear connectors with the same installation, spacing, and embedment into the NLT and the concrete as described for the direct shear tests. The edge distance of the truss plates in the longitudinal direction is 140 mm (5.5 inches). The exposed shear connectors can be seen in Figure 2.8a.

Solid sawn timber swells and shrinks with changing temperature and moisture conditions. Because of this, the author included an expansion gap within the NLT-concrete composite floor to prevent unintended stresses from developing over time, which is a common practice in NLT construction (NLT Design Guide 2017). The expansion gap is the width of one lamination, 38.1 mm (1.5 inches), and was located along the center of the floor. This location would decrease the flexural capacity of the floor the greatest in the event of a fire. A small piece of wood that was less than the full height of the NLT boards was lightly nailed in place along the bottom of the expansion gap, as shown in Figure 2.7b. In addition, a piece of plywood was placed on top of the expansion gap as formwork for the concrete.

Table 2.3. Concrete cylinder compression testing results for large-scale fire tests. Testing performed by researchers at the NRC

Age	No. cylinders tested	Avg. Compressive Strength	Max. Compressive Strength	Min. Compressive Strength	COV
days	**#**	**Mpa (ksi)**	**Mpa (ksi)**	**Mpa (ksi)**	**%**
28	3	34.4 (4.99)	35.5 (5.14)	33.7 (4.89)	2.68
Day of test (55 days)	5	36.1 (5.23)	37.1 (5.37)	35.3 (5.12)	2.05

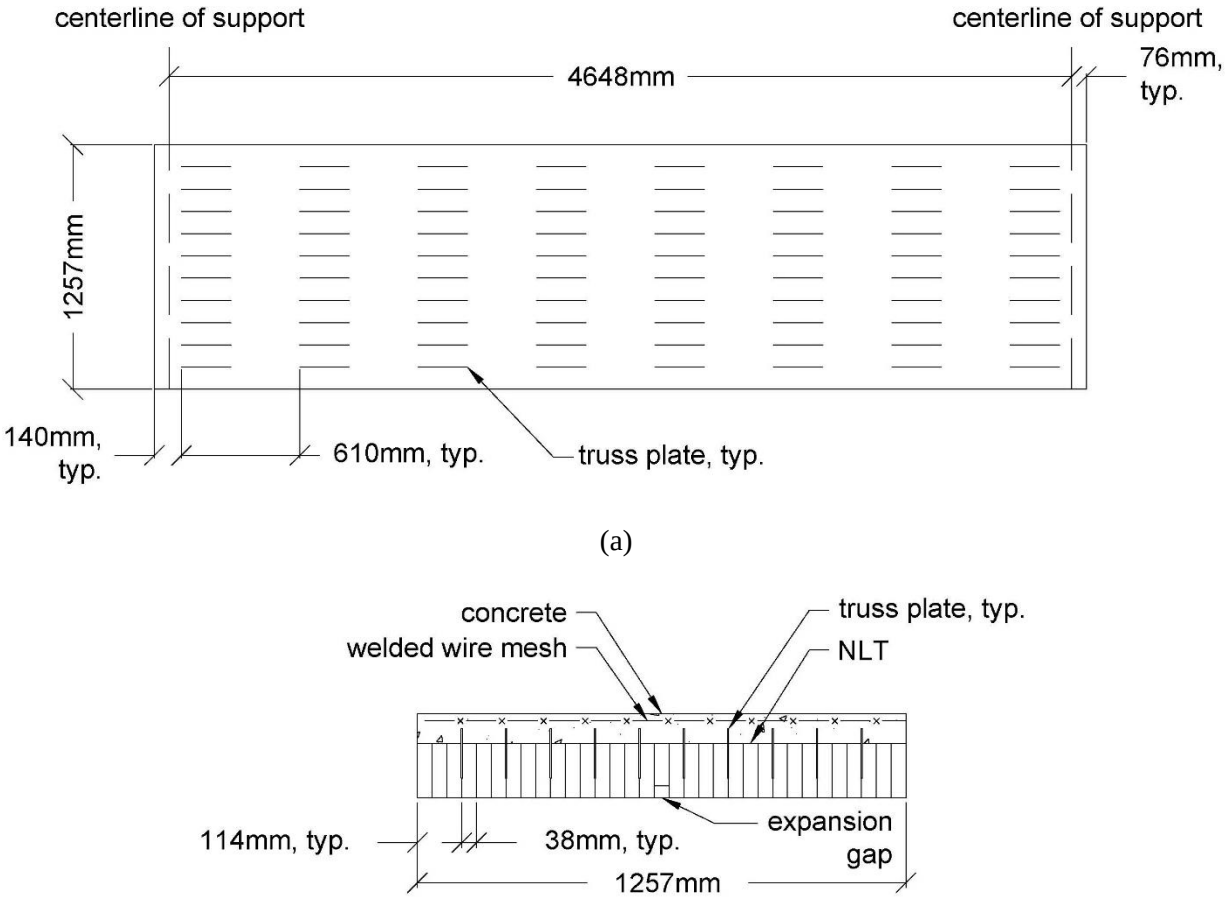

Fig. 2.7. NLT-concrete composite floor layout (a) plan view showing shear connector layout and (b) section through the expansion gap detail

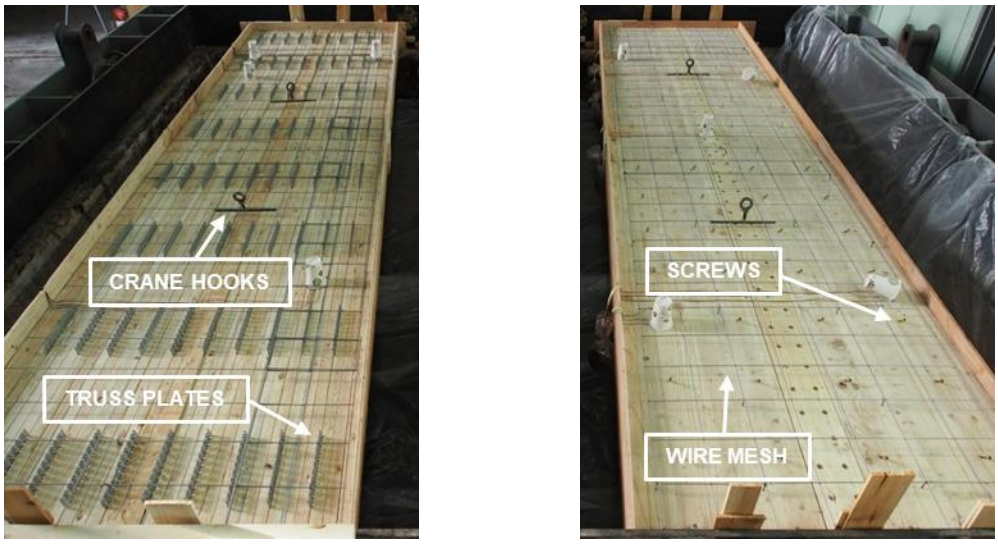

(a) (b)

Fig. 2.8. Photographs of the floors during construction showing shear connector layout for the (a) NLT- and (b) CLT-concrete composite floors

Loading protocol

The floors were tested side-by-side, as shown in Figure 2.9a. Floors were exposed to the ASTM E119 standard fire and loaded with a distributed service live load of 3.83 kPa (80 psf) using hydraulic rams and load distribution system (Figure 2.9b). The floors were supported on the edge of the furnace with roller supports. Insulation was placed between the floors to prevent flame-through, as shown in Figure 2.9a. Vertical deflections of the floors were permitted to be independent. Although both specimens were exposed to a standard fire, the test failure criterion was structural failure rather than the failure criteria associated with integrity failure in ASTM E119 (ASTM 2018). A limitation of side-by-side testing is that the test must stop (furnace shut off and load removed) when one of the floors collapses into the furnace. Consequently, the deflection rates of both floors were observed throughout the test. At the point of rapid increase in the deflection rate of one of the floors, per ASTM E119, the load was removed from that floor, and the test was continued.

(a) (b)

Fig. 2.9. (a) Photograph of the underside of the CLT- and NLT- concrete composite floors taken inside the furnace, and (b) distributed loading mechanism used to apply floor loads to floors

Instrumentation

Both floors were instrumented with Type K thermocouples to measure the temperature distribution along the length of the floor and through the cross-section at various locations, as shown in Figures 2.10 and 2.11. String potentiometers were used to measure the vertical displacement of the floor at the mid- and quarter- points along the length of the floor. Thermocouples were embedded at the same locations through the depth of the CLT- and NLT-concrete composite floors. Thermocouples were embedded through vertically drilled holes from the top of the concrete prior to the concrete pour. Thermocouples at the same location were offset to prevent locally weakening the timber and increasing potential for an integrity failure during the fire.

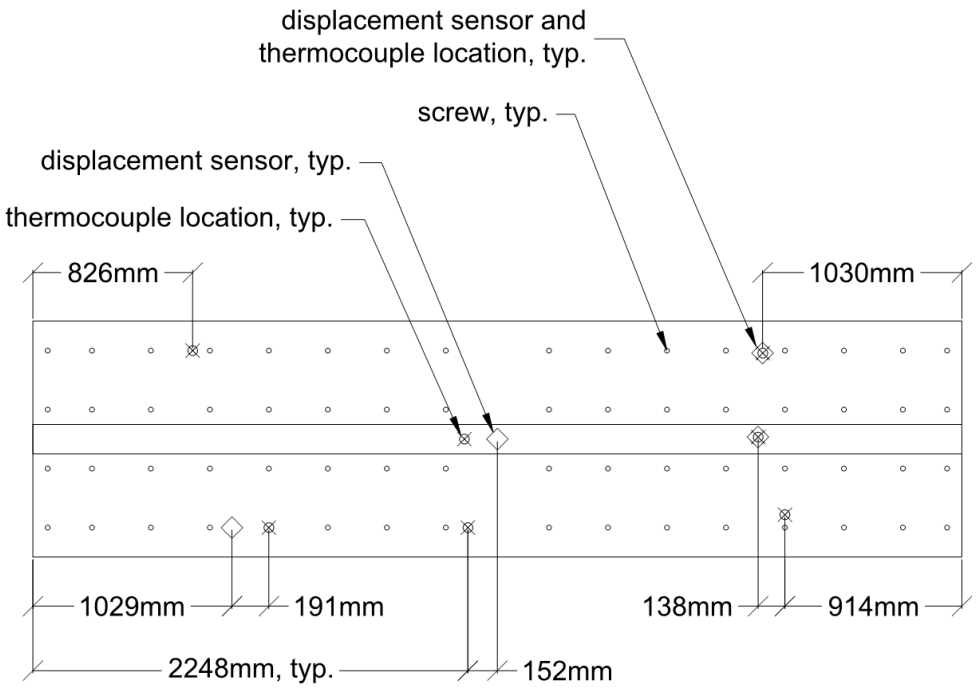

(a)

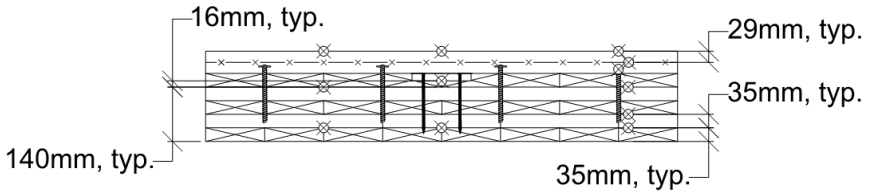

(b)

Fig. 2.10. CLT-concrete composite floor in (a) plan view showing thermocouple and displacement sensor locations and (b) section showing typical depths of thermocouples

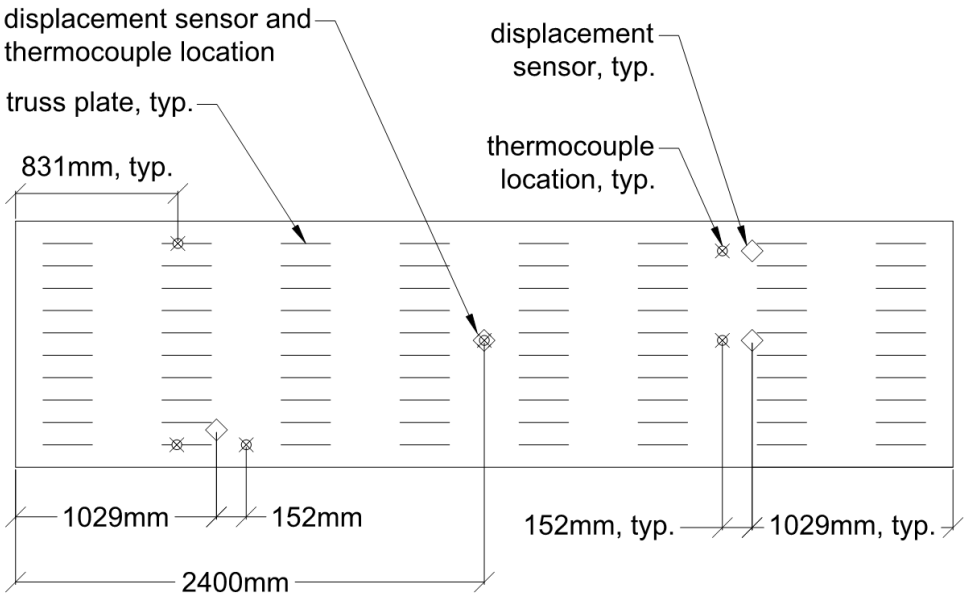

(a)

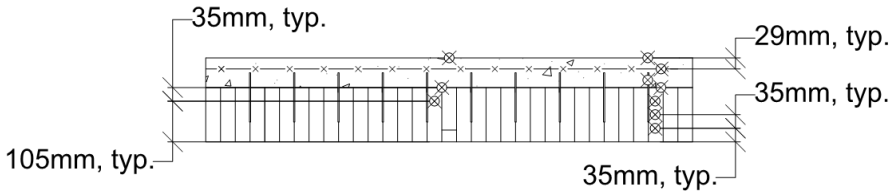

(b)

Fig. 2.11. NLT-concrete composite floor in (a) plan view showing thermocouple and displacement sensor locations and (b) section showing typical depths of thermocouples

Results

Direct shear tests

Numerical results

The results of the direct shear tests are presented in Tables 2.4 and 2.5, and the force-slip curves for each test are plotted in Figure 2.12. The slip modulus (k_s) was calculated per ISO 6891 (1983) and is shown for the fully-threaded screw and truss plate shear connectors in Tables 2.4 and 2.5, respectively. The maximum force (F_{max}) is the peak load measured during the test. Since the peak load occurred before 15mm of slip, this value also corresponds to F_{max} per ISO 6891 (1983). Though there was high variability of the slip modulus between specimens, there was consistency of the maximum force, the maximum displacement at the maximum force (δ_u), and the maximum displacement (δ_{max}) for both the CLT- and NLT-concrete composite direct shear tests.

Table 2.4. CLT-concrete composite specimen direct shear test results

Specimen	F_{max}	δ_u	δ_{max}	k_s
#	**kN (kip)**	**mm (inches)**	**mm (inches)**	**kN/mm (kip/inches)**
1	56.0 (12.6)	1.78 (0.07)	33.8 (1.33)	34.2 (195)
2	61.8 (13.9)	2.03 (0.08)	25.7 (1.01)	63.7 (364)
3	46.3 (10.4)	1.52 (0.06)	25.9 (1.02)	94.1 (538)
4	61.8 (13.9)	1.52 (0.06)	25.7 (1.01)	123 (701)
5	61.4 (13.8)	2.03 (0.08)	25.7 (1.01)	123 (700)
6	68.5 (15.4)	2.29 (0.09)	25.7 (1.01)	97.3 (556)
average	59.3 (13.3)	1.86 (0.07)	27.1 (1.07)	89.1 (509)
standard deviation	7.52 (1.69)	0.31 (0.01)	3.30 (0.13)	34.6 (198)

Table 2.5. NLT-concrete composite specimen direct shear test results

Specimen	F_{max}	δ_u	δ_{max}	k_s
#	**kN (kip)**	**mm (inches)**	**mm (inches)**	**kN/mm (kip/inches)**
1	134 (30.2)	6.10 (0.24)	15.0 (0.59)	24.9 (143)
2	132 (29.6)	5.33 (0.21)	12.7 (0.50)	45.1 (258)
3	127 (28.5)	6.10 (0.24)	13.7 (0.54)	70.8 (405)
4	135 (30.2)	5.84 (0.23)	14.0 (0.55)	84.5 (483)
5	133 (29.9)	9.65 (0.38)	16.5 (0.65)	32.8 (187)
6	134 (30.2)	6.10 (0.24)	12.4 (0.49)	264 (1510)
average	132 (29.8)	6.50 (0.30)	14.1 (0.55)	87.0 (497)
standard deviation	2.99 (0.67)	1.56 (0.06)	1.51 (0.06)	90.0 (512)

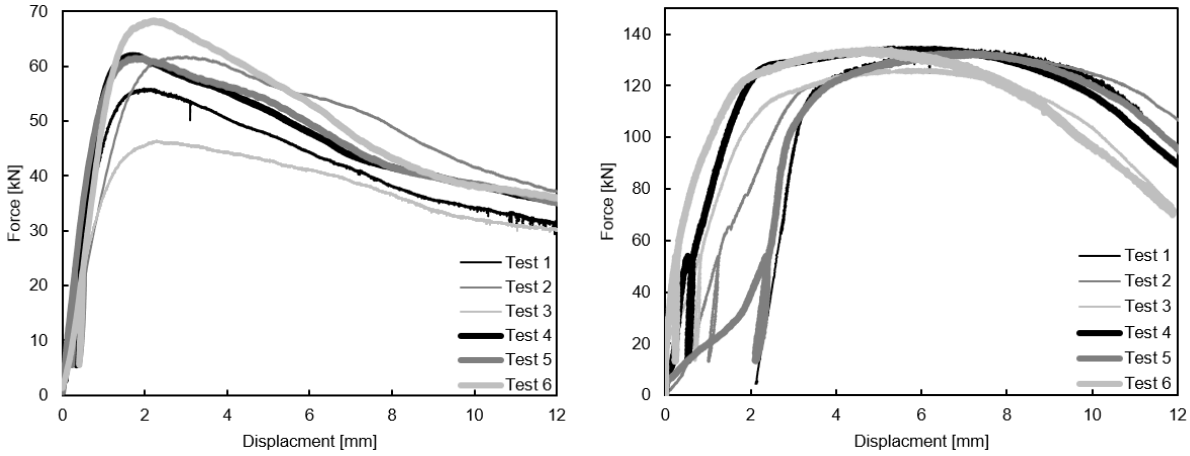

Fig. 2.12. Measured force-slip behavior of the shear connectors in the direct shear tests for the (a) CLT- and (b) NLT-concrete composite test specimens

A total of four LDVTs measured horizontal and vertical out-of-plane movement of the specimens. For the CLT-concrete composite specimen, the maximum vertical out-of-plane movement ranged from 0.406 to 4.45 mm (0.016 to 0.175 inches) and the maximum horizontal out-of-plane movement ranged from 0.127 to 1.40 mm (0.005 to 0.055 inches). For the NLT-concrete composite specimen, the maximum vertical out-of-plane movement ranged from 0.762 to 2.03 mm (0.030 to 0.080 inches) and the maximum horizontal out-of-plane movement ranged from 0.254 to 2.29 mm (0.01 to 0.09 inches). These movements were small enough to be considered negligible.

The fully-threaded screws had a higher initial stiffness than the truss plates. In addition, the post-peak behavior of the truss plates showed a faster decline of capacity than the fully-threaded screws. During the test, the author noticed that the laminations of NLT were not fully aligned in a single plane. This misalignment could contribute to the behavior of the specimens seen in Figure 2.12b. There is a larger difference in the plot of the initial loading ($0 – 0.4F_{est}$) and the loading to post-peak behavior ($0.1F_{est}$ onward) in the NLT-concrete composite specimens, which could be attributed to the misalignment of the laminations.

Observations

The shear connectors were examined after the test to provide additional insight into the behavior. Figure 2.13 shows two of the fully-threaded screws that were embedded into the CLT. These fully-threaded screws showed slight bending (Figure 2.13). The truss plates (Figure 2.14) showed significant damage at the NLT-concrete interface, including fracture of portions of the truss plate (Figures 2.14b and

14c). This damage can be indicative of yielding of the truss plate during the test. In both specimens, the author loaded to $0.5F_{est}$ in the post-peak region without any audible or visible failure of the specimens. Additional cracking of the concrete did occur throughout loading, particularly parallel with the shear connectors.

(a)

(b)

(c)

Fig. 2.13. Fully-threaded screw used in the CLT-concrete composite direct shear test (a) full view of the shear connector, (b) zoomed detail of the shear connector interface with concrete, and (c) zoomed detail of timber where the fully-threaded screw was embedded

(a)

(b) (c)

Fig. 2.14. Truss plates used in NLT-concrete composite direct shear test (a) full view of shear connector (b) zoomed detail of left-hand side, and (c) zoomed detail of the right-hand side

Large-scale fire tests

Observations

The floors were observed throughout the test through four cameras mounted in the laboratory, two of which provided visibility of the bottom of the floors in the furnace. After approximately 52 minutes into the test, the CLT-concrete composite floor began to have timber separate and fall into the furnace. Small pieces continued to fall intermittently until 92 minutes when larger pieces of the CLT

began to separate and fall into the furnace. This behavior is indicative of delamination. The deflection rate of the CLT-concrete composite floor began to rapidly increase at 105 minutes, at which time the load was removed from the floor. The furnace test continued for both specimens, but with only the NLT-concrete composite floor loaded. At 187 minutes, the CLT-concrete composite floor lost load-carrying capacity and failed in flexure. The load was removed from the NLT-concrete composite floor (which had not lost load-carrying capacity), the test was stopped, and the floors were removed from the furnace. The remaining ignited timber was extinguished with water. At no point throughout the tests was fire observed to penetrate through the floors.

Temperature data and char rate

The average experimental temperature distribution through each of the floors is plotted in Figure 2.15. The temperature of the concrete for both floors, on average, remained below 72°C. The maximum average temperature at the CLT-concrete interface was 59°C at 187 minutes, the end of the test. The maximum average temperature at the NLT-concrete interface was 78°C at 187 minutes. At temperatures below 100°C, concrete retains ambient temperature material properties in compression and tension (CEN 2004c).

The temperature measurements for the CLT-concrete composite floor, shown in Figure 2.15a, have sharp rises in temperature, particularly for temperatures associated with the timber. The CLT delaminated throughout the test, which will result in an increased char rate. Temperature measurements for the NLT-concrete composite floor shown in Figure 2.15b, do not show these sharp rises in temperatures, and the NLT did not exhibit signs of delamination.

The char rates were calculated by monitoring the 300°C isotherm. Using the thermocouple measurements and the temperature of the char isotherm, the author calculated the time-dependent location of the char isotherm throughout the experiment assuming the temperature variation between the locations of the thermocouples was linear. The resulting computed char rates from the experimental tests are shown in Table 2.6 for both floors. These char rates are specific to the thermocouple locations. The calculated char rates are smaller than the prescribed char rates. The difference between calculated and prescribed char rates is attributed to prescribed char rates including a 20% increase in char rate (AWC 2018) or a zero-strength layer (CEN 2004b; CSA Group 2016) to account for timber that has experienced pyrolysis, but has not yet charred. The char rates from Eurocode 5, the ANSI/AWC *National Design Specification for Wood Construction* (NDS), and the Canadian Standard CSA 086-14 (CSA 086) for timber without concrete or shear connectors are shown in Table 2.7 (CEN 2004b; AWC 2018; CSA Group 2016).

Standards for the performance of CLT adhesives at elevated temperatures were not included in ANSI/APA PRG 320 until 2018. To account for the potential of adhesive failure during a fire event, NDS and CSA 086 include an increased char rate for CLT consistent with delamination. The calculated char rate from the experimental data is comparable to the code prescribed values, which suggests that the concrete and the shear connectors of the TCC floor do not influence the char rate of the floor during a standard fire (ASTM 2018). This conclusion is consistent with Dagenais et al. (2016).

Measurements and observations of the floors were taken after the experiments. Four of the five laminations of the CLT were charred entirely during the test. The average remaining uncharred depth was 25 mm (1 inch) and 38 mm (1.5 inches) for the CLT- and NLT-concrete composite floors, respectively.

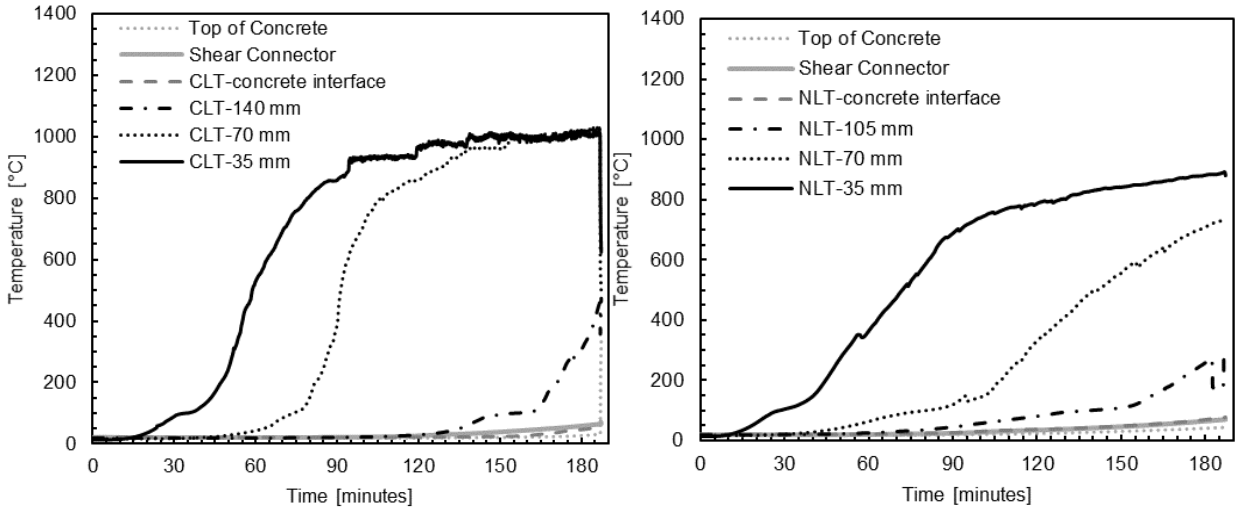

(a) (b)

Fig. 2.15. Average experimental temperature data for the (a) CLT- and (b) NLT-concrete composite floor

Table 2.6. Calculated char rates from experimentally measured temperatures

Location, mm (inches)	**Char rate, mm/min (inches/hr)**	
	CLT	NLT
35 (1.38)	0.66 (1.55)	0.68 (1.60)
70 (2.75)	0.80 (1.89)	0.57 (1.36)
105 (4.13)	NA	0.63 (1.50)
140 (5.50)	0.80 (1.90)	NA

Table 2.7. Code prescribed char rates (AWC 2018; CEN 2004b; CSA Group 2016)

Code	**Char rate, mm/min (inches/hr)**		
	CLT specific	Structural composite lumber	Timber
NDS	0.80 (1.90)	0.76 (1.80)	0.76 (1.80)
Eurocode 5	NA	0.70 (1.65)	0.80 (1.90)
CSA 086	0.80 (1.90)	0.70 (1.65)	0.80 (1.90)

Timber-concrete composite floor analytical model

General methodology

The flexural capacity of the TCC floors throughout the fire can be calculated with minor adjustments to the elasto-plastic model combined with the RCSM (Frangi and Fontana 2003; CEN 2004b). In the proposed methodology, the instant at which the capacity exceeds the flexural demands is defined as failure time.

The elasto-plastic model is an analytical model to calculate the stress distribution through a TCC cross-section joined with a ductile dowel-type fastener shear connector (Frangi and Fontana 2003). The model was initially developed for TCC beams and benchmarked against experimental tests. The initial assumptions of the elasto-plastic model are that: (1) the timber is subjected to combined tension and bending resulting in brittle behavior and therefore a linear elastic material behavior is assumed, (2) the timber portion of the TCC floor fails before the concrete exhibits plastic behavior, therefore, a linear-elastic model for concrete is used, (3) the concrete in tension is neglected, (4) in a fully-composite section, the connection between the timber and the concrete is rigid, and (5) the load-slip behavior of the shear connectors are rigid-perfectly plastic. The RCSM is defined in Eurocode 5 (CEN 2004b) for timber members assuming the mechanical properties of the uncharred timber remains constant throughout the fire, and the section size is reduced by the depth of char and the charred section is assigned zero-strength (e.g., Wiesner et al. 2017).

The proposed methodology, described in this section, can be used to estimate the capacity of a TCC floor as a function of time exposed to a fire and also the failure time of the TCC floor. The method is based on the elasto-plastic model and the RCSM, but modified to account for the additional timber width in a continuous floor as opposed to the discrete timber elements in a TCC beam, and to account for truss plate-type shear connectors.

The first modification pertains to the calculation of the depth of the neutral axis. The depth of the neutral axis is computed by equating the full elastic section modulus of the concrete and timber about the composite neutral axis. Note that in Figure 2.16 the stress diagrams are assumed equivalent stress diagrams over the CLT section, although it is expected that the true stress diagram would include relatively small stresses in the cross CLT plies, the second and fourth plies in Figure 2.16.

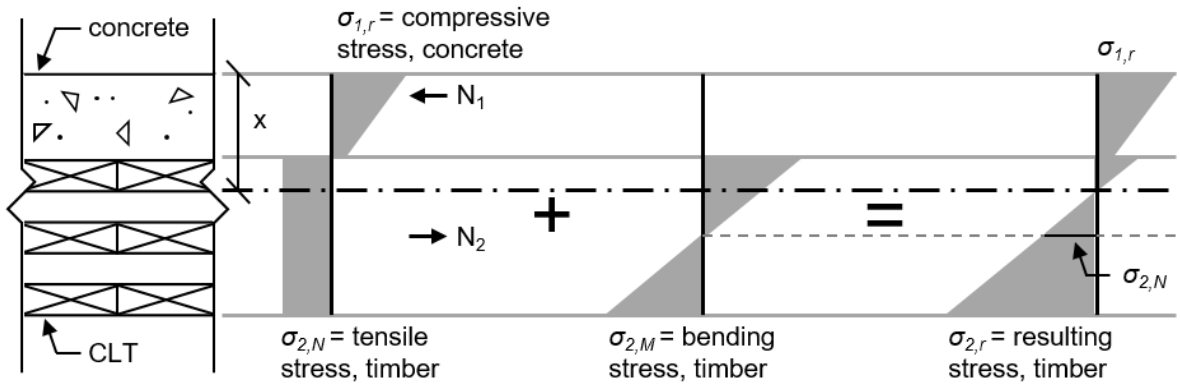

Fig. 2.16. Assumed stress field for the ultimate limit state of a fully-composite CLT-concrete composite floor based on fundamental principles of mechanics of materials. Stress field drawn assuming the neutral axis depth *x* is in the timber

The second adaptation pertains to the use of shear connectors that are not ductile dowel-type fastener shear connectors. In the case of the NLT-concrete composite floor, typical shear connectors may be in the form of truss plates. As shown above, the truss plates yield at the timber-concrete interface and potentially show signs of fracture at capacity, compared with ductile bending of the screws in a CLT-concrete composite floor. Therefore, the elasto-plastic model is modified to include the truss plates as tensile reinforcement of the timber. The stress field for the ultimate limit state of a fully composite NLT-concrete composite floor, as adapted from Frangi and Fontana (2003), is shown in Figure 2.17 with contribution from the steel truss plates. Similar to the CLT-concrete composite floor, the neutral axis is calculated by equating the elastic section modulus of the concrete in compression to that of the timber and truss plates.

Using the stress diagram in Figure 2.17a, assuming the truss plates resist the shear transfer uniformly along the length of the floor, and that the truss plates are yielding, the flexural capacity of the NLT-concrete composite floor is given by Equation 2.1.

$$M_{R,full} = A_2\sigma_{2,N}\left(\frac{h_2}{2} + h_1 - \frac{x}{3}\right) + f_y b_3 h_3 n_3\left(\frac{h_3}{2} + h_1 - \frac{x}{3}\right) + \sigma_{2,M}\frac{bh_2^{\,2}}{6} \tag{2.1}$$

Where x is the location of the neutral axis from the top of the concrete, $\sigma_{i,N}$ is the normal stress, $\sigma_{i,M}$ is the bending stress, A_i is the area of the sub-components, b is the width of the floor section, n_i is the ratio of mechanical stiffness of each subcomponent to that of the timber, and h_i is the height of the subcomponents with 1, 2, and 3, indicating concrete, timber, and connector, respectively. Note that, in Equation 2.1, the moment equilibrium was set about the location of the resultant N_1.

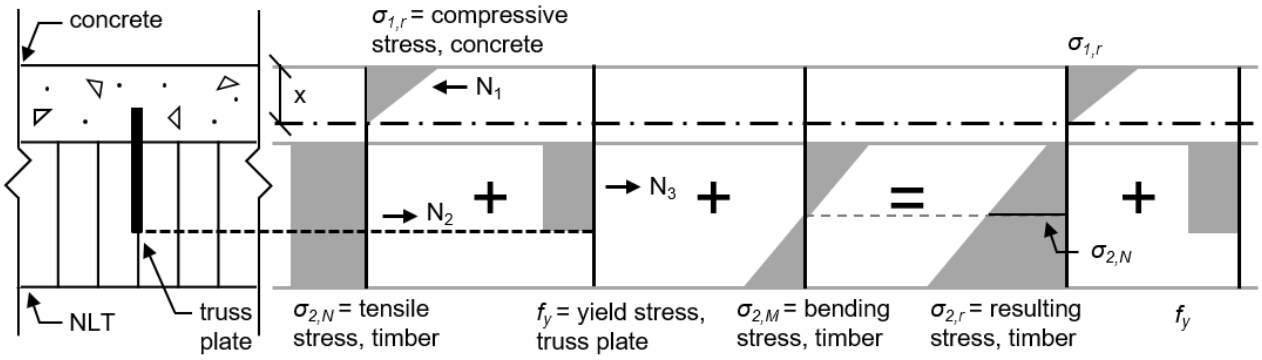

(a)

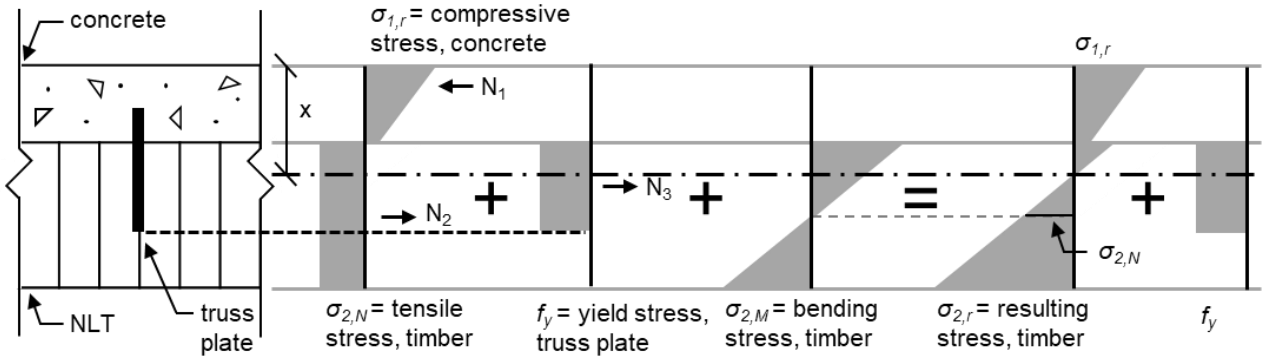

(b)

Fig. 2.17. Assumed stress field for the ultimate limit state of a fully composite NLT-concrete composite floor based on fundamental principles of mechanics of materials. Stress field drawn assuming the neutral axis depth x is in the (a) concrete and (b) timber

Application to large-scale fire tests

The flexural capacity of the tested TCC floors was calculated using the proposed methodology. The dotted lines in Figure 2.18 represent the flexural demands throughout the tests.

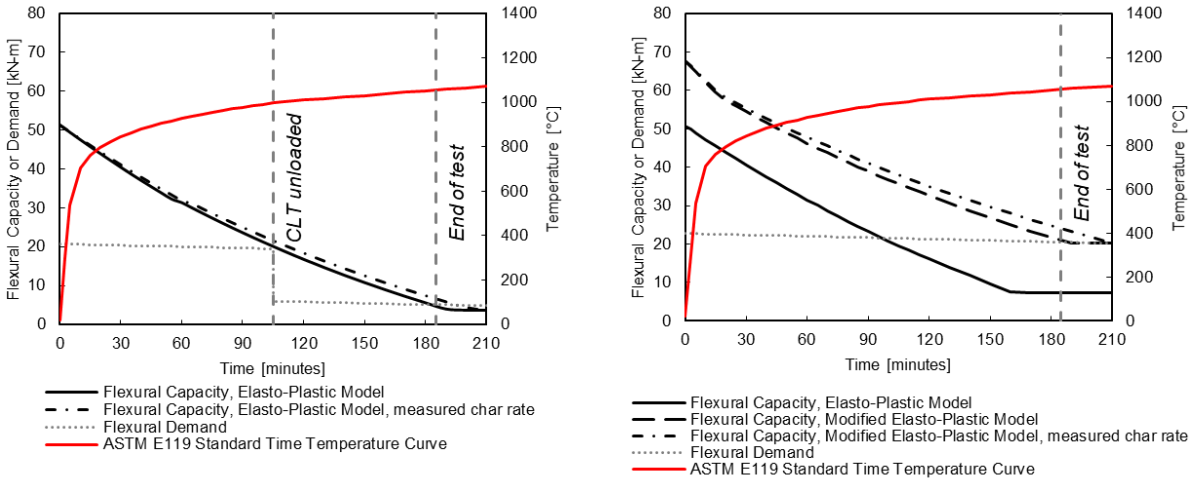

(a) (b)

Fig. 2.18. Flexural capacity of the tested TCC floors as a function of temperature computed using the elasto-plastic model with the RCSM (Frangi and Fontana 2003; CEN 2004b) (a) flexural capacity and imposed flexural demand of the CLT-concrete composite floor and (b) flexural capacity and imposed flexural demand of the NLT-concrete composite floor using the original and modified elasto-plastic model

From Figure 2.18a, it can be seen that the elasto-plastic model results align well with the experimental observations of the CLT-concrete composite floor at both the instant when the CLT panel was unloaded and at the end of test. The results of the elasto-plastic model show the reduction in flexural capacity over time due to the charring of the CLT. The black solid line denotes the calculated flexural capacity using the char rate prescribed for CLT of 0.80 mm/min (1.90 inches/hr), which accounts for delamination (AWC 2018; CSA Group 2016), while the dot dashed line denotes the calculated flexural capacity using the average experimentally measured char rate of 0.75 mm/min (1.78 inches/hr). At 105 minutes, the deflection rate of the CLT-concrete composite floor increased, indicating the floor was approaching failure (loss of load-carrying capacity). At this time, the calculated flexural capacity of the floor is 20.0 kN-m (14.8 kip-ft), which is +2.9% difference from the demand. At 105 minutes, the live load was removed from the CLT-concrete composite floor. The removal of the load is reflected in the reduction of the flexural demand on the floor. At 187 minutes of the experiment, the CLT-concrete composite floor failed in flexure in the concrete. At the time of failure, the average depth of uncharred timber was 25 mm (1 inch). The calculated failure time shown in Figure 2.18a is 190 minutes (+1.6% difference from the experimental observation).

Figure 2.18b shows the results of the flexural demand and capacity predictions using the original elasto-plastic model developed for dowel-type fasteners and the proposed modified elasto-plastic model as described in the previous section. In these calculations, the timber depth was reduced by a char rate

prescribed for structural composite lumber of 0.70 mm/min (1.65 inches/hr) (CEN 2004b; CSA Group 2016). Results indicate that the original elasto-plastic model does not compare well with the experimental observations (black solid line, Figure 2.18b). During the testing, the NLT-concrete composite floor was observed to begin to fail at about 187 minutes. The predicted time of failure shown in Figure 2.18b is 100 minutes (-47% difference from experimental observation). In contrast, results of the modified elasto-plastic model using the prescriptive char rate (dashed line, Figure 2.18b) show a predicted time of failure of 190 minutes (+1.6% difference from experimental observation). The modified elasto-plastic model using the average measured char rate of 0.63 mm/min (1.49 inches/hr) (dot dashed line, Figure 2.18b) shows a predicted time of failure of 210 minutes (+12% difference from the experimental observation). These two results correspond to a significant improvement and provide confidence in the use of this model for predicting failure times for NLT-concrete composite floor assemblies using both experimentally measured char rates and those prescribed through building codes and standards (AWC 2018; CEN 2004b; CSA Group 2016).

Application to Dagenais et al. (2016) SLT-concrete composite floor

To further investigate the flexural capacity of TCC floors using truss plate shear connectors, the experimental observations from Dagenais et al. (2016) large-scale floor tests were used to benchmark the developed analytical model to predict the flexural capacity of TCC floors throughout a fire. Dagenais et al. (2016) tested three configurations of TCC floors, this section focuses on the SLT-concrete composite floor.

The SLT-concrete composite floor was constructed from 38 mm x 184 mm (1.5 inches x 7.25 inches) solid sawn Grade No. 2 SPF. The screws joining the timber laminations were self-tapping 180 mm (7 inches) in length. The lamination screw pattern was two rows of nails spaced 610 mm (24 inches) staggered by 305 mm (12 inches) inclined at a 45° angle. The concrete was 89 mm (3.5 inches) in depth with a design compressive strength of 30 MPa (4.4 ksi) at 28 days and steel mesh for shrinkage reinforcement. The floor was 1715 mm (67.5 inches) wide and 4800 mm (189 inches) in length. MiTek MT20 truss plates were used as shear connectors between the timber and concrete to develop composite action. These are the same truss plates used in the NLT-concrete composite floors described in this chapter. As such, the measured maximum force for the truss plates from the direct shear tests will be used to model the SLT-concrete composite floor. The truss plates were embedded in the timber by a hydraulic press every fifth lamination and spaced 610 mm (24 inches) on center. 76.2 mm (3 inches) of the truss plate depth was embedded in the timber, while the remainder was embedded in the concrete topping. The edge distance of the truss plates in the longitudinal direction is 38 mm (1.5 inches).

The SLT-concrete composite floor was exposed to the CAN/ULC-S101 fire curve (similar exposure to the ASTM E119 standard fire), and loaded with a distributed service live load of 2.4 kPa (50 psf). Testing stopped at 214 minutes and the SLT-concrete composite floor did not reach failure at the end of the test.

The flexural capacity of the tested Dagenais et al. (2016) SLT-concrete composite floor was calculated using the elasto-plastic model and the modified elasto-plastic model (Equation 2.1) with the RCSM shown in Figure 2.19.

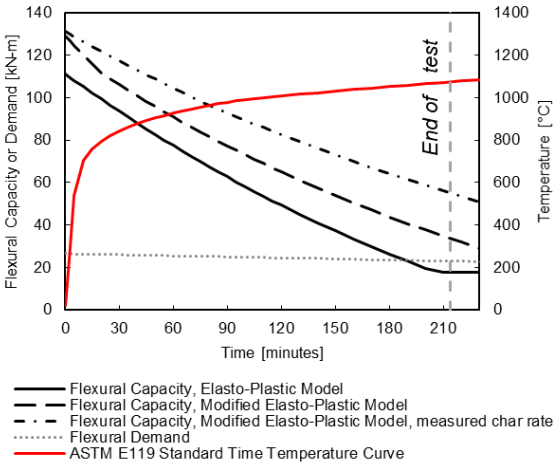

Fig. 2.19. Flexural capacity and imposed flexural demand of the SLT-concrete composite floor (Dagenais et al, 2016) using the original and modified elasto-plastic model with the RCSM (Frangi and Fontana 2003; CEN 2004b)

Figure 2.19 shows the results of the flexural demand and capacity predictions using the original elasto-plastic model developed for dowel-type fasteners and the proposed modified elasto-plastic model as described in the previous section. In these calculations, the timber depth was reduced by a char rate prescribed for structural composite lumber of 0.70 mm/min (1.65 inches/hr) (CEN 2004b; CSA Group 2016). Results indicate that the original elasto-plastic model (black solid line, Figure 2.19) does not compare well with the experimental observations. During the testing, the SLT-concrete composite floor did not reach failure by the end of test (214 minutes), therefore, the flexural demand did not exceed the flexural capacity throughout the test. The predicted time of failure shown in Figure 2.19 using the original elasto-plastic model is 190 minutes (24 minutes before the end of test). In contrast, results of the modified elasto-plastic model, using the prescriptive char rate, (long dashed line, Figure 2.19) never reaches failure (demand never intersects with capacity). The modified elasto-plastic model, using the average measured char rate (Dagenais et al. 2016) of 0.63 mm/min (1.49 inches/hr) (dot dashed line, Figure 2.19) never reaches failure (demand never intersects with capacity). These two results align with the experimental

observation of the SLT-concrete composite not reaching failure by the end of the test. These results correspond to an improvement and provide confidence in the use of this model for predicting failure times for TCC floors using truss plate shear connectors.

Proposed methodology comparison to state-of-the-practice

The design guidance North American engineers have for TCC floors both at ambient temperature and during a fire is the *Design Guide for Timber-Concrete Composite Floors in Canada* (Cuerrier-Auclair 2020) newly published by FPInnovations. This design guide provides methods for calculating the flexural capacity of the floors and the instantaneous deflections (which will be explored in Chapter 3).

Cuerrier-Auclair (2020) evaluates the flexural resistance of TCC floors by using the minimum result from two analytical models: (1) the elasto-plastic model and (2) γ-method. The elasto-plastic model, previously discussed in detail (*General methodology; Application to large-scale fire tests*), is based on equilibrium of force and beam theory, and assumes all shear connectors have yielded (Frangi and Fontana 2003). The γ-method was developed to estimate the effective bending stiffness of a composite beam from Euler-Bernoulli beam deflection equation and the following assumptions: (1) each layer is based on the Euler-Bernoulli beam theory, (2) each layer has the same deflection, rotation, and curvature, and (3) distributed shear stiffness is assumed between the two layers along the composite beam. The γ-method determines bending moment resistance to be that of the first subcomponent to reach its ultimate resistance and assumes the shear connectors do not yield (Cuerrier-Auclair 2020). The γ-method as a method to calculate deflection is discussed in detail in Chapter 3.

The comparison between the flexural capacity of the tested TCC floors calculated using the elasto-plastic model and the modified elasto-plastic model and the Cuerrier-Auclair (2020) methodology is shown in Figure 2.20. This comparison highlights that the Cuerrier-Auclair (2020) flexural capacity methodology is also developed for and applicable to dowel-type fasteners.

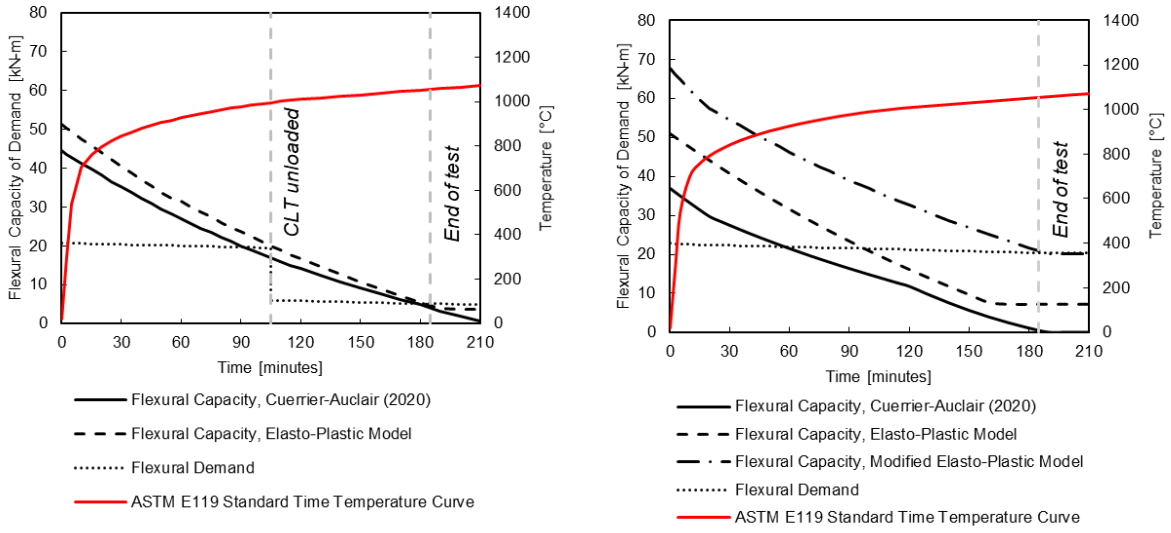

(a) (b)

Fig. 2.20. Flexural capacity of the tested TCC floors as a function of temperature computed using the Cuerrier-Auclair (2020) method and the elasto-plastic model with the RCSM (Cuerrier-Auclair 2020; Frangi and Fontana 2003; CEN 2004b) (a) flexural capacity and flexural demand of the CLT-concrete composite floor and (b) flexural capacity and flexural demand of the NLT-concrete composite floor using the original and modified elasto-plastic model

From Figure 2.20a, it can be seen that the Cuerrier-Auclair (2020) method results (black solid line) align well with the elasto-plastic model results (dashed line) for the CLT-concrete composite floor. For both calculations, the timber depth reduced by a char rate prescribed for CLT of 0.80 mm/min (1.90 inches/hr), which accounts for delamination (AWC 2018; CSA Group 2016). In particular, the Cuerrier-Auclair (2020) method aligns with the elasto-plastic model (and thus the experimental data) for the following: (1) the results show the reduction in flexural capacity over time due to the charring of the CLT, (2) results show alignment with the experimental observations at the instant when the CLT panel was unloaded (105 minutes), and (3) results show alignment with the experimental observations at the end of the test (187 minutes). The Cuerrier-Auclair (2020) method calculated the failure time as 95 minutes (-49% difference from the experimental observation). At 105 minutes, the Cuerrier-Auclair (2020) method calculated flexural capacity of the floor as 16.9 kN-m (12.4 kip-ft), which is -13% difference from the demand compared to +2.9% for the elasto-plastic model. At 187 minutes of the experiment, the CLT-concrete composite floor failed in flexure. The elasto-plastic model calculated the failure time as 190 minutes (+1.6% difference from the experimental observation). The Cuerrier-Auclair (2020) method is more conservative than the elasto-plastic model, under-estimating the time of failure, but both models calculate comparable flexural capacities throughout the standard fire.

The difference in the calculated flexural capacity of the TCC floors using the two models (Cuerrier-Auclair 2020; Frangi and Fontana 2003) is greatest at lower temperatures and decreases throughout the fire. This is due to Cuerrier-Auclair (2020) considering both the case where the full force-slip behavior of the shear connectors is considered (γ-method), and when the shear connectors are considered elastically-perfectly plastic (elasto-plastic model). The two models become increasingly similar throughout the fire as the Cuerrier-Auclair (2020) flexural capacity transitions from being limited by the γ-method to being limited by the elasto-plastic model. In addition, the author modified the elasto-plastic model to account for the additional timber width in a continuous floor and truss plate-type shear connectors. These modifications were not applied to the Cuerrier-Auclair (2020) method. If these modifications were applied to the Cuerrier-Auclair (2020) the two models would produce results that are more comparable. The results indicate either the Cuerrier-Auclair (2020) method or the elasto-plastic model can be used to estimate the flexural capacity of a CLT-concrete composite floor using dowel-type shear connectors during a standard fire (ASTM 2018), but only the elasto-plastic model can estimate failure time.

Figure 2.20b shows the results of the flexural demand and capacity predictions using the Cuerrier-Auclair (2020) method, the original elasto-plastic model developed for dowel-type fasteners and the modified elasto-plastic model as described in the previous section. In these calculations, the timber depth was reduced by a char rate prescribed for structural composite lumber of 0.70 mm/min (1.65 inches/hr) (CEN 2004b; CSA Group 2016). From Figure 2.20b, it can be seen that the Cuerrier-Auclair (2020) method results (black solid line) aligns well with the original elasto-plastic model results (dashed line) for the NLT-concrete composite floor and both models do not compare well with the experimental observations. During the testing, the NLT-concrete composite floor was observed to begin to fail at about 187 minutes. The predicted time of failure shown in Figure 2.20b is 60 minutes (-68% difference from experimental observation) and 100 minutes (-47% difference from experimental observation) for the Cuerrier-Auclair (2020) method and the original elasto-plastic model, respectively. In contrast, results of the modified elasto-plastic model (dashed line, Figure 2.20b) show a predicted time of failure of 190 minutes (+1.6% difference from experimental observation). These two results indicate neither the Cuerrier-Auclair (2020) method nor the original elasto-plastic model can be used to reasonably estimate the failure times of NLT-concrete composite floors using truss plate-type shear connectors during a standard fire (ASTM 2018). For this scenario, the modified elasto-plastic model corresponds to the experimental results and can be used to predict failure times for NLT-concrete composite floors using truss plate-type shear connectors.

Summary and conclusions

Two sets of experiments were performed to quantify the behavior of TCC floors and shear connectors that are used in both CLT- and NLT-concrete composite floors. Direct shear tests were performed on six CLT-concrete composite specimens with fully-threaded timber screws and six NLT-concrete composite specimens with truss plate shear connectors to quantify the force-slip behavior of these connectors (Table 2.4, Table 2.5). The results from these experimental tests include shear capacities of the connectors that can be used in analytical models, and force-slip behavior that can be used in finite element modeling. Structural fire tests were performed in a gas-fire furnace on large-scale TCC floors, one CLT- and one NLT-concrete composite floor. These tests demonstrated that the presence of shear connectors and a concrete topping have a negligible impact on the char rate of timber. The char rates prescribed in the NDS, Eurocode 5, and CSA 086 (AWC 2018; CEN 2004b; CSA Group 2016) for timber-only are comparable to the experimental char rates calculated for the TCC floors (Table 2.6, Table 2.7). The concrete remained near ambient temperature throughout the furnace test (Figure 2.15).

The flexural load-carrying capacity of the large-scale floor tests were calculated using the elasto-plastic model with modifications (Frangi and Fontana 2003) and RCSM (CEN 2004b). The flexural load-carrying capacity of the CLT-concrete composite floor during the fire test was reasonably estimated using the elasto-plastic model (Figure 2.18a). A modified elasto-plastic model accounting for the tensile capacity provided by the truss plate shear connectors was developed and showed to reasonably predict the NLT-concrete composite floor flexural capacity during the fire tests (Figure 2.18b). These results were further benchmarked by applying the proposed methodology to the SLT-concrete composite floor tests performed by Dagenais et al. (2016). Finally, the proposed methodology was compared to the Cuerrier-Auclair (2020) method to calculate flexural capacity. Similar to the original elasto-plastic model, the flexural load-carrying capacity of the CLT-concrete composite floor during the fire test was reasonably estimated, but the Cuerrier-Auclair (2020) method is unable to predict the failure time of the NLT-concrete composite floor (Figure 2.20).

CHAPTER 3: DEFLECTION OF TIMBER-CONCRETE COMPOSITE FLOORS IN FIRE

Introduction and motivation

Background

Analytical models are essential for the development of design methodologies. Without the ability to evaluate the capacity and behavior of structural members and frames, engineers are left using complex finite element method (FEM) models to simulate the performance of structures under gravity or extreme loads (e.g. seismic, fire). Engineers must be able to calculate both the strength and serviceability behavior of structural components.

The International Building Code (IBC) (ICC 2018) defines a condition beyond which a structure or member becomes unfit for service as a limit state. There are two types of limit states: (1) serviceability where a structure or member is judged to be no longer useful for its intended function and (2) strength where a structure or member has become unsafe (ICC 2018). Both serviceability and ultimate limit states need to be accounted for when developing design methodologies (Dias et al. 2016). The previous chapter discussed the evaluation of the structural resistance and fire integrity of timber-concrete composite (TCC) floors when exposed to fire through experimental shear and fire testing and the evaluation of TCC floors through the analytical modeling of the flexural capacity. To complete a thorough evaluation of TCC floors, this chapter examines the stiffness of TCC floors using the experimental data presented in the previous chapter and analytical modeling of the deflection.

Serviceability limit states for structural components ensure functionality of the structure. Limits on deflection are typically controlled by limiting deflection to limit damage to nonstructural components such as partition walls, finishes, and equipment. While the design of TCC floors in a fire will be controlled by strength (Chapter 2), for engineers to design mass timber buildings for functional recovery, calculating the deflections of the floors throughout a fire can inform whether the building is occupiable and functional after a fire, or will require remediation.

TCC floors have many advantages as compared to timber-only floors (Barbosa et al. 2018; Boccadoro and Frangi 2013; Deam et al. 2007; Dias et al. 2016; Lukaszewska et al. 2008; Yeoh et al. 2011a). This chapter will use experimental testing data from the large-scale fire tests presented in Chapter 2, and tests

performed by Dagenais et al. (2016) to benchmark analytical models for the prediction of the deflection of floors throughout a standard fire exposure (ASTM 2018).

Previous research on TCC floors

Researchers have used complex FEM models to simulate the stiffness of TCC floors thereby predicting the deflections of the floors throughout a fire (Caldova et al. 2015; Dagenais et al. 2016; O'Neill et al. 2014). These models require significant resources (time, computational knowledge, computing power, and financial) to execute. Therefore, while complex FEM models can provide significant insight into the behavior of structural components, they are not particularly applicable to design practice. Analytical models are an efficient and cost-effective substitute for experimental tests and numerical modeling. For TCC floors this means calculating the effective stiffness of the composite section considering the contributions of the timber, concrete, and the shear connectors.

Analytical models for calculating the effective stiffness of TCC beams and floors

The primary method to calculate the effective stiffness of TCC floors at ambient temperatures is the γ-method. The γ-method is a closed-form solution used to estimate the effective bending stiffness of a mechanically jointed composite beam with flexible elastic connections (Möhler 1956). More recently, the γ-method has been incorporated into Eurocode 5 (CEN 2004a) for calculating the effective stiffness of two timber elements connected with mechanical fasteners. The γ-method has been adapted for TCC beams (Girhammar 2009) and several researchers have demonstrated the ability of the γ-method to simulate the effective stiffness of TCC beams throughout a fire exposure (Frangi et al. 2010; O'Neill et al. 2011; Yeoh et al. 2011a). However, these researchers did not compare the γ-method to mass timber panel concrete composite floor (e.g. cross-laminated timber (CLT) or nail-laminated timber (NLT)). The γ-method has only been benchmarked against glulam-concrete and laminated-veneer lumber (LVL) concrete composite floors.

Girhammar (2009) generalized the Eurocode 5 method for analyzing and designing composite beams to account for varying boundary and loading conditions. The proposed model, which accounts for interlayer slip, calculates an effective stiffness of a TCC horizontal member (floor, beam) and is applicable to members with both partial and full composite action. Girhammar (2009) applied the developed model to several composite beam configurations (both timber-concrete and timber-timber) and the results were compared to the Eurocode 5 method and the exact solution. The proposed model produced smaller errors than the γ-method in Eurocode 5 when compared to the exact solution. However,

the proposed model is not benchmarked against experimental data, is developed for TCC beams rather than floors, and was not developed or benchmarked for fire exposure.

Frangi et al. (2010) performed large-scale fire tests on TCC beams to determine the fire behavior of self-drilling screws inclined at 45° used as a shear connector in TCC floors. Small-scale tests were performed to determine the loss of stiffness and strength of the self-drilling screws throughout a fire exposure. Full-scale fire tests were performed on TCC floors consisting of glulam beams and a concrete topping to investigate the impact the loss of stiffness and strength of the shear connectors has on the behavior of the floor. The γ-method and reduced cross-section method (RCSM) were used to calculate the deflections of the floors throughout the fire exposure. Modification factors were developed and applied to the γ-method and the RCSM to account for the loss of stiffness and strength of the timber, concrete, and shear connectors as a function of temperature. The calculated deflection was slightly smaller than the experimental deflection values measured during the full-scale fire tests. This research provides valuable information on the application of the γ-method and the RCSM to determine the deflection of glulam beam-concrete composite floors. However, this model has not been applied to mass timber panel concrete composite floors, particularly using US construction practices and varying shear connector types.

Yeoh et al. (2011a) demonstrated the applicability of the γ-method to LVL-concrete composite floors. Eleven short-term collapse tests were performed on 8 m x 10 m (26 ft x 33 ft) LVL-concrete composite floors. Shear connectors used included triangular and rectangular timber notches reinforced with a coach screw and a truss plate with perforated holes embedded in the concrete. Yeoh et al. (2011a) showed that the γ-method could reasonably predict the short-term deflection of the tested floors. This research demonstrated the capability of the γ-method to LVL-concrete composite floors; however, these tests were performed at ambient temperature.

State-of-the-practice

Several researchers have developed design guidelines for TCC floors at ambient temperature (Crews et al. 2010; Ceccotti 1995; SOM 2017). Ceccotti (1995) created a design procedure for timber beams composite with concrete toppings where the effective bending stiffness of the cross-section is calculated per the γ-method. Crews et al. (2010) developed a preliminary design method for TCC floors based upon Eurocode 5 design procedures (CEN 2004a), which are recommended for use in New Zealand and Australia. The objective was to promote the use of TCC floors and other timber framing systems in non-residential buildings in Australia and New Zealand. While these design procedures are useful for ambient

temperature and for TCC floors with timber beams, these design guidelines have not been benchmarked against mass timber panel concrete composite floors or TCC floors in fires.

SOM (2017) adapted the γ-method for the specific case of CLT-concrete composite floors. A conservative assumption was made to neglect the shear stiffness of the concrete due to the potential for shrinkage cracks or negative bending tensile cracks. The method was applied to the TCC floors tested by Higgins et al. (2017) and was found to give reasonable predictions for the floor deflection behavior. This design guide has not been benchmarked against TCC floors with other mass timber panels or for TCC floors exposed to fire.

More recently, a TCC floor design guide was published (Cuerrier-Auclair 2020) applying the γ-method in general terms to TCC floors. This design guide is mainly focused on the strength and stiffness of TCC floors at ambient temperatures; however, has a chapter devoted to the fire behavior of TCC floors and worked examples. This chapter will utilize the γ-method presented in Cuerrier-Auclair (2020) to demonstrate the ability of this design guide to predict the effective stiffness of a variety of TCC floors throughout a fire.

Chapter objectives

The objective of this chapter is to benchmark an analytical approach to predict the deflection of TCC floors throughout a fire. Mass timber panel type, concrete thickness, and shear connector type will be varied to demonstrate the wide applicability of the γ-method coupled with the RCSM to predict the deflection of TCC floors throughout a standard fire exposure (ASTM 2018). In the previous chapter, the large-scale structural fire tests on two TCC floors in a gas-fire furnace were introduced. In this chapter, the experimental deflection data from those tests will be used to benchmark the γ-method (CEN 2004a). For further investigation, the model was benchmarked against large-scale TCC floor fire tests from existing literature. The results demonstrated that practicing engineers can predict deflection of TCC floors for fire scenarios using the γ-method coupled with the RCSM, therefore aiding practicing engineers in employing structural fire engineering on mass timber buildings.

In this chapter, the methodology for calculating the deflection of TCC floors in fire will be presented, a demonstration of the applicability of the γ-method will then be presented for CLT-, NLT-, and screw-laminated timber (SLT) concrete composite floors. The results of the calculations will be presented and compared with experimental data from literature (Dagenais et al. 2016) and from the large-scale tests described in Chapter 2.

Methodology for calculating deflection of TCC floors in fire

The deflection of TCC floors during a fire can be calculated using the γ-method and the RCSM (CEN 2004a; CEN 2004b). The proposed methodology, described in this section, uses the reduced timber height calculated with the RCSM in the γ-method to calculate the effective stiffness of a TCC floor as a function of time exposed to a fire. The deflection used in this chapter is the maximum vertical deflection at the center of a floor simply supported with a uniformly distributed load.

γ-method

Deflection of TCC floors can be determined by calculating the effective bending stiffness $(EI)_{eff}$ with the γ-method (Eq. 3.1). Per Eurocode 5, the initial assumptions of the γ-method are: (1) design method based on the theory of linear elasticity, (2) beams are simply supported with a span *l*, (3) individual parts span the full length *l* and are wood or wood-based panels, (4) the individual parts are joined by mechanical fasteners, (5) spacing between the fasteners is constant or varies per CEN 2004a, (6) applied load is acting in the z-direction (perpendicular to the span) giving a moment varying sinusoidally or parabolically (CEN2004a).

$$(EI)_{eff} = (EI)_1 + (EI)_2 + \gamma_1 (EA)_1 a_1^{\,2} + \gamma_2 (EA)_2 a_2^{\,2} \tag{3.1}$$

Where E_i is the elastic modulus, I_i is the moment of inertia, A_i is the area and a_i is the distance from the neutral axis of the subcomponent *i* to the neutral axis *x* of the section (Figure 3.1, Eq. 3.2, Eq. 3.3). Subscript *i* indicates the subcomponent where 1 and 2 indicate the concrete and timber respectively.

$$a_1 = \frac{\gamma_2 (EA)_2}{\gamma_1 (EA)_1 + \gamma_2 (EA)_2} r \tag{3.2}$$

$$a_2 = \frac{\gamma_1 (EA)_1}{\gamma_1 (EA)_1 + \gamma_2 (EA)_2} r \tag{3.3}$$

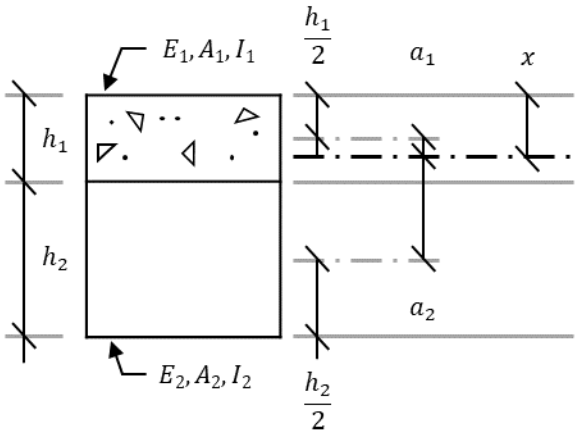

Fig. 3.1. Cross-section of TCC floor

In Eq. 3.1, γ_i is a unitless factor representing the composite action of the section (Eq. 3.4, Eq. 3.5). When $\gamma_2 = 0$ there is no composite action between the two subcomponents and the stiffness *K* (Eq. 3.6) of the shear connector is zero. When $\gamma_2 = 1$ there is full composite action between the two subcomponents.

$$\gamma_1 = 1 \tag{3.4}$$

$$\gamma_2 = \frac{1}{1 + \frac{\pi^2 (EA)_2}{KL^2}} \tag{3.5}$$

$$K = \frac{mk}{s} \tag{3.6}$$

Where *L* is the length of the floor, *m* is the number of shear connectors in the section width, *s* is the spacing of the shear connectors along the length of the floor, *k* is the slip modulus of one shear connector.

In addition to the initial assumptions adopted by Eurocode 5, this chapter assumes concrete in tension is not contributing to the stiffness of the section. Thus, the height of concrete should be reduced to only represent the height of concrete above the neutral axis *x* (Figure 3.2). This assumption is consistent with the design methodology presented in Cuerrier-Auclair (2020).

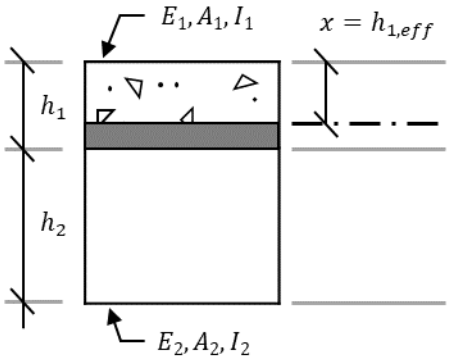

Fig. 3.2. Cross-section of TCC floor with concrete in tension indicated in grey

Therefore, when the neutral axis of the composite section is in the concrete, the effective depth of the concrete $h_{1,eff}$ is the distance to the plastic neutral axis as measured from the top of the concrete as calculated by Eq. 3.7.

$$h_{1,eff} = \sqrt{\alpha^2 + \alpha(h_2 + 2h_1)} - \alpha \tag{3.7}$$

$$\alpha = \frac{\gamma_2 (EA)_2}{\gamma_1 E_1 b_1} \tag{3.8}$$

Where b_1 is the width of the concrete and α is a term to simplify Eq. 3.7 (Cuerrier-Auclair 2020).

Slip modulus

To calculate the stiffness of the connection K (Eq. 3.7) the slip modulus of one shear connector k must be defined. The slip modulus can be calculated using data from direct shear tests, as was calculated in Chapter 2. However, experimental testing is costly and time consuming and experimental testing data is not always readily available. In order for the proposed methodology to be useful for design purposes of practicing engineers, non-experimentally calculated value of slip moduli must be available. A simplified design method for calculating the slip moduli of a variety of shear connector types is available in Eurocode 5 (CEN 2004a).

Eurocode 5 provides calculation methods for two slip moduli: (1) for the serviceability state K_{ser} and (2) for the ultimate limit state K_u. For dowel-type fasteners Eq. 3.9 can be used to determine serviceability slip modulus in N/mm.

$$K_{ser} = \rho_m^{1.5} \frac{d}{23} \tag{3.9}$$

Where d is the diameter of the fastener in mm and ρ_m is the density of the two jointed wood-based members in kg/m^3. For concrete-to-timber connections, ρ_m should be equal to the density of the timber member and K_{ser} may be multiplied by 2.0 (CEN 2004a). The methodology in this chapter considers the ultimate limit state, therefore, the slip modulus of a connection for the ultimate limit state can be calculated per Eq. 3.10.

$$K_u = \frac{2}{3} K_{ser} \tag{3.10}$$

Char rates of timber

During a fire, timber chars and experiences a reduction of mechanical properties. To account for the loss of height due to the formation of a char layer and the reduced stiffness and strength, the RCSM is used for analytical modeling of timber during a fire. The RCSM reduces the height of timber by a prescribed char rate. The newly formed char layer is assumed to have zero stiffness and strength. The remaining uncharred timber is assumed to retain ambient temperature mechanical properties. The deflection of a TCC floor throughout the duration of a fire can be calculated by using the RCSM with the γ-method. The RCSM is defined in Eurocode 5 (CEN 2004b) as are char rates for different types of timber. Char rates are also defined for timber in NDS (2018) and CSA 086 (CSA Group 2016). These prescribed char rates are tabulated in Chapter 2 (Table 2.7) and were shown to be applicable to TCC floors.

Experimentally measured char rates (Table 2.6) were calculated using data from the large-scale fire tests performed on the CLT- and NLT-concrete composite floors (Chapter 2). To benchmark the proposed methodology against the experimental tests from Chapter 2, both the prescribed char rates and the measured char rate are used in the proposed methodology.

Large-scale TCC floor fire tests

Large-scale fire tests were performed on one CLT- and one NLT-concrete composite floor at the National Research Council (NRC). The complete materials and methods for the design and testing of the two TCC floors, includes material grades and properties, instrumentation, and loading protocols, can be

found in Chapter 2. The information provided below consists of the specific information essential to the deflection of the floors throughout the standard fire exposure (ASTM 2018).

The CLT- and NLT-concrete composite floors were exposed to the ASTM E119 standard fire and loaded with a distributed service live load of 3.83 kPa (80 psf) (Figure 2.9b). The defined failure criterion for the test was structural failure. The floors were tested side-by-side, a testing configuration that requires the furnace to be shut off and the load removed when one of the floors collapses. To avoid a premature end of test for one floor due to the other collapsing, the deflection rates were monitored to be able to observe and remove the load from the floor approaching collapse, and allow the test to continue. Approaching collapse was defined as the point of rapid increase in deflection rate, per ASTM E119.

The temperature distribution along the length of the floor and through the cross-section of the timber was measured by thermocouples (Figure 2.10; Figure 2.11) and the vertical displacement of the floor was measured by string potentiometers. Figure 3.3 shows the locations of the string potentiometers (diamonds) for the CLT- and NLT-concrete composite floors. The displacements were measured at the center and quarter points of the floors both along the length and width of the specimens. These locations were chosen to measure any potential out-of-plane movement of the floors throughout the test.

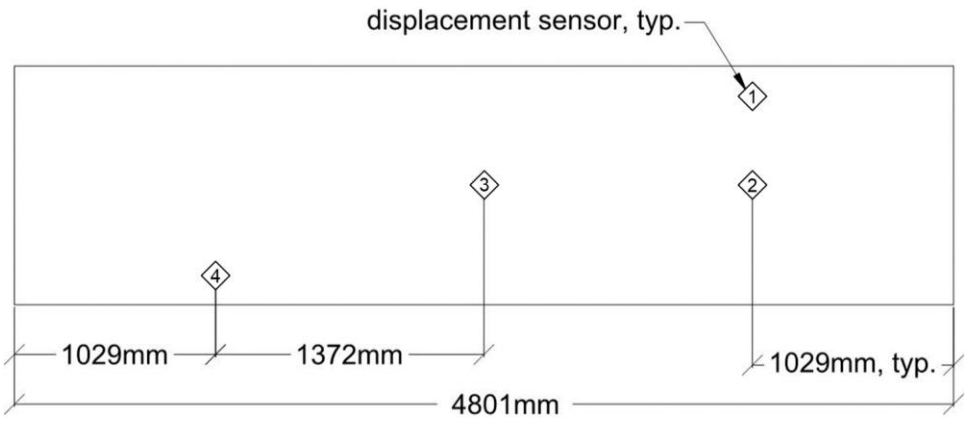

Fig. 3.3. Approximate location and number of displacement sensors used in the large-scale fire tests of the TCC floors. Drawings shown in plan of one floor

After initial preloading, deflection was 0.22 cm (0.56 in) for both assemblies. For the first 105 minutes, the deflection of the NLT-concrete composite floor was greater than that of the CLT-concrete composite floor (as shown in Figure 3.4). The black solid line in Figure 3.4 is the midspan deflection of the NLT-concrete composite floor and the dotted black line in Figure 3.4 is the midspan deflection of the CLT-concrete composite floor. At approximately 103 minutes, the CLT-concrete composite floor midspan deflection surpassed the NLT-concrete composite floor midspan deflection. At 105 minutes, the

deflection rate of the CLT-concrete composite floor increased, indicating the floor was approaching failure (loss of load-carrying capacity). At 105 minutes, the live load was removed from the CLT-concrete composite floor to prevent structural collapse and allow the test to continue. After the removal of the live load, the deflection of the CLT-concrete composite floor remained less than that of the NLT-concrete composite floor for the remainder of the test. The CLT-concrete composite floor failed at 187 minutes and the test was ended. Maximum deflection occurred at the end of the test and was 12.5 cm (4.93 inches) and 13.3 cm (5.24 inches) for the CLT- and NLT-concrete composite specimens respectively.

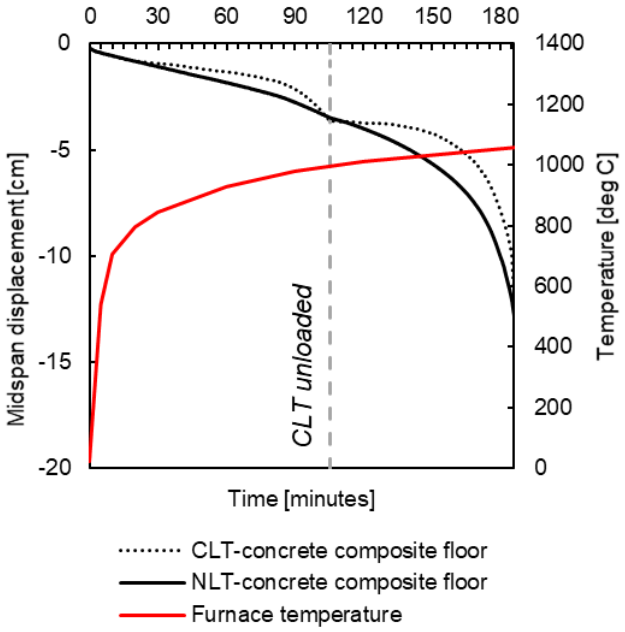

Fig. 3.4. Midspan displacement and furnace temperature during large-scale fire test

The deflection was always largest at the mid-point of both specimens throughout the test, and the quarter point measured displacements indicated no out-of-plane rotation of the floors (Figure 3.5). Figure 3.5 shows the deflection measured at each location of the string potentiometers (shown in Figure 3.3) for the CLT- (a) and NLT- (b) concrete composite floors.

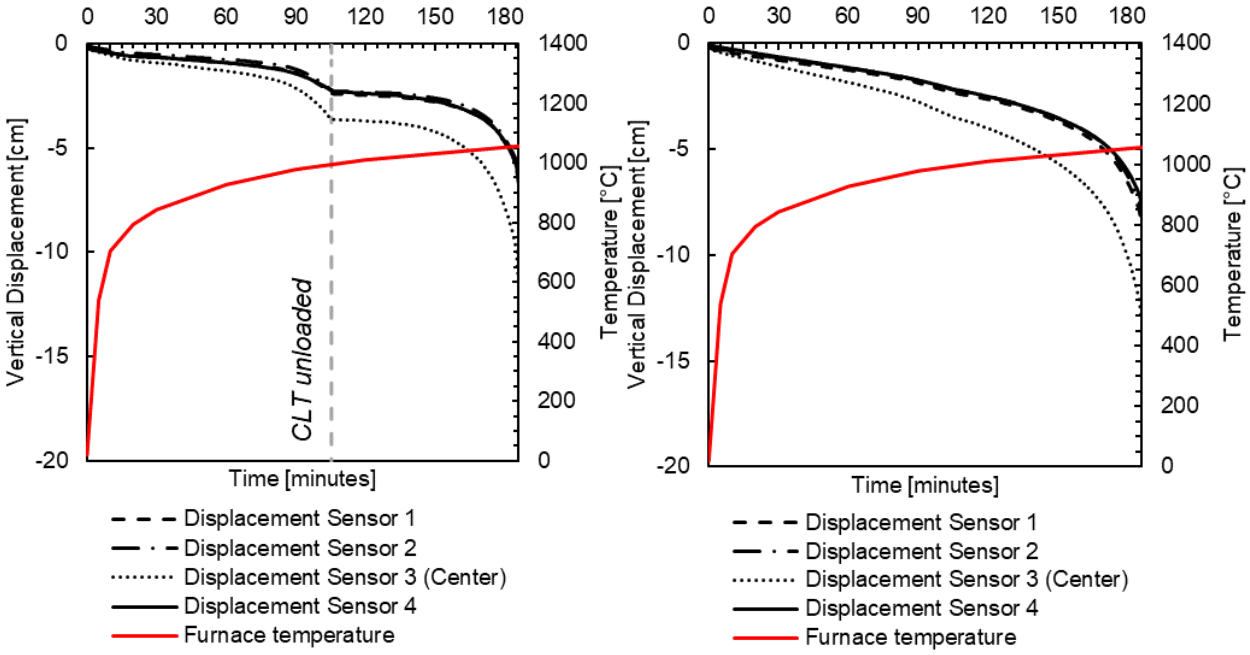

(a) (b)

Fig. 3.5. Experimental deflection data for the (a) CLT- and (b) NLT-concrete composite floor

Application of γ-method for calculating deflection of TCC floors in fire

CLT- and NLT-concrete composite floors

The γ-method with RCSM (CEN 2004a; CEN 2004b) was used to calculate the deflections of the CLT- and NLT-concrete composite floors throughout the standard fire exposure. The analytical model uses the measured secant slip modulus at maximum load from the direct shear tests (Chapter 2). The secant slip modulus at maximum load assumes the shear connectors have reached their ultimate capacity, as would be the case at the time of failure of the TCC floors. This slip modulus was selected because this assumption is compatible with the aim of the analytical model, which is to calculate the deflection of the TCC floor during a standard fire until failure. The results of these calculations are plotted in Figure 3.6.

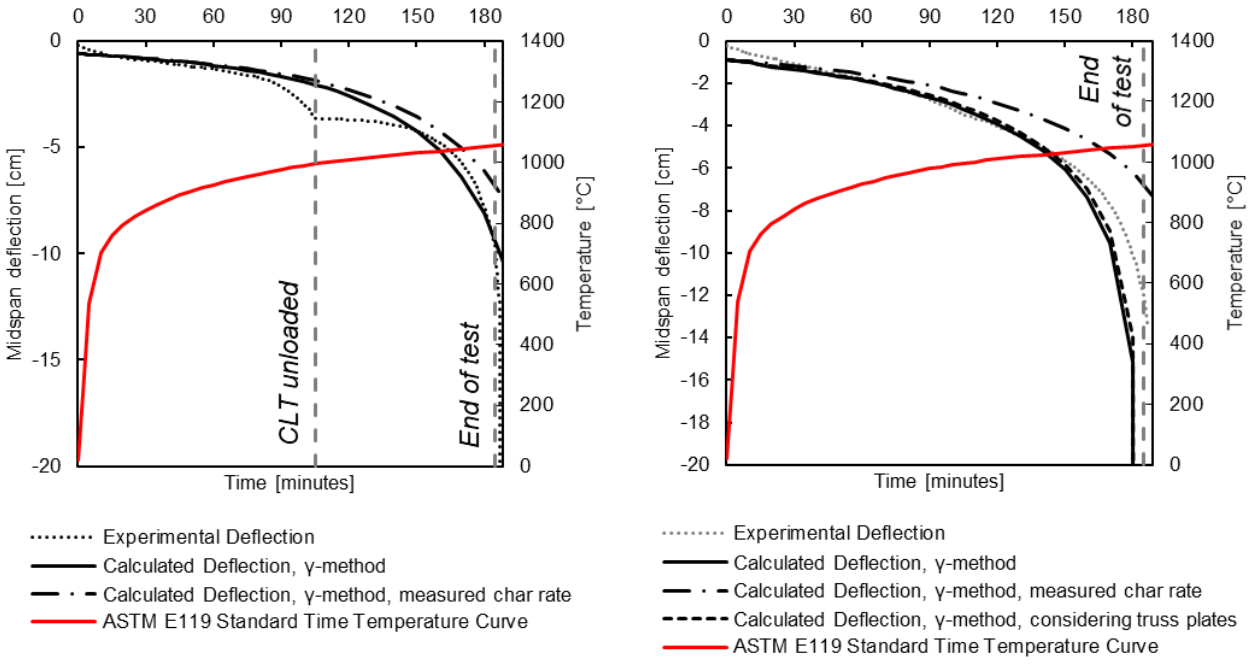

(a) (b)

Fig. 3.6. Deflection of the tested TCC floors as a function of temperature computed using the γ-method with the RCSM (CEN 2004a; CEN 2004b) (a) deflection of the CLT-concrete composite floor and (b) deflection of the NLT-concrete composite floor using the original and adapted γ-method

For the CLT-concrete composite floor the calculated deflection aligns with the experimental data (Figure 3.6a). The black solid line denotes the calculated deflections using the prescribed char rate for CLT of 0.80 mm/min (1.90 inches/hr), which accounts for delamination (AWC 2018; CSA Group 2016). From the beginning of the test to 90 minutes the calculated deflection follows the same trend as the experimental data. At 90 minutes the experimental deflection is 2.13 cm (0.84 inches) and the calculated deflection is 1.68 cm (0.66 inches) (-21% difference from the experimental observation). The dot dashed line denotes the calculated deflections using the experimentally measured char rate of 0.75 mm/min (1.78 inches/hr). Though the two calculated deflections are similar, the calculated effective stiffness of the CLT-concrete composite floor was larger using the measured char rates resulting in smaller calculated deflections throughout the fire exposure. The difference between the two calculated deflections increases throughout the test.

At 105 minutes, the experimental deflection rate of the CLT-concrete composite floor increased, indicating the floor was approaching failure (loss of load-carrying capacity). At this time, the calculated deflection of the floor (using the prescribed char rate) is 2.07 cm (0.81 inches), which is –43% difference from the experimental deflection. At 105 minutes, the live load was removed from the CLT-concrete

composite floor. From experimental observation, there is plasticity occurring in the CLT-concrete composite floor as the deflection of the floor continues to increase after the applied load is removed. The analytical model presented in this chapter was not able to account for the plastic deformation occurring in the CLT-concrete composite floor. The calculated deflections shown in Figure 3.6a do not consider the removal of the load from the floor. As such, results from the beginning of the test to the time of flexural demand removal (105 minutes) will be the only results discussed.

For the NLT-concrete composite floor, the calculated deflections are compared with the experimentally measure deflections in Figure 3.6b. Figure 3.6b shows the results of the calculated deflection not considering (black solid line) and considering (long dashed line) the added stiffness of the truss plates. In these calculations, the timber depth was reduced by a char rate prescribed for structural composite lumber of 0.70 mm/min (1.65 inches/hr) (CEN 2004b; CSA Group 2016). Results indicate both methods align well with the experimental deflection data, and that the stiffness of the truss plates does not contribute significantly to the effective stiffness of the composite section. From the beginning of the test to 150 minutes the calculated deflection (using the prescribed char rate) follows the same trend as the experimental data. At 150 minutes the experimental deflection is 5.7 cm (2.2 inches) and the calculated deflection not considering truss plates is 6.1 cm (2.4 inches) (+7.5% difference). After 150 minutes the difference between the calculated and experimental deflection increases. During the testing, the NLT-concrete composite floor was observed to approach failure at about 187 minutes indicated by runaway deflection (ASTM E119). The calculated deflection demonstrates similar behavior indicative of failure. At 180 minutes the experimental deflection is 10.0 cm (3.9 inches) and the calculated deflection not considering truss plates is 15.2 cm (6.0 inches) (+51% difference). The γ-method, using the average measured char rate of 0.63 mm/min (1.49 inches/hr) (dot dashed line, Figure 3.6b) follows the same trend as the experimental data. Though less conservative than the prescribed char rate, the results are more similar to the end behavior with the calculated deflection at 180 minutes being 6.2 cm (2.4 inches) (-38% difference from the experimental observation). These results provide confidence in the use of the γ-method with RCSM for predicting the deflection of NLT-concrete composite floors with truss plate-type shear connectors during a standard fire (ASTM 2018).

Dagenais et al. (2016) large-scale SLT-concrete composite floor fire test

A limitation of this experimental program is one floor for each configuration was tested providing only one set of experimental data against which to benchmark the results of the analytical model. To further investigate the deflection of TCC floors using truss plate shear connectors, the experimental deflection data from Dagenais et al. (2016) large-scale floor tests was used to compare against the γ-

method with RCSM (CEN 2004a; CEN 2004b). Dagenais et al. (2016) tested three configurations of TCC floors, this section will focus on the SLT-concrete composite floor.

The SLT-concrete composite floor was consisted of 38 mm x 184 mm (1.5 inches x 7.25 inches) solid sawn Grade No. 2 SPF joined by self-tapping screws and a 89 mm (3.5 inches) concrete topping with a design compressive strength of 30 MPa (4.4 ksi) at 28 days and steel mesh for shrinkage reinforcement. The shear connectors used to develop composite action between the timber and concrete were the same as the large-scale fire test NLT-concrete composite floor (Chapter 2), MiTek MT20 truss plates. The measured secant slip modulus at maximum load for the truss plates will be used to model the SLT-concrete composite floor.

The CAN/ULC-S101 fire curve, similar exposure to the ASTM E119 standard fire, was used for the furnace temperature (ASTM 2018; ULC 2014). The SLT-concrete composite floor was loaded with a distributed service live load of 2.4 kPa (50 psf), and did not reach failure at the end of the test (214 minutes). The deflection of the SLT-concrete composite floor was calculated using the γ-method with RCSM (CEN 2004a; CEN 2004b) and compared the experimental data reported from Dagenais et al. (2016). The comparison of these results is shown in Figure 3.7.

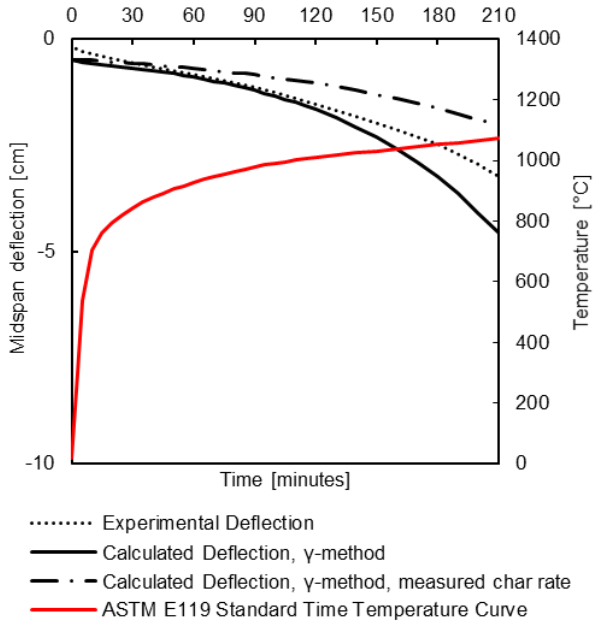

Fig. 3.7. Deflection of the tested SLT-concrete composite floor (Dagenais et al. 2016) as a function of temperature computed using the γ-method with the RCSM (CEN 2004a; CEN 2004b)

In the calculated deflections shown in Figure 3.7, the deflection is calculated with the prescribed char rate of 0.70 mm/min (1.65 inches/hr) (CEN 2004b; CSA Group 2016) and the average experimentally measured char rate of 0.51 mm/min (1.2 inches/hr) (Dagenais et al. 2016). The calculated deflection using the prescribed char rate (black solid line, Figure 3.7) follows the trend of the experimental deflection consistently throughout the test. The difference between the experimental data and the calculated deflection remains less than half a centimeter until 180 minutes. At 180 minutes, the difference between the experimental data and the calculated deflection begins to increase. At the end of the test, the experimental deflection is 3.25 cm (1.28 inches). The calculated deflection using the prescribed char rate (black solid line, Figure 3.7) is 4.56 cm (1.80 inches), which is a +40% difference from the experimental deflection. The calculated deflection using average measured char rate (dot dashed line, Figure 3.7) follows the same trend as the experimental data as well. Though less conservative than the prescribed char rate, the results are as similar to the end behavior with the calculated deflection using the average measured char rate being 2.00 cm (0.79 inches), which is a -38% difference from the experimental data. These results provide confidence in the use of the γ-method with RCSM (CEN 2004a; CEN 2004b) for predicting the deflection of a TCC floor with truss plate-type shear connectors during a standard fire (ASTM 2018).

Application of γ-method for design

The CLT-concrete composite floor tested by Dagenais et al. (2016) used proprietary shear connectors, and therefore, no direct shear test data was provided in the published results. Eurocode 5 (CEN 2004a) provides a simplified design method for calculating the slip modulus, as was presented earlier in the chapter. This method will be applied to the Dagenais et al. (2016) CLT-concrete composite test to be used in the γ-method with RCSM to predict the deflection of the floor throughout the test.

The CLT-concrete composite floor was comprised of 2012 ANSI/APA PRG 320 (ANSI 2012) compliant 5-ply, 175 mm (6.88 inches) thick E1 CLT, 89 mm (3.5 inches) normal-weight concrete topping with a design compressive strength of 30 MPa (4.4 ksi) at 28 days and steel mesh for shrinkage reinforcement. The floor was 1829 mm (72 inches) wide and 4800 mm (189 inches) in length. Self-tapping wood screws 180 mm (7.1 inches) in length were used as shear connectors between the CLT and concrete to develop the composite action. The self-tapping wood screws were oriented in the same direction at 45° and embedded in the CLT for a depth of 100 mm (3.9 inches). The remainder of the fully-threaded screw was embedded in the concrete topping. The self-tapping wood screws were oriented in the strong position, facing toward the nearest support, spaced at 406 mm (16 inches) along the length of the specimen.

The deflection of the Dagenais et al. (2016) CLT-concrete composite floor was calculated using the γ-method with RCSM (CEN 2004a; CEN 2004b), the Eurocode 5 calculated slip modulus, K_u, and the prescribed char rate for CLT of 0.80 mm/min (1.90 inches/hr), which accounts for delamination (AWC 2018; CSA Group 2016). This calculated deflection is compared to the experimental data reported from Dagenais et al. (2016). The comparison of these plots is shown in Figure 3.8.

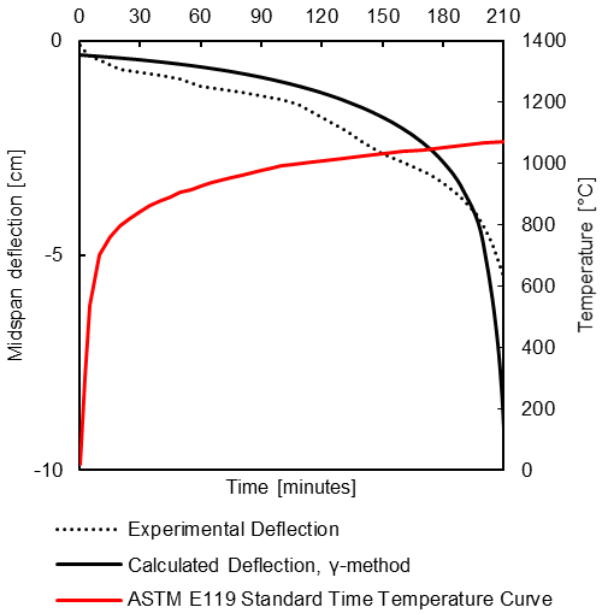

Fig. 3.8. Deflection of the tested CLT-concrete composite floor from Dagenais et al. (2016) as a function of temperature computed using the γ-method with the RCSM and K_u (CEN 2004a; CEN 2004b)

The results show the increase in deflection over time due to the charring of the CLT. During the test at 200 minutes the rate of deflection increased and the floor failed soon after at 214 minutes. Immediately before failure, the maximum recorded deflection of the CLT-concrete composite floor was 7.5 cm (3.0 inches). The calculated deflection rate begins to increase rapidly at approximately 200 minutes. At 210 minutes the experimental deflection is 5.5 cm (2.2 inches) and the calculated deflection is 8.7 cm (3.4 inches), which is a +58% difference from the experimental data. At 214 minutes the calculated deflection increases even more rapidly indicating approaching failure. The calculated deflection aligns with the experimental deflection throughout the test and reflects the rapid increase in deflection at the end of the test. These results demonstrate the use of the prescribed char rate and K_u in the proposed methodology is comparable to the experimental deflection data.

Summary and conclusions

The experimental deflection data from the large-scale TCC floor fire tests was used to benchmark the γ-method (CEN 2004a) and the RCSM (CEN 2004b). The deflection of two CLT-, a NLT-, and a SLT-concrete composite floor exposed to a standard fire (ASTM 2018; ULC 2014) was reasonably estimated using the γ-method (CEN 2004a) and the RCSM (CEN 2004b). This calculation methodology assumed the concrete in tension did not contribute to the stiffness of the composite section, which is consistent with the state-of-practice (Cuerrier-Auclair 2020). In addition, this methodology demonstrated that while the truss plates used as shear connectors in the NLT-concrete composite floor contributed to the strength of the floor, they did not contribute to the stiffness throughout a fire.

Lastly, the work in this chapter demonstrated that when experimental load-slip data is not readily available for shear connectors the simplified calculation method to calculate the slip modulus K_u (CEN 2004a) can be used to calculate the deflection of CLT-concrete composite floors with dowel-type shear connectors throughout a standard fire exposure (ASTM 2018; ULC 2014).

CHAPTER 4: GENERAL CONCLUSIONS

Research summary

Recently North American construction trends have turned toward mass timber structures. Rather than using timber-only floors in these structures, engineers commonly add a concrete topping to meet the International Building Code (IBC) (ICC 2018) requirements for vibration and acoustics. The performance of the timber-only floor under gravity, seismic, and fire loading can be improved by creating composite action with the concrete topping using shear connectors. No codes and standards in North America provide design methodologies for timber-concrete composite (TCC) floors nor does the IBC (ICC 2018) consider TCC floors improved fire performance compared to timber-only floors in the prescriptive approach for fire resistant design. The focus of this thesis is to aid practicing engineers in the design of TCC floors through the development and benchmarking of analytical models to predict the behavior of TCC floors throughout a fire. Experimental and analytical investigations were performed to accomplish the objectives of this thesis.

A series of cross-laminated timber (CLT) and nail-laminated timber (NLT) concrete composite small-scale specimens were tested under direct shear to experimentally quantify the force-slip behavior of shear connectors used in TCC floors. Fully-threaded screws were tested as a part of CLT-concrete composite assemblies and truss plates were tested as a part of NLT-concrete composite assemblies. The fully-threaded screws had a higher initial stiffness than the truss plates and the post-peak behavior of the truss plates showed a faster decline of capacity than the fully-threaded screws. The shear connectors were examined after testing. The fully-threaded screws showed slight bending, but the truss plates showed significant damage, potentially indicative of yielding of the truss plate during the tests. The slip modulus was calculated for both shear connectors using experimental data.

One CLT- and one NLT-concrete composite floor were tested in a gas-fired furnace to evaluate the structural resistance and fire integrity of TCC floors when exposed to fire and gravity loads, collect experimental deflection data on TCC floors subjected to fire and gravity loads, and to benchmark existing char rates for TCC floors against those intended for solid timber members. The CLT-concrete composite floor demonstrated behavior indicative of delamination and had to be unloaded at 105 minutes into testing due to behavior indicative of approaching failure (rapidly increasing deflection rate). The test continued with only the NLT-concrete composite floor loaded. The CLT-concrete composite floor failed in flexure at 197 minutes and the test ended. The NLT-concrete composite floor was experimentally observed to be

approaching failure, but maintained load-carrying capacity until the end of the test. The temperature of the concrete and timber-concrete interface remained below 100°C, indicating the concrete retained ambient temperature material properties in compression and tension (CEN 2004c). Using the thermocouple measurements and assuming temperature of the char isotherm to be 300°C, the experimental char rate was calculated and found to be comparable to the code prescribed values for timber-only, which suggests that the concrete and the shear connectors of the TCC floor do not influence the char rate of the floor during a standard fire.

The flexural capacity of TCC floors during a fire can be calculated using the elasto-plastic model with the reduced cross-section method (RCSM) (Frangi and Fontana 2003; CEN 2004b). This existing analytical model was benchmarked and improved upon using the results from the experimental investigations. Modifications were made to account for the additional timber width in a continuous floor and to account for truss plate-type shear connectors. The original elasto-plastic model, developed for dowel-type fasteners such as the fully-threaded screws used in the CLT-concrete composite floor, results aligned well with the experimental observations of the CLT-concrete composite floor at both the instant when the CLT panel was unloaded and at the end of test. The original elasto-plastic model results did not align well with the experimental observations of the NLT-concrete composite floor. The elasto-plastic model was modified to include yielding of the truss plates and to include the truss plates as tensile reinforcement of the timber. This modified elasto-plastic model aligned well with the experimental observations of the NLT-concrete composite floor throughout the fire exposure. The modified elasto-plastic model was applied to an screw-laminated timber (SLT) concrete composite floor (Dagenais et al. 2016) and found to agree well with the experimental observations. The Cuerrier-Auclair (2020) method, developed for dowel-type fasteners, was able to reasonably estimate the failure time of the CLT-concrete composite floor, but was unable to estimate the failure time of the NLT-concrete composite floor.

The deflection of TCC floors during a fire can be calculated using the γ-method and the reduced cross-section method (RCSM) (CEN 2004a; CEN 2004b). The γ-method was able to reasonably predict the deflections throughout a standard fire for the CLT- and NLT-concrete composite floors described in Chapter 2 and the CLT- and SLT-concrete composite floors tested by Dagenais et al. (2016). However, the γ-method was unable to account for the plastic deformation observed following the load removal for the CLT-concrete composite floor test described in this thesis. Lastly, the γ-method can be applied to TCC floors even when there is no slip modulus data on the shear connectors. A simplified design method for calculating the slip modulus of dowel-type shear connectors (CEN 2004a) was applied to the CLT-concrete composite floor from Dagenais et al. (2016). The calculated slip modulus value was used in the proposed methodology and the results aligned well with the experimental deflection data.

Conclusions

Based on the experimental investigations performed on small-scale TCC specimens the following conclusions are drawn:

1. The fully-threaded screws have a higher initial stiffness than the truss plates and the truss plates have a more rapid loss of capacity than the fully-threaded screws post-peak.
2. The fully-threaded screws showed slight bending, but the truss plates showed significant damage at the NLT-concrete interface, including fracture of portions of the truss plate, indicative of yielding.

Based on the experimental investigations performed on large-scale TCC floors the following conclusions are drawn:

1. The calculated experimental char rates are comparable to prescribed char rates in the NDS, Eurocode 5, and CSA 086 (AWC 2018; CEN 2004b; CSA Group 2016) for timber-only, indicating the concrete and shear connectors do not impact the char rate of timber.
2. Throughout a fire, a large thermal gradient develops within a TCC floor resulting in the concrete portion remaining at near ambient temperature throughout the standard fire exposure.

Based on the analytical investigations of large-scale TCC floors' flexural capacity the following conclusions are drawn:

1. The original elasto-plastic model and the Cuerrier-Auclair (2020) method can be used to reasonably estimate the flexural capacity of a TCC floor with dowel-type shear connectors during a standard fire.
2. The elasto-plastic model, modified to account for the additional timber width in a continuous floor and to account for truss plate-type shear connectors, can be used to reasonably estimate the flexural capacity of a TCC floor with truss plate-type shear connectors during a standard fire.

Based on the analytical investigations of large-scale TCC floors' deflection the following conclusions are drawn:

1. The deflection of TCC floors during a fire can be calculated using the γ-method and the RCSM (CEN 2004a; CEN 2004b).

2. For TCC floors with truss plate-type shear connectors considering the contribution of the stiffness of the truss plates has negligible impact on the results of the proposed deflection calculation methodology.
3. The slip modulus for dowel-type shear connectors calculated with the simplified design method (CEN 2004a) can be used to reasonably approximate the deflection of TCC floors in fire when used with the γ-method and the RCSM (CEN 2004a; CEN 2004b)

Suggestions for future work

The results from the experimental investigations are a cohesive package of data demonstrating the performance of TCC floors and shear connectors. However, the results and conclusions produced from these experimental tests only apply to members similar to those physically tested. The data collected can be used to benchmark numerical models of TCC floors exposed to a standard fire. Improving numerical simulation methods will allow a greater variety of TCC floors to be investigated with fewer resources and minimal cost. Additionally, this data can be used to develop and improve prescriptive methods for the design of TCC floors during a fire. Design methodologies that have been benchmarked against experimental tests and validated for finite element models will allow for greater ease of design for structural engineers regarding TCC floors at ambient temperature and during a fire.

Large-scale fire tests on CLT-concrete composite floors manufactured in accordance with the most recent ANSI/APA PRG 320 (ANSI 2018), which includes standards for the performance of CLT adhesives at elevated temperature, are recommended to better understand how the new adhesive performance requirements affect the fire resistance of CLT-concrete composite floors. Large-scale fire tests on CLT-concrete composite floors with different types of panel to panel connections are recommended to better understand the impact inter-panel joints have on the fire performance of CLT-concrete composite floors.

The deflection of the TCC floors during the fire test was reasonably estimated using the γ-method (CEN 2004a) and the RCSM (CEN 2004b). The effects of temperature on the mechanical properties of the shear connectors were not considered in the calculation of the composite bending stiffness. Additionally, the effect of loss of penetration depth due to timber charring was not considered in the calculation of the shear connector stiffness. Further investigation is recommended to evaluate the impact temperature dependent and penetration depth dependent properties of the shear connectors used in TCC floors have on the composite stiffness during a fire event.

BIBLIOGRAPHY

American Society for Testing and Materials (ASTM). (2012). "ASTM C39 Standard Test Method for Compressive Strength of Cylindrical Concrete Specimens." *ASTM International,* West Conshohocken, PA.

American Society for Testing and Materials (ASTM). (2012). "ASTM C39 Standard Test Method for Compressive Strength of Cylindrical Concrete Specimens." *ASTM International,* West Conshohocken, PA.

American Society for Testing and Materials (ASTM). (2018). "ASTM E119-16a Standard Test Methods for Fire Tests of Building Construction and Materials." *ASTM International,* West Conshohocken, PA.

American Society of Civil Engineers (ASCE). (2016). "Minimum Design Loads for Buildings and Other Structures (ASCE 7-16)." *ASCE,* Reston, VA.

American Wood Council (AWC). (2018). "National Design Specifications for Wood Construction (ANSI/AWC NDS 2018)." *AWC,* Leesburg, VA.

ANSI. (2017). "Standard for Performance-Rated Cross-Laminated Timber (ANSI/APA PRG 320 2017)." *APA – The Engineering Wood Association,* Tacoma, WA.

ANSI. (2018). "Standard for Performance-Rated Cross-Laminated Timber (ANSI/APA PRG 320 2018)." *APA – The Engineering Wood Association,* Tacoma, WA.

Barber, D., Gerard, R. (2015). "Summary of the fire protection foundation report – fire safety challenges of tall wood buildings." *Fire Sciences Reviews*, 4(5), 1-15.

Barbosa, A.R., Rodrigues, L.G., Sinha, A., Higgins, C., DeMeza, B., Zimmerman, R., Breneman, S., Pei, S., van de Lindt, J.W., Berman, J., McDonnell, E., Branco, J.M., Neves, L.A.C. (2018). "Numerical Modeling of CLT And CLT-Concrete Composite Diaphragms Tested on a Shake Table Experiment." *16th World Conference on Timber Engineering*, Seoul, Republic of Korea.

Binational Softwood Lumber Council. (2017). "Nail-laminated Timber: U.S. Design and Construction Guide (NLT Design Guide)." *Binational Softwood Lumber Council,* Minneapolis, MN.

Boccadoro, L., Frangi, A. (2013). "Experimental analysis of the structural behavior of timber–concrete composite slabs made of beech-laminated veneer lumber." *Journal of Performance of Constructed Facilities,* 28(6), 1-10.

Branco, J.M., Kekeliak, M., Lourenco, P.B. (2015). "In-plane stiffness of timber floors strengthened with CLT." *European Journal of Wood and Wood Products,* 73(3), 313-323.

Brenenman, S., Timmers, M., Richardson, D. (2019). "Tall Wood Buildings in the 2021 IBC Up to 18 Stories of Mass Timber." *WoodWorks Wood Products Council,* Washington, DC.

Buchanan, A. H., Abu, A. K. (2017). "Structural design for fire safety." *John Wiley & Sons, Ltd.,* United Kingdom.

Buchanan, A., Ostman, B., Frangi, A. (2014) “Fire resistance of timber structures, a report for the National Institute of Standards and Technology (NIST).” *NIST*, Gaithersburg, MD.

Caldova, E., Vymlatil, P, Wald, F., Kuklikova, A. (2015). “Timber Steel Fiber-Reinforced Concrete Floor Slabs in Fire: Experimental and Numerical Modeling.” *Journal of Structural Engineering,* 141(9).

Canadian Standards Association (CSA Group). (2016). “Engineering design in wood (CSA 086-14).” *CSA Group,* Mississauga, Ontario, Canada.

Ceccotti, A. (1995). “Timber-concrete composite structures.” *Timber engineering, step*, 2(1).

Ceccotti, A., Fragiacomo, M., Giordano, S. (2006). “Long-term and collapse tests on a timber–concrete composite beam with glued-in connection.” *Materials and Structures,* 40(1), 15–25.

Crews, K., John, S., Gerber, C., Buchanan, A., Smith, T., Pampanin, S. (2010). “Innovative engineered timber building systems for non-residential applications, utilizing timber concrete composite flooring capable of spanning up to 8–10 m. Forest and Wood Products Australia Report PNA012-0708.” *Forest and Wood Products Australia Limited, ISBN: 978-1-920883-99-7,* Melbourne, Australia.

Cuerrier-Auclair, S. (2020). “Design Guide for Timber-Concrete Composite Floors in Canada.” *FPInnovations,* Canada.

Dagenais, C., Ranger, L., Cuerrier-Auclair, S. (2016). “Understanding Fire Performance of Wood-Concrete Composite Floor Systems.” *World Conference on Timber Engineering*, Vienna, Austria.

Deam, B.L., Fragiacomo, M., Buchanan, A.H. (2007). “Connections for composite concrete slab and LVL flooring systems.” *Materials and Structures,* 41(3), 495–507.

Dias, A. M. P. G., Skinner, J., Crews, K., Tannert, T. (2016). “Timber-concrete-composites increasing the use of timber in construction.” *European Journal of Wood and Wood Products,* 74(3), 443-451.

Emberley, R., Putynska, C.G., Bolanos, A., Lucherini, A., Solarte, A., Soriguer, D., Gonzalez, M.G., Humphreys, K., Hidalgo, J.P., Maluk, C. and Law, A. (2017). “Description of small and large-scale cross laminated timber fire tests.” *Fire Safety Journal,* 91, 327-335.

European Committee for Standardization (CEN). (2004a). “Design of timber structures – Part 1-1: General –Common rules and rules for buildings.” *EN 1995-1-1*, Brussels, Belgium.

European Committee for Standardization (CEN). (2004b). “Design of timber structures – Part 1-2: General – Structural fire design.” *EN 1995-1-2*, Brussels, Belgium.

European Committee for Standardization (CEN). (2004c). “Design of concrete structures – Part 1-2: General rules and rules for buildings.” *EN 1992-1-2*, Brussels, Belgium.

Fragiacomo, M., Menis, A., Clemente, I., Bochicchio, G., Tessadri, B. (2012). “Experimental and Numerical Behaviour of Cross-Laminated Timber Floors in Fire Conditions.” *World Conference on Timber Engineering,* Auckland, New Zealand.

Frangi, A., Fontana, M. (2003). “Elasto-Plastic Model for Timber-Concrete Composite Beams with Ductile Connection,” *Structural Engineering International.* 13(1), 47-57.

Frangi, A., Fontana, M., Hugi, E., Jöbstl, R. (2009). "Experimental analysis of cross-laminated timber panels in fire." *Fire Safety Journal,* 44(8), 1078–1087.

Frangi, A., Fontana, M., Knobloch, M., Bochicchio, G. (2008). "Fire Behaviour of Cross-Laminated Solid Timber Panels." *Fire Safety Science,* 9, 1279-1290.

Frangi, A., Knobloch, M., Fontana, M. (2010). "Fire Design of Timber-Concrete Composite Slabs with Screwed Connections." *Journal of Structural Engineering,* 136(2), 219-228.

Gelfi, P., Giuriani, E., Marini, A. (2002). "Stud Shear Connection Design for Composite Concrete Slab and Wood Beams." *Journal of Structural Engineering,* 128(12), 1544-1550.

Gerard, R., Barber, D., Wolski, A. (2013). "Fire safety challenges of tall wood buildings." *National Fire Protection Research Foundation,* Quincy, Massachusetts.

Girhammar, U.A. (2009). "A simplified analysis method for composite beams with interlayer slip." *International Journal of Mechanical Sciences,* 51(7), 515-530.

Higgins, C., Barbosa, A.R., Blank, C. (2017). "Structural Tests of Concrete Composite-Cross-Laminated Timber Floors." *Oregon State University,* Corvallis, OR.

Hopkin, D., Bisby, L., Kotsovinos, P., Wilkinson, P. (2014). "Fire resistance: structural design for fire safety." *International fire professional,* 10, 22-26.

Hozjan, T., Bedon, C., Ogrin, A., Cvetkovska, M., Klippel, M. (2019). "Literature review on Timber-Concrete Composite Structures in Fire." *Journal of Structural Engineering,* 145(11).

International Code Council (ICC). (2018). "International Building Code (IBC)." *ICC,* Washington, D.C.

International Organization for Standardization (ISO). (1983). "Timber structures – Joints made with mechanical fasteners – General principles for the determination of strength and deformation characteristics." *ISO 6891,* Geneva, Switzerland.

Klippel, M., Leyder, C., Frangi, A., and Fontana, M. (2014). "Fire Tests on Loaded Cross-laminated Timber Wall and Floor Elements." *Fire Safety Science - Proceedings of the Eleventh International Symposium,* International Association for Fire Safety Science, University of Canterbury, New Zealand, 626–639.

Li, X., McGregor, C., Medina, A., Sun, X., Barber, D., Hadjisophocleous, G. (2016). "Real-scale fire tests on timber constructions." *World Conference on Timber Engineering,* Vienna, Austria.

Lineham, S.A., Thomson, D., Bartlett, A.I., Bisby, L., Hadden, R.M. (2016). "Structural response of fire-exposed cross-laminated timber beams under sustained loads." *Fire Safety Journal,* 85, 23-24.

Lukaszewska, E., Fragiacomo, M., Johnsson, H. (2008). "Laboratory tests and numerical analyses of prefabricated timber– concrete composite floors." *Journal of Structural Engineering,* 136(1), 46–55.

Mai, K.Q., Park, A., Lee, Kihak. (2018). "Experimental and numerical performance of shear connections in CLT-concrete composite floor." *Materials and Structures,* 51(84), 1-12.

Miotto, J.L., Dias, A.A. (2011). "Evaluation of perforated steel plates as connection in glulam-concrete composite structures." *Construction and Building Materials,* 28, 216-223.

Möhler, K. (1956). “On the load carrying behavior of beams and columns of compound sections with flexible connections.” *Habilitation, Technical University of Karlsruhe,* Germany.

O’Neill, J.W., Carradine, D., Moss, P.J., Fragiacomo, M., Dhakal, R., Buchanan, A.H. (2011). “Design of Timber-Concrete Composite Floors for Fire Resistance.” *Journal of Structural Fire Engineering,* 2(3), 231-242.

O'Neill, J., Abu, A., Carradine, D., Moss, P., Buchanan, A. (2014). “Modelling the fire performance of structural timber-concrete composite floors.” *Journal of structural fire engineering,* 5(2).

Osborne, L., Dagenais, C., and Benichou, N. (2012). “Preliminary CLT Fire Resistance Testing Report. Project No 301006155.” *FPInnovations,* Canada.

Pei, S., Van De Lindt, J.W., Popovski, M., Berman, J.W., Dolan, J.D., Ricles, J., Sause, R., Blomgren, H., Rammer, D.R. (2014). "Cross-laminated timber for seismic regions: Progress and challenges for research and implementation." *Journal of Structural Engineering,* 142(4), 1-11.

Richart, F. E., Williams, C. B. (1943). “Tests of composite timber and concrete beams.” University of Illinois Bulletin, 40(38).

Rodrigues, J. N., Dias, A. M. P. G., Providência, P. (2013). “Timber-Concrete Composite Bridges: State-of-the-Art Review.” BioResources, 8(4), 6630-6649.

Sathre, R., O’Connor, J. (2010). “Meta-analysis of greenhouse gas displacement factors of wood product substitution.” *Environmental science & policy*, 13(2), 104-114.

Schaub, O. (1931). “Wood reinforced concrete structural member.” United States Patent Office, Alexandria, VA.

Skidmore, Owings, & Merrill, LLP. (SOM). (2017). “Timber Tower Research Project. Physical Testing Report #1. Composite Timber Floor Testing at OSU. Final Report.” *SOM,* Chicago, IL.

Smartlam North Americam (Smartlam). (2020). “Cross-Laminated Timber 2020 Specification Guide.” *Smartlam,* Columbia Falls, MT.

Structurlam. (2020). “Crosslam CLT Technical Design Guide.” *Structurlam,* Penticton, BC, Canada.

Underwriters Laboratories (UL). (2011). “Standard for Fire Tests of Building Construction and Materials (UL 263).” *UL/ANSI,* Northbrook, IL.

Underwriters Laboratories of Canada (ULC). (2014). “CAN/ULC S101 - Standard Method of Fire Endurance Tests of Building Construction Materials.” *ULC,* Toronto, Ont., Canada.

White, R. H. (2008). “Analytical methods for determining fire resistance of timber members.” *SFPE Handbook of Fire Protection Engineering, 4th ed. National Fire Protection Association,* Quincy, MA.

Wiesner, F., Randmael, F., Wan, W., Bisby, L., Hadden, R. (2017). “Structural Response of Cross-Laminated Timber Compression Elements Exposed to Fire.” *Fire Safety Journal,* 91, 56-67.

Wood Handbook. (2010). “Wood handbook - Wood as an Engineering Material. General Technical Report FPL-GTR-190.” *Forest Products Laboratory, USDA Forest Service,* Madison, WI.

Yeoh, D., Fragiacomo, M., Deam, B. (2011a). “Experimental behaviour of LVL–concrete composite floor beams at strength limit state.” *Engineering Structures,* 33(9), 2697–2707.

Yeoh, D., Fragiacomo, M., Franceschi, M. D., Boon, K. H. (2011b). “State of the Art on Timber-Concrete Composite Structures: Literature Review.” Journal of Structural Engineering, 137(10), 1085-1095.

Appendix A: Slip modulus example calculation

Slip modulus calculation
CLT-concrete composite specimen
Specimen #1
Per ISO 6891 (1983)

Description

The results of the direct shear tests (Chapter 2) were used to calculate the slip modulus of the CLT- and NLT-concrete composite specimens (Table 2.4 and Table 2.5, respectively). The slip modulus k_s was calculated per ISO 6891 (1983). The example calculation provided below is for the first CLT-concrete composite specimen tested.

Slip modulus calculation (ISO 6891 1983)

For Specimen #1, the estimated maximum load F_{est} was defined as 6 kips on the basis of previous experimental data. For Specimens #2 to #6, F_{est} will be defined as F_{max} measured from Specimen #1. For the slip modulus calculations, F_{est} was defined as F_{max} measured from Specimen #1. Due to variability of data for the first loading cycle, the displacement values used for calculations are from the second loading cycle.

Estimated maximum load (F_{max} measured from Specimen #1)

$F_{est} := 12.6kip$ $\quad F_{est} = 56 \cdot kN$

$0.1 \cdot F_{est} = 1.26 \cdot kip$ $\quad 0.1 \cdot F_{est} = 5.6 \cdot kN$

$0.4 \cdot F_{est} = 5.04 \cdot kip$ $\quad 0.4 \cdot F_{est} = 22 \cdot kN$

Second loading, slip at $0.1F_{est}$

$\upsilon_{21} := 0.1143mm$ $\quad \upsilon_{21} = 0.005 \cdot in$

Second loading, slip at $0.4F_{est}$

$\upsilon_{24} := 0.3607mm$ $\quad \upsilon_{24} = 0.014 \cdot in$

Second loading, slip modulus

$$k_s := \frac{1}{2} \cdot \frac{0.4 \cdot F_{est} - 0.1 \cdot F_{est}}{\upsilon_{24} - \upsilon_{21}}$$

$$\boxed{k_s = 195 \cdot \frac{kip}{in}} \qquad \boxed{k_s = 34 \cdot \frac{kN}{mm}}$$

Appendix B: Loading calculations

Loading calculations for the large-scale fire test
CLT- and NLT-concrete composite floor

Description

Loading calculations to determine the flexural demand on the CLT- and NLT-concrete composite floors during the large-scale fire test.

All concrete properties are from the mix design for this study. All timber properties are from the National Design Specifications for Wood Construction (NDS 2018) unless otherwise indicated.

Ambient Section Geometry

Length of floor $L_p := 15.75ft$

Depth of concrete, CLT-concrete floor $h_{1.c} := 2.25in$

Depth of concrete, NLT-concrete floor $h_{1.n} := 3.0in$

Depth of timber, CLT-concrete floor $h_{2.c} := 6in + \frac{7}{8}in$

Depth of timber, NLT-concrete floor $h_{2.n} := 5.5in$

Depth of section, CLT-concrete floor $h_c := 2.25in + 6in + \frac{7}{8}in = 9.125 \cdot in$

Depth of section, NLT-concrete floor $h_n := 3.0in + 5.5in = 8.5 \cdot in$

Width of section, CLT-concrete floor $b_c := 48in$

Width of section, NLT-concrete floor $b_n := 49.5in$

Total floor width $b_s := b_c + b_n = 97.5 \cdot in$

Total floor area $A_s := b_s \cdot L_p = 128 \cdot ft^2$

Loading Protocol Details

Number of actuators $n_a := 60$

Equation for the factored distributed load $w_u = 1 \cdot D + 1 \cdot L$

Service live load (ICC 2018) $L_a := 80psf$

Total applied load $P_L := L_a \cdot A_s = 10.2 \cdot kip$

Load per actuator $P_a := \frac{P_L}{n_a} = 171 \cdot lbf$

Material properties

Density, concrete

$$\rho_{conc} := 150pcf$$

Density, SPF

$$\rho_{spf} := 485\frac{kg}{m^3} = 0.941\cdot\frac{slug}{ft^3}$$

Self-weight, SL-V4 CLT (Smartlam 2020)

$$D_{2.c} := 16.5psf$$

Loading calculations

Self-weight, concrete, CLT-concrete composite floor

$$D_{1.c} := \rho_{conc}\cdot h_{1.c} = 28.1\cdot psf$$

Self-weight, concrete, NLT-concrete composite floor

$$D_{1.n} := \rho_{conc}\cdot h_{1.n} = 37.5\cdot psf$$

Self-weight, timber, NLT-concrete composite floor

$$D_{2.n} := \rho_{spf}\cdot h_{2.n}\cdot g = 13.9\cdot psf$$

Total demand, CLT-concrete composite floor

$$\boxed{D_c := D_{1.c} + D_{2.c} + L_a = 125\cdot psf}$$

Total demand, NLT-concrete composite floor

$$\boxed{D_n := D_{1.n} + D_{2.n} + L_a = 131\cdot psf}$$

Appendix C: Elasto-plastic model example calculation

Elasto-plastic model flexural capacity calculation
Applied to the NLT-concrete composite floor
Exactly per Frangi and Fontana (2003)

Description

The elasto-plastic model is an analytical model to calculate the stress distribution through a TCC cross-section joined with a ductile dowel-type fastener shear connector (Frangi and Fontana 2003). The example calculation provided below is for the ambient temperature flexural capacity of the NLT-concrete composite floor tested (Chapter 2).

All concrete properties are from the mix design for this study. All timber properties are from the National Design Specifications for Wood Construction (NDS 2018).

Material Properties

Compressive strength, concrete $f'_c := 5000psi$

Tensile strength, timber $F_t := 450psi$

Bending strength, timber $F_b := 875psi$

Elastic modulus, concrete $E_1 = 4031 \cdot ksi$

Elastic modulus, timber $E_2 := 1400ksi$

Ambient Section Geometry

Length of floor $L_p := 15.75ft$

Depth of section, concrete $h_1 := 3in$

Depth of section, timber $h_2 := 5.5in$

Width of section, concrete $b_1 := 49.5in$

Width of section, timber $b_2 := b_1$

Area of section, concrete $A_1 := h_1 \cdot b_1 = 148.5 \cdot in^2$

Area of section, timber $A_2 := h_2 \cdot b_2 = 272.25 \cdot in^2$

Ratio, elastic moduli $n := \frac{E_1}{E_2} = 2.88$

Thickness, accoustic layer $t := 0$

Neutral axis calculation

Equation simplification factor

$$\beta := \frac{A_2}{n \cdot b_1} = 1.91 \cdot in$$

Neutral axis depth from the top of the section, assuming neutral axis in concrete

$$x := \sqrt{\beta^2 + \beta \cdot \left(h_2 + 2 \cdot t + 2 \cdot h_1\right)} - \beta = 3.15 \cdot in$$

Check if the neutral axis is in the concrete.

$$x = 3.15 \cdot in \quad . \leq . \quad h_1 = 3 \cdot in$$ **Not OK.**

If the neutral axis is greater that the depth of the concrete the assumption the neutral axis is in the concrete is incorrect. The neutral depth calculation needs to be recalculated assuming the neutral axis is in the timber.

Neutral axis depth from the top of the section, assuming neutral axis in timber

$$x := \frac{n \cdot A_1 \cdot \frac{h_1}{2} + A_2 \cdot \left(\frac{h_2}{2} + t + h_1\right)}{n \cdot A_1 + A_2} = 3.15 \cdot in$$

Stress calculations and checks

Relation between timber bending and tensile stress

$$\alpha := \frac{h_2}{h_2 + 2 \cdot t + 2 \cdot h_1 - 2 \cdot x} = 1.06$$

Tensile stress, timber

$$\sigma_{2.N} := \frac{F_t \cdot F_b}{F_b + \alpha \cdot F_t} = 291 \cdot psi$$

Bending stress, timber

$$\sigma_{2.M} := \alpha \cdot \sigma_{2.N} = 309 \cdot psi$$

Check is the ultimate limit state for timber in combined bending and tension met

$$\frac{\sigma_{2.N}}{F_t} + \frac{\sigma_{2.M}}{F_b} = 1 \quad . \leq . \quad 1$$ **OK.**

Check Compressive stress, concrete (neutral axis in concrete)

$$\sigma_{1.r} := \frac{2 \cdot \sigma_{2.M} \cdot n \cdot x}{h_2} = 1.02 \cdot ksi \quad . \leq . \quad f'_c = 5 \cdot ksi$$ **OK.**

Check Compressive stress, concrete (neutral axis in timber)

$$\sigma_{1.r} := \frac{2 \cdot \sigma_{2.M} \cdot n \cdot h_1}{h_2} = 0.97 \cdot ksi \quad . \leq . \quad f'_c = 5 \cdot ksi$$ **OK.**

Moment capacity calculation

Flexural capacity, composite section

$$M_R := A_2 \cdot \sigma_{2.N} \cdot \left(\frac{h_2}{2} + t + h_1 - \frac{x}{3}\right) + \sigma_{2.M} \cdot \frac{b_2 \cdot h_2^2}{6}$$

$$M_R = 37.5 \cdot kip \cdot ft$$

Appendix D: Modified elasto-plastic model example calculation

Modified elasto-plastic model flexural capacity calculation
NLT-concrete composite floor
Modified from Frangi and Fontana (2003) to consider full elastic section modulus and contribution from the truss plates

Description

Two minor adjustments were made to the elasto-plastic model (Frangi and Fontana 2003). The first modification pertains to the calculation of the depth of the neutral axis. The second adaptation pertains to the use of shear connectors that are not ductile dowel-type fastener shear connectors. The example calculation provided below is for the ambient temperature flexural capacity of the NLT-concrete composite floor tested (Chapter 2).

All concrete properties are from the mix design for this study. All timber properties are from the National Design Specifications for Wood Construction (NDS 2018).

Material Properties

Compressive strength, concrete $f'_c := 5000psi$

Tensile strength, timber $F_t := 450psi$

Bending strength, timber $F_b := 875psi$

Elastic modulus, concrete $E_1 := 4030.5087ksi$

Elastic modulus, timber $E_2 := 1400ksi$

Ambient Section Geometry

Length of floor $L_p := 15.75ft$

Depth of section, concrete $h_1 := 3in$

Depth of section, timber $h_2 := 5.5in$

Width of section, concrete $b_1 := 49.5in$

Width of section, timber $b_2 := b_1$

Area of section, concrete $A_1 := h_1 \cdot b_1 = 148.5 \cdot in^2$

Area of section, timber $A_2 := h_2 \cdot b_2 = 272.25 \cdot in^2$

Ratio, elastic moduli $n_a := \frac{E_1}{E_2} = 2.88$

Shear connector properties

Number of connectors in width of floor $m := 10$

Total thickness, connector $b_3 := m \cdot 0.0356in = 0.36 \cdot in$

Depth of connector in timber

$$h_3 := 3in$$

Yield stress, steel

$$f_y := 40ksi$$

Tensile capacity, truss plates

$$N_3 := f_y \cdot b_3 \cdot h_3 = 42.7 \cdot kip$$

Elastic modulus, steel

$$E_3 := 29000ksi$$

Ratio, elastic moduli

$$n_b := \frac{E_3}{E_2} = 20.71$$

Neutral axis calculation

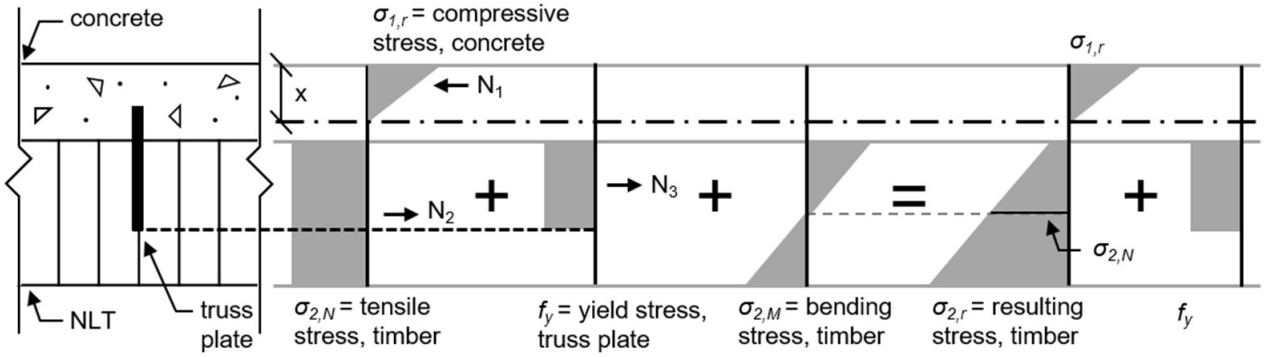

Fig. D.1. Assumed stress field for a fully composite timber-concrete composite floor with the neutral axis in the concrete

Full elastic section modulus, concrete

$$S_1 = \frac{1}{6} \cdot b \cdot x^2 + b \cdot x \cdot \frac{x}{2}$$

Full elastic section modulus, timber

$$S_2 = \frac{1}{6} \cdot b \cdot {h_2}^2 + b \cdot h_2 \cdot \left(\frac{h_2}{2} + h_1 - x \right)$$

Full elastic section modulus, connector

$$S_3 = \frac{1}{6} \cdot b_3 \cdot {h_3}^2 + b_3 \cdot h_3 \cdot \left(\frac{h_3}{2} + h_1 - x \right)$$

Summing the full section modulus of all subcomponents yields the following equation:

$$n_a \cdot S_1 = S_2 + S_3 \cdot n_b$$

Combining equations and simplifying results in the following quadratic equation:

$$0 = \frac{2}{3} \cdot n \cdot b_1 \cdot x^2 + \left(n_b \cdot b_3 \cdot h_3 + b_2 \cdot h_2 \right) \cdot x \ldots + -\left(n_b \cdot \frac{2}{3} \cdot b_3 \cdot {h_3}^2 + b_3 \cdot h_3 \cdot h_1 \cdot n_b \right) \ldots + -\left(\frac{1}{6} \cdot b_1 \cdot {h_2}^2 + b_2 \cdot h_2 \cdot h_1 + b_2 \cdot {h_2}^2 \cdot \frac{1}{2} \right)$$

Using the quadratic formula we can solve for the neutral axis depth with respect to the top of the

$$a := \frac{2}{3} \cdot n_a \cdot b_1 = 95 \cdot in$$

section:

$$b := n_b \cdot b_3 \cdot h_3 + b_2 \cdot h_2 = 294 \cdot in^2$$

$$c := -\left(n_b \cdot \frac{2}{3} \cdot b_3 \cdot h_3^{\,2} + b_3 \cdot h_3 \cdot h_1 \cdot n_b \ \ldots \right.$$
$$\left. + \frac{1}{6} \cdot b_1 \cdot h_2^{\,2} + b_2 \cdot h_2 \cdot h_1 + b_2 \cdot h_2^{\,2} \cdot \frac{1}{2} \right) = -1926 \cdot in^3$$

Neutral axis depth from the top of the section

$$x := \max\left(\frac{-b + \sqrt{b^2 - 4 \cdot a \cdot c}}{2 \cdot a}, \frac{-b - \sqrt{b^2 - 4 \cdot a \cdot c}}{2 \cdot a} \right) = 3.21 \cdot in$$

Check if the neutral axis is in the concrete. $x = 3.21 \cdot in \quad .\leq. \quad h_1 = 3 \cdot in$ **Not OK.**

If the neutral axis is greater that the depth of the concrete the assumption the neutral axis is in the concrete is incorrect. The neutral depth calculation needs to be recalculated assuming the neutral axis is in the timber.

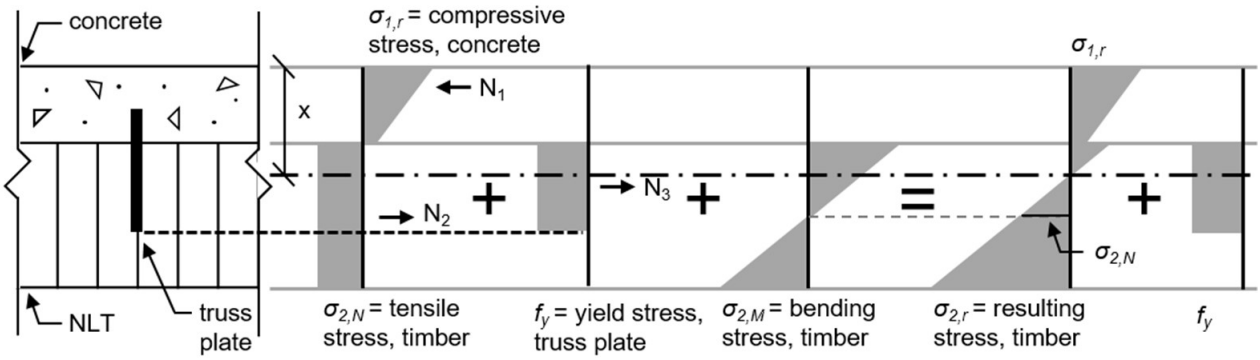

Fig. D.2. Assumed stress field for a fully composite timber-concrete composite floor with the neutral axis in the timber

Full elastic section modulus, concrete

$$S_1 = \frac{1}{6} \cdot b \cdot h_1^{\,2} + b \cdot h_1 \cdot \left(x - \frac{h_1}{2} \right)$$

Full elastic section modulus, timber

$$S_2 = \frac{1}{6} \cdot b \cdot h_2^{\,2} + b \cdot h_2 \cdot \left(\frac{h_2}{2} + h_1 - x \right)$$

Full elastic section modulus, connector

$$S_3 = \frac{1}{6} \cdot b_3 \cdot h_3^{\,2} + b_3 \cdot h_3 \cdot \left(\frac{h_3}{2} + h_1 - x \right)$$

Summing the full section modulus of all subcomponents yields the following equation:

$$n_a \cdot S_1 = S_2 + S_3 \cdot n_b$$

Combining equations and simplifying results in the following equation for the depth of neutral axis from the top of the section:

$$x := \frac{\frac{n_a \cdot b_1 \cdot h_1^{\,2}}{3} + \frac{2 \cdot b_2 \cdot h_2^{\,2}}{3} + b_2 \cdot h_2 \cdot h_1 + \left(\frac{2 \cdot b_3 \cdot h_3^{\,2}}{3} + b_3 \cdot h_3 \cdot h_1 \right) \cdot n}{n_a \cdot b_1 \cdot h_1 + b_2 \cdot h_2 + b_3 \cdot h_3 \cdot n_b}$$

Check if the neutral axis is in the concrete. $x = 3.26 \cdot in \quad . \geq . \quad h_1 = 3 \cdot in$ **OK.**

Stresses

Relation between timber bending and tensile stress

$$\alpha := \frac{h_2}{h_2 + 2 \cdot h_1 - 2 \cdot x} = 1.1$$

Tensile stress, timber

$$\sigma_{2.N} := \frac{F_t \cdot F_b}{F_b + \alpha \cdot F_t} = 287 \cdot psi$$

Bending stress, timber

$$\sigma_{2.M} := \alpha \cdot \sigma_{2.N} = 317 \cdot psi$$

Check is the ultimate limit state for timber in combined bending and tension met

$$\frac{\sigma_{2.N}}{F_t} + \frac{\sigma_{2.M}}{F_b} = 1 \quad . \leq . \quad 1$$ **OK.**

Check Compressive stress, concrete (neutral axis in concrete)

$$\sigma_{1.r} := \frac{2 \cdot \sigma_{2.M} \cdot n_a \cdot x}{h_2} = 1.08 \cdot ksi \quad . \leq . \quad f'_c = 5 \cdot ksi$$ **OK.**

Check Compressive stress, concrete (neutral axis in timber)

$$\sigma_{1.m} := \frac{2 \cdot \sigma_{2.M} \cdot n_a \cdot h_1}{h_2} = 1 \cdot ksi \quad . \leq . \quad f'_c = 5 \cdot ksi$$ **OK.**

Moment capacity

Flexural capacity, composite section (neutral axis in concrete)

$$M_R := A_2 \cdot \sigma_{2.N} \cdot \left(\frac{h_2}{2} + h_1 - \frac{x}{3} \right) + \sigma_{2.M} \cdot \frac{b_2 \cdot h_2^2}{6} \ldots + f_y \cdot b_3 \cdot h_3 \cdot \left(\frac{h_3}{2} + h_1 - \frac{x}{3} \right)$$

$$M_R = 49 \cdot kip \cdot ft$$

Flexural capacity, composite section (neutral axis in timber)

$$M_R := A_2 \cdot \sigma_{2.N} \cdot \left(\frac{h_2}{2} + \frac{2h_1}{3} \right) + \sigma_{2.M} \cdot \frac{b_2 \cdot h_2^2}{6} \ldots + N_3 \cdot \left(\frac{h_3}{2} + \frac{2h_1}{3} \right)$$

$$M_R = 50 \cdot kip \cdot ft$$

Appendix E: γ-method example calculation

γ-method deflection calculation
NLT-concrete composite floor
Exactly per Eurocode 5 (CEN 2004a)

Description

Deflection of TCC floors can be calculated by evaluating the effective bending stiffness, $(EI)_{eff}$, with the γ-method per Eurocode 5 (CEN 2004a). The example calculation provided below is for the ambient temperature deflection of the NLT-concrete composite floor tested (Chapter 3).

All concrete properties are from the mix design for this study. All timber properties are from the National Design Specifications for Wood Construction (NDS 2018).

Material Properties

Compressive strength, concrete $f'_c := 5000psi$

Tensile strength, timber $F_t := 450psi$

Bending strength, timber $F_b := 875psi$

Elastic modulus, concrete $E_1 = 4031 \cdot ksi$

Elastic modulus, timber $E_2 := 1400ksi$

Ambient Section Geometry

Length of floor $L_p := 15.75ft$

Depth of section, concrete $h_1 := 3in$

Depth of section, timber $h_2 := 5.5in$

Width of section, concrete $b_1 := 49.5in$

Width of section, timber $b_2 := b_1$

Moment of inertia, concrete $I_1 := b_1 \cdot h_1^3 \cdot \frac{1}{12} = 111 \cdot in^4$

Moment of inertia, timber $I_2 := b_2 \cdot h_2^3 \cdot \frac{1}{12} = 686 \cdot in^4$

Area of section, concrete $A_1 := h_1 \cdot b_1 = 148.5 \cdot in^2$

Area of section, timber $A_2 := h_2 \cdot b_2 = 272.25 \cdot in^2$

Ratio, elastic moduli $n := \frac{E_1}{E_2} = 2.88$

Connector Properties

Number of connectors in width of floor

$m := 10$

Connector spacing

$s := 24in$

Average experimental maximum force, per connector

$$T_r := \frac{(30.18 + 29.61 + 28.48 + 30.24 + 29.89 + 30.18)\cdot kip}{6\cdot 4}$$

Average experimental displacement at maximum force

$$\Delta := \left(\frac{0.28 + 0.29 + 0.22 + 0.21 + 0.28 + 0.19}{6}\right)in$$

Stiffness, connector

$$k := \frac{T_r}{\Delta} = 30.4\cdot\frac{kip}{in}$$

Effective stiffness calculations

Reduction factor, composite action

$$\gamma := \frac{1}{1 + \frac{\pi^2\cdot E_1\cdot A_1\cdot s}{m\cdot k\cdot L_p^{\,2}}} = 0.07$$

Distance between the centroid of the timber layer and the neutral axis

$$a_2 := \frac{\gamma\cdot E_1\cdot A_1\cdot(h_1 + h_2)}{2\cdot(\gamma\cdot E_1\cdot A_1 + E_2\cdot A_2)} = 0.43\cdot in$$

Distance between the centroid of the concrete layer and the neutral axis

$$a_1 := \frac{h_1 + h_2}{2} - a_2 = 3.82\cdot in$$

Effective stiffness, composite section

$$EI_{ef} := E_1\cdot I_1 + E_2\cdot I_2 + E_1\cdot A_1\cdot\gamma\cdot a_1^{\,2} + E_2\cdot A_2\cdot a_2^{\,2}$$

$$EI_{ef} = 2101013\cdot kip\cdot in^2$$

Deflection Calculations

Flexural demand (See Appendix B)

$w := 131psf\cdot b_1 = 540\cdot plf$

Deflection at midspan

$$\Delta := \frac{5}{384}\cdot\frac{w\cdot L_p^{\,4}}{EI_{ef}} = 0.36\cdot in$$

Units: w [pli], L_p [in], EI_{ef} [lbf-in^2]

Appendix F: Adapted γ-method example calculation

Adapted γ-method deflection calculation
Applied to the NLT-concrete composite floor
Per Eurocode 5 (CEN 2004a), FPInnovations Design Guide (Cuerrier-Auclair 2020)

Description

Deflection of TCC floors can be calculated by evaluating the effective bending stiffness, $(EI)_{eff}$, with the γ-method per Eurocode 5 (CEN 2004a). Two minor adaptations are made to the γ-method. The first adaptation pertains neglecting the height of the concrete in tension. The second adaptation pertains to the use of shear connectors that are not ductile dowel-type fastener shear connectors. The example calculation provided below is for the ambient temperature deflection of the NLT-concrete composite floor tested (Chapter 3).

All concrete properties are from the mix design for this study. All timber properties are from the National Design Specifications for Wood Construction (NDS 2018).

Material Properties

Compressive strength, concrete $f'_c := 5000psi$

Tensile strength, timber $F_t := 450psi$

Bending strength, timber $F_b := 875psi$

Elastic modulus, concrete $E_1 = 4031 \cdot ksi$

Elastic modulus, timber $E_2 := 1400ksi$

Ambient Section Geometry

Length of floor $L_p := 15.75ft$

Depth of section, concrete $h_1 := 3in$

Depth of section, timber $h_2 := 5.5in$

Width of section, concrete $b_1 := 49.5in$

Width of section, timber $b_2 := b_1$

Moment of Inertia, concrete $I_1 := b_1 \cdot h_1^3 \cdot \frac{1}{12} = 111 \cdot in^4$

Moment of Inertia, timber $I_2 := b_2 \cdot h_2^3 \cdot \frac{1}{12} = 686 \cdot in^4$

Area of section, concrete $A_1 := h_1 \cdot b_1 = 148.5 \cdot in^2$

Area of section, timber $A_2 := h_2 \cdot b_2 = 272.25 \cdot in^2$

Ratio, elastic moduli $n_a := \frac{E_1}{E_2} = 2.88$

Connector Properties

Number of connectors in width of floor

$m := 10$

Connector spacing

$s := 24in$

Average experimental maximum force, per connector

$T_r := \frac{(30.18 + 29.61 + 28.48 + 30.24 + 29.89 + 30.18)\cdot kip}{6\cdot 4}$

Average experimental displacement at maximum force

$\Delta := \left(\frac{0.28 + 0.29 + 0.22 + 0.21 + 0.28 + 0.19}{6}\right)in$

Stiffness, connector

$k := \frac{T_r}{\Delta} = 30.4\cdot\frac{kip}{in}$

Total thickness, connector

$b_3 := m\cdot 0.0356in = 0.36\cdot in$

Depth of connector in timber

$h_3 := 3in$

Area of section, connector

$A_3 := m h_3\cdot b_3 = 10.68\cdot in^2$

Moment of Inertia, connector

$I_3 := \frac{m\cdot b_3\cdot {h_3}^3}{12} = 8.01\cdot in^4$

Elastic modulus, steel

$E_3 := 29000ksi$

Combining Timber and Connector Sections

Ratio, elastic moduli

$n_b := \frac{E_3}{E_2} = 20.71$

Centroid, timber, measured from top of timber section

$x_2 := \frac{1}{2}\cdot h_2 = 2.75\cdot in$

Centroid, truss plate, measured from top of timber section

$x_3 := \frac{1}{2}\cdot h_3 = 1.5\cdot in$

Centroid, timber and truss plate, measured from top of timber section

$y := \frac{A_2\cdot x_2 + A_3\cdot x_3\cdot n_b}{A_2 + A_3\cdot n_b} = 2.19\cdot in$

Moment of inertia, timber and truss plate

$I_{23} := \left[I_2 + A_2\cdot\left(x_2 - y\right)^2\right] + \left[n_b\cdot I_3 + n_b\cdot A_3\cdot\left(x_3 - y\right)^2\right]$

$I_{23} = 1043\cdot in^4$

Area, connector and timber combined

$A_{23} := A_2 + A_3\cdot n_b = 493\cdot in^2$

Effective Stiffness Calculations, FP Innovations Design Guide

Reduction factor, composite action, concrete

$$\gamma_1 := 1$$

Reduction factor, composite action, timber

$$\gamma_2 := \frac{1}{1 + \frac{\pi^2 \cdot E_2 \cdot A_{23} \cdot s}{m \cdot k \cdot L_p^2}} = 0.062$$

Axial stiffness, concrete

$$EA_1 := E_1 \cdot b_1 \cdot h_1 = 598531 \cdot kip$$

Distance between timber and concrete centroids

$$r := y + \frac{h_1}{2} = 3.69 \cdot in$$

Distance between the centroid of the concrete layer and the neutral axis

$$a_1 := \frac{\gamma_2 \cdot E_2 \cdot A_{23} \cdot r}{\gamma_1 \cdot EA_1 + \gamma_2 \cdot E_2 \cdot A_{23}} = 0.25 \cdot in$$

Check if a_1 is greater than the height of the concrete. If yes, then the entire thickness of the concrete is in compression and $h_{1,eff} = h_1$. But if not, then a_1 needs to be recalculated to neglect the portion of concrete in tension.

$$a_1 = 0.25 \cdot in \quad . \geq . \quad \frac{h_1}{2} = 1.5 \cdot in$$ **Not OK.**

Equation simplification factor

$$\alpha := \frac{\gamma_2 \cdot E_2 \cdot A_{23}}{\gamma_1 \cdot E_1 \cdot b_1} = 0.22 \cdot in$$

Effective depth, concrete

$$h_{1.eff} := \sqrt{\alpha^2 + \alpha \cdot (2 \cdot y + 2 \cdot h_1)} - \alpha = 1.29 \cdot in$$

Axial stiffness, concrete

$$EA_{1.eff} := E_1 \cdot b_1 \cdot h_{1.eff} = 258361 \cdot kip$$

Bending stiffness, concrete

$$EI_{1.eff} := \frac{1}{12} E_1 \cdot b_1 \cdot h_{1.eff}^3 = 36105 \cdot kip \cdot in^2$$

Distance between timber and concrete centroids

$$r_{eff} := y + h_1 - \frac{h_{1.eff}}{2} = 4.54 \cdot in$$

Distance between the centroid of the concrete layer and the neutral axis, using effective concrete height

$$a_{1.eff} := \frac{\gamma_2 \cdot E_2 \cdot A_{23} \cdot r_{eff}}{\gamma_1 \cdot EA_{1.eff} + \gamma_2 \cdot E_2 \cdot A_{23}} = 0.65 \cdot in$$

Distance between the centroid of the timber layer and the neutral axis

$$a_{2.eff} := \frac{\gamma_1 \cdot EA_{1.eff} \cdot r_{eff}}{\gamma_1 \cdot EA_{1.eff} + \gamma_2 \cdot E_2 \cdot A_{23}} = 3.89 \cdot in$$

Effective stiffness

$$EI_{ef} := EI_{1.eff} + E_2 \cdot I_{23} + \gamma_1 \cdot EA_{1.eff} \cdot a_{1.eff}^2 \ldots + \gamma_2 \cdot E_2 \cdot A_{23} \cdot a_{2.eff}^2$$

$$EI_{ef} = 2256031 \cdot kip \cdot in^2$$

Deflection Calculations

Flexural demand (See Appendix B)

$$w := 131psf \cdot b_1 = 540 \cdot plf$$

Deflection at midspan

$$\Delta := \frac{5}{384} \cdot \frac{w \cdot L_p^4}{EI_{ef}} = 0.33 \cdot in$$

Units: w [pli], L_p [in], EI_{ef} [lbf-in^2]

Appendix G: Cuerrier-Auclair (2020) design method example calculation

FPInnovations design method for flexural capacity of TCC floors
Applied to the NLT-concrete composite floor
Per FPInnovations Design Guide (Cuerrier-Auclair 2020)

Description

Flexural capacity of TCC floors can be calculated with the FPInnovations design method. FPInnovations evaluates the bending moment resistance of TCC floors by using the minimum result from two analytical models: (1) the elasto-plastic model and (2) γ-method. The example calculation provided below is for the ambient temperature flexural capacity of the NLT-concrete composite floor tested (Chapter 2).

All concrete properties are from the mix design for this study. All timber properties are from the National Design Specifications for Wood Construction (NDS 2018).

Concrete Properties

Specified compression strength $f'_c := 5000psi$

Elastic modulus $E_1 = 4031 \cdot ksi$

Density $\rho_1 := 150pcf$

Width $b_1 := 49.5in$

Height $h_1 := 3in$

Area $A_1 := b_1 \cdot h_1 = 148 \cdot in^2$

Timber Properties

Elastic modulus, timber $E_2 := 1400ksi$

Width $b_2 := 49.5in$

Height $h_2 := 5.5in$

Area $A_2 := b_2 \cdot h_2 = 272 \cdot in^2$

Moment of inertia $I_2 := \frac{1}{12} b_2 \cdot h_2^3 = 686 \cdot in^4$

Tensile strength, timber $F_t := 450psi$

Bending strength, timber $F_b := 875psi$

Bending moment resistance $M_{r,2} := \frac{1}{6} \cdot F_b \cdot A_2 \cdot h_2 = 218 \cdot kip \cdot in$

Tension resistance $T_{r,2} := F_t \cdot A_2 = 123 \cdot kip$

Connector Properties

Shear resistance (Average experimental maximum force, per connector)

$V_{r,3} = 7.4 \cdot kip$

Shear stiffness of a single connector in the span direction (experimental, see Appendix 3)

$k_s = 30.4 \cdot \frac{kip}{in}$

No. of connectors along width

$n := 10$

Spacing of shear connector along the span

$s := 24in$

Ambient Section Geometry

Span length

$L := 15.75ft$

Thickness, accoustic layer

$t := 0in$

Calculation of the Effective Bending Stiffness

Effective spacing of shear connector along the span (for this case, equal to spacing)

$s_{eff} := s = 24 \cdot in$

Distributed shear stiffness in the span direction

$K := \frac{n \cdot k_s}{s_{eff}} = 12.7 \cdot ksi$

Non-dimensional factor for composite action, concrete layer

$\gamma_1 := 1$

Non-dimensional factor for composite action, timber layer

$$\gamma_2 := \frac{1}{1 + \frac{\pi^2}{L^2} \cdot \frac{E_2 \cdot A_2}{K}} = 0.11$$

Equation simplification factor

$$\alpha := \frac{\gamma_2 \cdot (E_2 \cdot A_2)}{\gamma_1 \cdot E_1 \cdot b_1} = 0.2 \cdot in$$

Effective height of concrete

$$h_{1.eff} := \sqrt{\alpha^2 + \alpha \cdot (h_2 + 2 \cdot h_1 + 2 \cdot t)} - \alpha = 1.3 \cdot in$$

Effective height of accoustic layer (for this case, no accoustic layer)

$t_{eff} := 0$

Distance between timber and concrete centroids

$$r := \frac{h_2}{2} + t_{eff} + h_1 - \frac{h_{1.eff}}{2} = 5.1 \cdot in$$

Bending stiffness, concrete

$$EI_1 := E_1 \cdot \frac{b_1 \cdot h_{1.eff}^3}{12} = 40350 \cdot kip \cdot in^2$$

Axial stiffness, concrete

$EA_1 := E_1 \cdot b_1 \cdot h_{1.eff} = 268114 \cdot kip$

Distance between the centroid of the concrete layer and the neutral axis, using effective concrete height

$$a_1 := \frac{\gamma_2 \cdot E_2 \cdot A_2 \cdot r}{\gamma_1 \cdot EA_1 + \gamma_2 \cdot \left(E_2 \cdot A_2\right)} = 0.7 \cdot in$$

Distance between the centroid of the timber layer and the neutral axis

$$a_2 := \frac{\gamma_1 \cdot EA_1 \cdot r}{\gamma_1 \cdot EA_1 + \gamma_2 \cdot \left(E_2 \cdot A_2\right)} = 4.41 \cdot in$$

Effective stiffness

$$EI_{eff} := EI_1 + E_2 \cdot I_2 \ldots + \gamma_1 \cdot EA_1 \cdot a_1^{\,2} + \gamma_2 \cdot E_2 \cdot A_2 \cdot a_2^{\,2}$$

$$EI_{eff} = 1916002 \cdot kip \cdot in^2$$

Calculation of Bending Moment Resistance (1-3)

(1) γ-method

Bending moment resistance, limited by timber

$$M_{r,\gamma,2} := \frac{EI_{eff} \cdot T_{r,2} \cdot M_{r,2}}{\gamma_2 \cdot E_2 \cdot A_2 \cdot a_2 \cdot M_{r,2} + E_2 \cdot I_2 \cdot T_{r,2}} = 27.2 \cdot kip \cdot ft$$

(2) γ-method

Section modulus, concrete

$$S_1 := \frac{EI_{eff}}{E_1 \cdot \left(0.5 \cdot h_{1.eff} + \gamma_1 \cdot a_1\right)} = 354 \cdot in^3$$

Bending moment resistance, limited by concrete

$$M_{r,\gamma,1} := 0.9 \cdot f'_c \cdot S_1 = 179.9 \cdot kN \cdot m$$

(3) Elasto-plastic method

See Appendix C for the design example of the elasto-plastic model applied to the NLT-concrete composite floor.

Bending moment resistance, elasto-plastic model

$$M_{r,EP} := 37.5 kip \cdot ft$$

(4) Bending Moment Resistance

Bending Moment Resistance

$$M_r := \min\left(M_{r,\gamma,2}, M_{r,\gamma,1}, M_{r,EP}\right) = 27.2 \cdot kip \cdot ft$$

Appendix H: Spline calculation

Spline calculations for the large-scale fire test
CLT-concrete composite floor

Description

Calculations to determine the number of screws needed for the surface spline inter-panel connection. Calculations follow design procedure suggested by Simpson Strong-Tie for typical Wood-to-Wood application.

Calculations assume dry and normal temperature conditions, maximum shear stress at location of neutral axis, and uniform shear flow.

National Design Specifications for Wood Construction (NDS 2018) factors

Wet Service Factor $C_M := 1.0$

Temperature Factor $C_t := 1.0$

Load Duration Factor $C_D := 1.0$

Connection and shear connector properties

Type of spline APA rated Sturd-I-Floor wood structural panel

Type of screw SDWS Timber Screws 6" SDWS 22600 DB

Screw allowable for SPF timber and a surface spline $S_v := 335lbf$

Width of connection $b_c := 6in$

Timber and floor properties

Height, timber $h_2 := 6in + \frac{7}{8}in$

Length, floor $L_p := 15ft + 9in$

Location of support centerline $x := 3in$

Moment of inertia, timber $I := \frac{1}{12}\cdot b_c\cdot {h_2}^3 = 162\cdot in^4$

Loading

Applied load, live load and concrete dead load (See Appendix B) $w := 80psf + 28.1psf$

Shear force at supports $V := w\cdot b_c\cdot\left(\frac{L_p}{2} - x\right) = 0.412\cdot kip$

Partial cross-section area $A' := b_c\cdot\left(\frac{1}{2}\cdot h_2\right) = 20.6\cdot in^2$

Distance to centroid of A' from neutral axis

$$y_{bar} := \frac{\frac{1}{2}\cdot h_2}{2} = 1.7\cdot in$$

Shear force at supports

$$Q := A'\cdot y_{bar} = 35\cdot in^3$$

Shear flow at supports

$$q := \frac{V\cdot Q}{I} = 1079\cdot plf$$

Number of screws required

Number of screws

$$N_s := \frac{q}{S_v\cdot C_D\cdot C_t\cdot C_M}$$

Number of screws

$$N_s = 3.2\cdot\frac{1}{ft}$$

Thus, **(4) SDWS timber screws per foot** spaced 3" o.c. on each side of the spline are required.